LIÈGE université
Gembloux
Agro-Bio Tech

COMMUNAUTÉ FRANÇAISE DE BELGIQUE
UNIVERSITÉ DE LIÈGE – GEMBLOUX AGRO-BIO TECH

ECOHYDROLOGICAL RESPONSE OF A GRASSLAND SPECIES TO DROUGHT FROM AN ISOTOPIC AND HYDRAULIC PERSPECTIVE

Paulina Alejandra DESEANO DIAZ

Dissertation originale présentée en vue de l'obtention du grade de doctorat en sciences agronomiques et ingénierie biologique

Promoteur(s) : Prof. Dr. Youri Rothfuss
Année civile (= année du dépôt) : 2024

Abstract

Water flow from the soil through the plants and into the atmosphere is not only passively determined by above- and below-ground environmental conditions. Plants actively control water loss through certain physiological properties (e.g., stomatal closure) following external and internal, chemical and physical triggers (e.g., internal signaling with abscisic acid, production of mucilage, extreme dry conditions around the roots or the leaves). The study of the degree and timing of the vegetation's avoidance of unproductive water loss sheds light into not only the resilience and plasticity of a certain species, but also into the links between environmental conditions and plant physiology that ultimately determine water flow in the soil-plant-atmosphere continuum. Understanding the dynamic interactions between biotic and abiotic processes underlying water fluxes across scales has become even more relevant since the frequency of weather extremes (e.g., drought and heatwaves) is observed to increase due to climate change, especially affecting ecosystems that depend strongly on water from precipitation such as grasslands. These ecosystems provide forage for livestock, are biodiversity hotspots, can store significant amounts of carbon, and represent a considerable area of agricultural land (in Europe, over 30%). The threats posed by drought, reduced precipitation, and heatwaves (e.g., loss of biodiversity, carbon-storage capacity, and productivity) are not only environmental, but also societal and financial.

Water stable isotopic monitoring has been used for several decades as a tracer tool in ecohydrological studies aiming at elucidating interactions between biotic and abiotic processes. More specifically, quantifying root water uptake and investigating its dynamics and drivers with isotopic measurements of soil and plant water in probabilistic multi-source mixing models is now a relatively common strategy. Insights into the mechanisms at the soil-root interface influencing water uptake, especially in dry soils, have been gained with physically-based transfer models, i.e., accounting for soil and root hydraulic properties. This mechanistic understanding of the couplings in the soil-plant-atmosphere continuum ultimately enables accurate water flux estimations across scales and accurate predictions of the impacts of climate change. Thus, vulnerability of grasslands to hydrological extremes can be investigated in part through the assessment of the drought response of the species in this ecosystem at the single plant and community scale.

Nevertheless, the potential of water stable isotopes for root water uptake quantification is limited by the uncertainties associated with the techniques used to extract soil and plant water. Firstly, the reliance of many established water recovery techniques following destructive sampling (e.g., cryogenic vacuum distillation, centrifugation, direct water vapor equilibration) leads to non-negligible measurement uncertainty. In situ non-destructive techniques that rely on continuous soil water vapor isotopic measurements have contributed to reducing this uncertainty source while providing estimates of root water uptake patterns at higher temporal resolution, which is of key interest for modeling purposes. Secondly, vegetation might extract water of which the delta is different from what can be recovered by the range of (destructive

and non-destructive) techniques because of the pore-scale heterogeneity resulting from soil texture-soil water isotope interactions and associated fractionation. Thus, challenging the assumption made in isotopic mixing models that roots take up water from a well-mixed soil water source at the pore-scale.

In chapter 1 of this thesis, I outline the theoretical framework about grasslands, their response to drought and vulnerability to hydrological extremes, about water stable isotopes terminology, their transport in soil and within plants, and about mechanistic transfer modelling. At the end of this section, I formulate the main and specific objectives, as well as accompanying hypothesis of this doctoral project. In chapters 2 through 4, I describe in detail the methodological framework and I present and discuss the results of the three studies constituting this doctoral project:

1. In the first study (chapter 2), I investigated the potential soil-texture- and soil-water-tension-related isotopic fractionating effects on soil water though a comparison of water extracted via pressure, with three destructive isotopic techniques and measured with an in situ non-destructive technique in two types of soil. Describing potential soil water isotopic fractionation caused by a particular soil via in situ non-destructive determinations was a prerequisite to eliminate potential biases in the second study.
2. In a second study, I assessed the ecohydrological response of the forb species *Centaurea jacea* L., native to grasslands in Europe, to varying above- and below-ground conditions in a semi-automated laboratory experiment at the single-plant scale. For this, plant physiological and environmental conditions were continuously monitored. This species was the dominant forb species in the semi-natural temperate grassland, where the ecohydrological assessment of the response to drought and nitrogen loading of the plant community was performed in the framework of the same research program the present doctoral project was embedded in.
3. In the third and final study, I modelled root water uptake and the hydraulic parameters of the aforementioned laboratory experiment with a macroscopic mechanistic hydraulic model to describe links between processes at the soil-root and plant-atmosphere interfaces. I also compared probabilistic and physically-based root water uptake patterns.

The conclusions in the first study are i) two isotopically distinct water pools successively added to a “chemically inert” soil (quartz sand) mix, albeit not consistently across the considered soil volume in the horizontal axis; ii) the isotopic composition of soil water changed as a function of soil water potential in a loamy sand due most likely to methodological constraints and enhanced by low soil water potential values; and iii) the isotopic determinations of three destructive methods (cryogenic vacuum distillation, centrifugation, and direct water vapor equilibration) and the in situ non-destructive online technique were not comparable. Since the unsatisfactory accuracy of the in situ method in the first study was rooted in methodological issues and the results were not affected by horizontal spatial heterogeneities, it was determined that no additional corrections of the soil water isotopic determinations using this method and the loamy sand were necessary.

The root water uptake profiles obtained in the second study enabled by the semi-automated experimental setup evidenced a consistent reliance of *Centaurea jacea* L. on water in shallow depths: up to 79% of water uptake occurred in soil layer 0-15 cm, while up to 44% occurred in soil layer 45-60 cm. Moreover, this grassland drought-resistant species was able to maintain high transpiration rates – by withstanding very low leaf water potential values – and relatively constant water use efficiency in dry conditions, traits also observed in the field in other studies. In the final days of the drought part of the experiment, a steady decrease in canopy conductance at relatively high soil water content was recorded.

To test the hypothesis that this decrease in canopy conductance might have been related to a decrease in root or soil hydraulic conductivity, the ecohydrological assessment was broadened by adding a hydraulic perspective. In these final days of the drought part of the experiment, a steep decrease of the root system conductance and hydraulic conductance near the soil-root interface of *C. jacea* L. under dry conditions was modelled using a macroscopic mechanistic hydraulic model. Consequently, there were slight discrepancies between the probabilistic and physically-based root water uptake patterns, since not only root density or water availability but hydraulic states in the soil and the plant were part of the analysis. Assumptions regarding overestimations of soil water content and absorbing root surface were also part of this extended isotopic and hydraulic approach.

An important task in future studies is disentangling methodology-related and "naturally" occurring fractionating processes in ecohydrological systems and determining the biases and uncertainties they introduce in probabilistic isotope-based root water uptake quantification. These biases and uncertainties could be minimized through standardized methodological frameworks overarching experimental design, sampling, and isotopic determinations. Investigating isotope discrimination in the soil (due to texture, tension or root presence), during transport into the roots (due to e.g., mycorrhizal activity or the root membrane) or through the xylem (due to e.g., molecular transport mechanisms or mixing of storage and conduit water) is still needed. By addressing these knowledge gaps, the potential of water stable isotopes as tracers in the mechanistic understanding of still unknown biotic-abiotic dynamic processes and the identification of climate-related breaking or tipping points in the soil-plant-atmosphere continuum will increase. Moreover, fully coupling probabilistic and physically-based transfer models accounting also for relevant and until now overlooked processes influencing water, carbon, and nutrient cycling (e.g., fine root biomass) without making them unnecessarily complicated can assist in achieving this mechanistic understanding and provide accurate predictions of the impacts of climate change on grasslands and the related ecological, social, and financial consequences.

Résumé

Le flux d'eau du sol à travers les plantes et vers l'atmosphère n'est pas seulement déterminé passivement par les conditions environnementales au-dessus et au-dessous du sol. Les plantes contrôlent activement la perte d'eau grâce à certaines propriétés physiologiques (par exemple, la fermeture des stomates) à la suite de déclencheurs externes et internes, chimiques et physiques (par exemple, la signalisation interne avec l'acide abscissique, la production de mucilage, les conditions de sécheresse extrême autour des racines ou des feuilles). L'étude du degré et du moment où la végétation évite les pertes d'eau improductives nous éclaire non seulement sur la résilience et la plasticité d'une certaine espèce, mais aussi sur les liens entre les conditions environnementales et la physiologie des plantes qui déterminent en fin de compte le flux d'eau dans le continuum sol-plante-atmosphère. Comprendre les interactions dynamiques entre les processus biotiques et abiotiques qui sous-tendent les flux d'eau à travers les échelles est devenu encore plus pertinent depuis que l'on a observé que la fréquence des extrêmes météorologiques (par exemple, la sécheresse et les vagues de chaleur) augmentait en raison du changement climatique, affectant particulièrement les écosystèmes qui dépendent fortement de l'eau provenant des précipitations, tels que les prairies. Ces écosystèmes fournissent du fourrage pour le bétail, sont des points chauds de biodiversité, peuvent stocker des quantités importantes de carbone et représentent une surface considérable de terres agricoles (en Europe, plus de 30 %). Les menaces posées par la sécheresse, la diminution des précipitations et les vagues de chaleur (par exemple, la perte de biodiversité, de capacité de stockage du carbone et de productivité) ne sont pas seulement environnementales, mais aussi sociétales et financières.

Les isotopes stables de l'eau sont utilisés depuis plusieurs décennies comme outil de traçage dans les études éco-hydrologiques visant à étudier les interactions entre les processus biotiques et abiotiques. Plus précisément, la quantification de l'absorption d'eau par les racines, l'étude de sa dynamique et de ses moteurs à l'aide de mesures isotopiques de l'eau du sol et de la plante dans des modèles de mélange multi-source probabiliste constituent désormais une stratégie relativement courante. Des modèles de transfert basés sur la physique, c'est-à-dire tenant compte des propriétés hydrauliques du sol et des racines, ont permis de mieux comprendre les mécanismes à l'interface sol-racine qui influencent l'absorption d'eau, en particulier dans les sols secs. Cette compréhension mécanistique des couplages dans le continuum sol-plante-atmosphère permet en fin de compte d'estimer avec précision les flux d'eau à toutes les échelles et de prédire avec précision les impacts du changement climatique. Ainsi, la vulnérabilité des prairies aux évènements hydrologiques extrêmes peut être étudiée en partie par l'évaluation de la réponse à la sécheresse des espèces de cet écosystème à l'échelle de la plante unique et de la communauté.

Néanmoins, le potentiel des isotopes stables de l'eau pour la quantification de l'absorption d'eau par les racines est limité par les incertitudes associées aux techniques utilisées pour extraire l'eau du sol et des plantes. Tout d'abord, le recours à de nombreuses techniques établies de récupération de l'eau après un échantillonnage

destructif (par exemple, distillation cryogénique sous vide, centrifugation, équilibrage direct de la vapeur d'eau) entraîne une incertitude de mesure non négligeable. Les techniques non destructives in situ qui reposent sur des mesures isotopiques continues de la vapeur d'eau du sol ont contribué à réduire cette source d'incertitude tout en fournissant des estimations des schémas d'absorption de l'eau par les racines à une résolution temporelle plus élevée, ce qui est d'un intérêt essentiel pour la modélisation. Deuxièmement, la végétation peut extraire de l'eau dont la composition isotopique est différente de celle qui peut être récupéré par les diverses techniques (destructives et non destructives) en raison de l'hétérogénéité à l'échelle des pores résultant des interactions entre la texture du sol et les isotopes de l'eau du sol et du fractionnement associé. Cela remet donc en question l'hypothèse faite dans les modèles de mélange isotopique selon laquelle les racines absorbent l'eau d'une source bien mélangée à l'échelle des pores.

Dans le chapitre 1 de cette thèse, je présente le cadre théorique des prairies, leur réponse à la sécheresse et leur vulnérabilité aux extrêmes hydrologiques, la terminologie des isotopes stables de l'eau, leur transport dans le sol et à l'intérieur des plantes, et la modélisation mécanistique du transfert. À la fin de cette section, je formule les objectifs principaux et spécifiques, ainsi que les hypothèses liées aux objectifs spécifiques de ce projet de doctorat. Dans les chapitres 2 à 4, je décris en détail le cadre méthodologique et je présente et discute les résultats des trois études constituant ce projet doctoral :

1. Dans la première étude (chapitre 2), j'ai étudié les effets potentiels de fractionnement isotopique liés à la texture du sol et à la tension de l'eau du sol sur l'eau du sol en comparant l'eau extraite par pression, avec trois techniques isotopiques destructives et mesurée avec une technique non destructive in situ dans deux types de sol. La description du fractionnement isotopique potentiel de l'eau du sol causé par un sol particulier au moyen de déterminations non destructives in situ était une condition préalable à l'élimination des biais potentiels dans la deuxième étude.
2. Dans une deuxième étude, j'ai évalué la réponse éco-hydrologique de l'espèce d'herbacée *Centaurea jacea* L., originaire des prairies d'Europe, à des conditions atmosphériques et de sol variables dans une expérience de laboratoire semi-automatisée à l'échelle de la plante. Pour ce faire, les conditions physiologiques des plantes et environnementales ont été contrôlées en permanence. Cette espèce était l'espèce dominante de la prairie tempérée semi-naturelle, où l'évaluation éco-hydrologique de la réponse de la communauté végétale à la sécheresse et à la fertilisation en azote a été réalisée dans le cadre du même programme de recherche que celui dans lequel s'inscrit le présent projet de doctorat.
3. Dans la troisième et dernière étude, j'ai modélisé l'absorption d'eau par les racines et les paramètres hydrauliques de l'expérience de laboratoire susmentionnée à l'aide d'un modèle hydraulique mécanistique macroscopique afin de décrire les liens entre les processus aux interfaces sol-racine et plante-

atmosphère. J'ai également comparé les modèles d'absorption d'eau par les racines probabiliste et hydraulique.

Les conclusions de la première étude sont les suivantes : i) deux réservoirs d'eau isotopiquement distincts successivement ajoutés à un sol « chimiquement inerte » (sable de quartz) se sont mélange, mais pas de manière complètement homogène dans le volume de sol considéré sur l'axe horizontal ; ii) la composition isotopique de l'eau du sol a changé en fonction du potentiel hydrique du sol dans un sable limoneux, probablement en raison de contraintes méthodologiques et de faibles valeurs du potentiel hydrique du sol ; et iii) les déterminations isotopiques de trois méthodes destructives (distillation cryogénique sous vide, centrifugation et équilibrage direct de la vapeur d'eau) et de la technique non destructive in situ n'étaient pas comparables. Étant donné que la précision insatisfaisante de la méthode in situ dans la première étude était due à des problèmes méthodologiques et que les résultats n'étaient pas affectés par des hétérogénéités spatiales horizontales dans le volume de sol considéré, il a été déterminé qu'aucune correction supplémentaire des déterminations isotopiques de l'eau du sol à l'aide de cette méthode et du sable limoneux n'était nécessaire.

Les profils d'absorption d'eau par les racines obtenus lors de la deuxième étude rendue possible par le dispositif expérimental semi-automatique ont mis en évidence une dépendance constante de *Centaurea jacea* L. à l'égard de l'eau près de la surface du sol : jusqu'à 79 % de l'absorption d'eau s'est produite dans la couche de sol 0-15 cm, tandis que jusqu'à 44 % s'est produite dans la couche de sol 45-60 cm. En outre, cette espèce de prairie résistante à la sécheresse a été capable de maintenir des taux de transpiration élevés - en supportant des valeurs de potentiel hydrique foliaire très basses - et une efficacité d'utilisation de l'eau relativement constante dans des conditions sèches, des caractéristiques également observées sur le terrain dans d'autres études. Au cours des derniers jours de la partie de l'expérience consacrée à la sécheresse, une diminution constante de la conductance du couvert végétal a été enregistrée à une teneur en eau du sol relativement élevée.

Pour tester l'hypothèse selon laquelle cette diminution de la conductance du couvert aurait pu être liée à une diminution de la conductivité hydraulique des racines ou du sol, l'évaluation éco-hydrologique a été élargie par l'ajout d'une perspective hydraulique. Au cours de ces derniers jours de la partie sécheresse de l'expérience, une forte diminution de la conductance du système racinaire et de la conductance hydraulique près de l'interface sol-racine de *C. jacea* L. en conditions sèches a été modélisée à l'aide d'un modèle hydraulique mécanistique macroscopique. Par conséquent, il y a eu de légères divergences entre les modèles d'absorption d'eau par les racines probabiliste et ceux du modèle hydraulique, étant donné que l'analyse du dernier ne portait pas uniquement sur la densité des racines ou la disponibilité de l'eau, mais aussi sur les états hydrauliques du sol et de la plante. Les hypothèses concernant la surestimation de la teneur en eau du sol et de la surface absorbante des racines faisaient également partie de cette approche isotopique et hydraulique élargie.

Une tâche importante des études futures consistera à démêler les processus de fractionnement liés à la méthodologie et ceux qui se produisent « naturellement » dans les systèmes éco-hydrologiques et à déterminer les biais et les incertitudes qu'ils

introduisent dans la quantification probabiliste de l'absorption d'eau par les racines basée sur les isotopes. Ces biais et incertitudes pourraient être minimisés grâce à des cadres méthodologiques normalisés couvrant la conception expérimentale, l'échantillonnage et les déterminations isotopiques. Il est encore nécessaire d'étudier la discrimination isotopique dans le sol (en raison de la texture, de la tension ou de la présence de racines), pendant le transport dans les racines (en raison, par exemple, de l'activité mycorhizienne ou de la membrane racinaire) ou à travers le xylème (en raison, par exemple, des mécanismes de transport moléculaire ou du mélange de l'eau de stockage et de l'eau de conduite). En comblant ces lacunes, le potentiel des isotopes stables de l'eau en tant que traceurs dans la compréhension mécanistique des processus dynamiques biotiques-abiotiques encore inconnus et l'identification des points de rupture ou de basculement liés au climat dans le continuum sol-plante-atmosphère augmentera. En outre, le couplage complet de modèles de transfert probabilistes et physiques tenant également compte de processus pertinents et jusqu'à présent négligés influençant le cycle de l'eau, du carbone et des nutriments (par exemple, la biomasse des racines fines), sans les compliquer inutilement, peut aider à parvenir à cette compréhension mécanistique et à fournir des prévisions précises des impacts du changement climatique sur les prairies et des conséquences écologiques, sociales et financières qui en découlent.

(Texte traduit avec DeepL® le 2 Novembre 2024 et corrigé par Samuel Le Gall).

Acknowledgements

I am immensely grateful to my supervisor, Youri Rothfuss, for having given me the chance at the great adventure that was my doctoral project. I am thankful for the constant meaningful scientific and personal support and for having shown me repeatedly that the best strategy to overcome difficulties is to remain calm and make the best out of ever changing circumstances. I am grateful for his kindness and for having been challenged to achieve more than I thought to be capable of.

I thank Maren Dubbert, Mathieu Javaux, Nicolas Brüggemann, Jan Vanderborght, and Harry Vereecken for always giving useful feedback and delivering constructive criticism in a graceful manner. Thanks to their willingness to share their expertise, I was able to overcome numerous challenges and move forward in the project, improve significantly all manuscripts and experimental approaches, question my assumptions and decisions, and gain a deeper understanding of my project and what my contribution to the field was.

Many thanks to Lutz Weihermüller for the numerous personal tutorials on soil physics, HYDRUS, the soil retention curves, and the scientific and technical support for the experiments of the first study described in chapter 2.

I am thankful for the pivotal and committed involvement of Dagmar van Dusschoten in the second study described in chapter 3. My time working with him and his team conducting MRI measurements and building the elements of my experimental setup was one of the most challenging and rewarding in my project. It was entirely uncharted territory, but I had incredibly skilled and agreeable guides.

The successful completion of the experiments described in chapters 2 and 3 is in great part due to the scientific and technical support of Marco Dautzenberg, Johannes Kochs, Daniel Pflugfelder, Normen Hermes, and Moritz Harings, who reminded me how exciting and rewarding engineering and hands-on work are. Thankfully, they brought structure and flexibility into the experimental phase, which was decisive for the success of my project despite the restrictions during the corona pandemic.

I feel lucky to have met and engaged in scientific exchanges with two brilliant young scientists: Valentin Couvreur and Angelika Kübert. These interactions were crucial to the realization of the third study described in chapter 4. Moreover, every conversation with them was nourishment not only for the brain, but also for the soul. This study also profited significantly from the on-point remarks and meaningful insights of Jan Vanderborght. He dedicated his valuable time to provide key results and a framework, together with Valentin Couvreur and Mathieu Javaux, for the third study with the hydraulic approach to root water uptake.

Furthermore, the invaluable support and contributions of Andreas Weihermüller, Barbara Herbstritt, Heike Weller, Nelly Weis, Holger Wissel, Sirgit Kummer, Franz Leistner, and Beate Uhlig were also essential during my experiments in Forschungszentrum Jülich and the University of Gießen. Moreover, their patience and readiness to engage with me during my first attempts at communicating in German rocketed my progress in this language and contributed greatly to my adaptation process in a land that I now call home.

I am grateful for the opportunity of working together with and co-supervising Sandi Moyo and Thai Nong and for their inventive workarounds during the experimental phase of this project. I feel lucky to have been part of an incredible research group with nice and collegial PhDs and Post-Docs. Thank you Samuel Le Gall, Daniel Schulz, Katharina Neubert, Nikos Kaloterakis, Rüdiger Reichel, Otavio Leal, Matthias Claß, and Muhammad Islam for the funny and relaxed lunches and coffee breaks together, that I am still allowed to attend. A especial thanks to Samuel Le Gall for checking the translation into French of the abstract and providing the valuable information for the perspectives of the second study.

I would also like to thank Jean-Thomas Cornelis and Sarah Garré for having been part of my thesis committee and hope they are successful in their new exciting career opportunities following the University of Liège. Likewise, I thank Bernard Longdoz for his scientific and administrative advice for the completion of my doctoral project and Hélène Soyeurt for voluntarily taking over the role of chair of the jury.

Thanks to the co-authors of the published studies and the members of my thesis committee and jury for valuable contributions that resulted in significant improvements of the manuscripts and this doctoral thesis.

I am deeply grateful for the unwavering support and love, as well as the constant and inspiring presence in my life of my mom, Elvia, my sister, Daniela, and my oldest friends Marian, Ezequiel, Jessica, and Karla. I consider myself extremely lucky for having been raised by a generous, hard working, fair, and, above all, kind mother and learning important life lessons from my little sister. I am also thankful for the friendship and emotional support of Susana, Corinna, Daniela, Lya, Jimena, and Gaby that kept my head above the water during personal and professional crisis in the past five years.

I thank the chain of fortuitous events that led me to meeting my husband, Stefan. I feel blessed for being able to grow and mature together through disagreements, moments of silly laughter, and travelling. Thank you for never doubting us and forgiving me for doing so in the past.

Finally, I am grateful to my father- and mother-in-law, Karl and Armgard, for their crucial support at the beginning of our marriage, when we were pursuing personal, financial, and professional stability and independence. With your and my mom’s support, we made it.

Table of contents

List of figures

List of tables

List of acronyms

A	CO_2 assimilation rate	μmol s^{-1} m^{-2}
B_z	Geometrical factor	
bi	Best iteration	
CF	Centrifugation	
c_{in}	CO_2 mixing ratio of the water vapor in the plant chamber's inlet airstream	
c_{out}	CO_2 mixing ratio of the water vapor in the plant chamber's outlet airstream	
CRDS	Cavity ring-down spectrometer	
CVD	Cryogenic vacuum distillation	
DaS	Days after seeding	
DVE	Direct water vapor equilibration	
dz	Thickness of soil layer z	cm
GMWL	Global Meteoric Water Line	
GRESP	Greenland Summit Precipitation	
G_s	Canopy conductance	mmol s^{-1} m^{-2}
H_{collar}	Water potential at the plant collar	MPa
$H_{s,r}$	Water potential in the soil-root interface	cm
HTr	High transpiration rate	
IAEA	International Atomic Energy Agency	
IPCC	Intergovernmental Panel on Climate Change	
IRIS	Isotope Ratio Infrared Spectrometer	
IS	In situ online isotopic method	
iWUE	Intrinsic water use efficiency	μmol $mmol^{-1}$
K_{eq}	Equivalent hydraulic conductance	cm^3 hPa^{-1} d^{-1}
K_r	Radial hydraulic conductance	cm hPa^{-1} d^{-1}

k_r	Radial hydraulic conductivity	$cm^3\ hPa^{-1}\ d^{-1}$
K_{rs}	Root system equivalent hydraulic conductance	$cm^3\ hPa^{-1}\ d^{-1}$
k_s	Soil hydraulic conductivity	$cm^2\ hPa^{-1}\ d^{-1}$
k_{sat}	Soil hydraulic conductivity at saturation	
K_x	Axial hydraulic conductance	$cm^3\ hPa^{-1}\ d^{-1}$
k_x	Axial hydraulic conductivity	$cm^4\ hPa^{-1}\ d^{-1}$
LED	Light-Emitting Diode	
LL	Lower Limit in the Bland-Altman plot	‰
LMWL	Local Meteoric Water Line	
LTr	Low Transpiration rate	
L_z	Thickness of soil layer z	cm
MFC	Mass flow controller	
mfv	Most frequent value	
MRI	Magnetic Resonance Imaging	
MS	Multi-Source	
n	Factor describing the nature of the transport through the layer above an evaporating surface	
n_A	Number of observations per subject using method A	
n_B	Number of observations per subject using method B	
nk	Factor describing the nature of the transport through the layer above the evaporating front in soil	
$N_{segments}$	Number of dz-long root segments	
OF	Objective function	
P_{air}	Vapor saturation pressure at air temperature	kPa
PC	Pressure controller	

P_{canopy}	Canopy xylem pressure	
PID	Piping and instrumentation diagram	
P_{leaf}	Vapor saturation pressure at leaf temperature	kPa
PPE	Pressure plate extractor	
ppmV	Parts per million volume	
PTFE	Polytetrafluoroethylene	
PVC	Polyvinyl chloride	
Q	Flux rate of water into the roots	$L^3\ T^{-1}$
RC	Repeatability coefficient	‰
rh	Air relative humidity	%
rh’	Relative humidity normalized to leaf temperature	%
RLD	Root length density	cm cm^{-3}
RL	Root length	cm
RMSE	Root Mean Square Error	
rRLD	Relative root length density	
r_{root}	Weighted mean of the root radius	cm
R_{sample}	Isotope ratio in a sample	‰
$R_{standard}$	Isotope ratio in a standard	‰
RWU	Root water uptake	$V\ T^{-1}\ V^{-1}$
s	Soil surface area of the isotopic column	m^2
s_{diff}	Standard deviation of the differences in soil water isotopic composition determined with method A and method B	‰
$\hat{s}_{diff}$	Corrected standard deviation of the differences in soil water isotopic composition determined with method A and method B	‰
SIAR	Stable Isotope Analysis with R	

SLAP2	Standard Light Antarctic Precipitation 2	
S_{root}	Root surface area	cm^2
SUF	Standard uptake fraction	
SUF_{iso}	Standard uptake fraction considered equal to relative root water uptake	
SUF_{Knet}	Standard uptake fraction from the conductance network	
SUF_{root}	Standard uptake fraction considered equal to relative root length	
SV	Soil-filled vessel	
s_w	Within-subject standard deviation	‰
s_{wA}	Within-subject standard deviation of the isotopic determinations with method A	‰
s_{wB}	Within-subject standard deviation of the isotopic determinations with method B	‰
SWaP	Soil Water Profiler	
T_{act}	Actual transpiration rate	$cm^3\ s^{-1}$
$T_{act\ day}$	Actual transpiration rate during day (LED panel on)	$cm^3\ s^{-1}$
$T_{act\ night}$	Actual transpiration rate during night (LED panel off)	$cm^3\ s^{-1}$
T_{air}	Air temperature	°C
T_{leaf}	Leaf temperature	°C
Tr	Plant transpiration rate	$mmol\ m^{-2}\ s^{-1}$
u_{in}	Molar air flow into the plant chamber	$mmol\ s^{-1}$
UL	Upper Limit in the Bland-Altman plot	‰
vpd	Vapor pressure deficit	kPa
vpd_l	Air-to-leaf vapor pressure deficit	kPa

V-SMOW2	Vienna Standard Mean Ocean Water 2	
V_z	Soil volume of layer z	cm^3
w_{in}	Water vapor mixing ratio in the plant chamber's inlet airstream	
w_{out}	Water vapor mixing ratio in the plant chamber's outlet airstream	
$w_{tap\ water}$	Amount of deionized tap water remaining after the pressure-extraction	g
w_{mix}	Sum of remaining tap water and added isotopically enriched water	g
WUE	Instantaneous water use efficiency	µmol $mmol^{-1}$
WV	Water-filled vessel	
$x_{tap\ water}$	Fraction of tap water in the soil water mixture after re-saturation	
α_{eq}	Equilibrium fractionation factor	‰
α_k	Kinetic fractionation factor	‰
ρ_z	Ratio of the distance between roots and the root averaged diameter in soil layer z	
δ_{Aj}	Isotopic composition of soil water in vessel j determined with method A	‰
$\delta_{(A-B)j}$	Difference in isotopic composition of soil water in vessel j determined with method A and with method B	‰
$\bar{\delta}_{A-B}$	Mean of differences in isotopic composition determined with method A and B	‰
$\bar{\delta}_{A,Bj}$	Mean of the δ-values obtained with methods A and B	‰

δ_{Bj}	Isotopic composition of soil water in vessel j determined with method B	‰
$\delta_{enriched\ water}$	Isotopic composition of enriched water	‰
$\delta_{extracted\ water}$	Isotopic composition of (pressure-)extracted water	‰
δ_{LW}	Isotopic composition of leaf water	‰
δ_{mix}	Isotopic composition of the mixture of tap water and isotopically enriched water in soil	‰
$\delta_{tap\ water}$	Isotopic composition of tap water	‰
δ_{Tr}	Isotopic composition of plant transpiration	‰
$\delta_{soil\ water}$	Isotopic composition of soil water	‰
δ-value	Water isotopic composition	‰
δ^2H	Relative ratio of ^{2}H to ^{1}H	‰
$\delta^{18}O$	Relative ratio of ^{18}O to ^{16}O	‰
$\bar{\delta}^2H$	Mean δ^2H	‰
$\bar{\delta}^{18}O$	Mean δ^{18}O	‰
Δ	Difference in isotopic composition to a reference	‰
θ	Volumetric soil water content	$cm^3\ cm^{-3}$
θ_{res}	Residual volumetric soil water content	$cm^3\ cm^{-3}$
θ_{sat}	Saturated volumetric soil water content	$cm^3\ cm^{-3}$
θ_z	Volumetric soil water content in soil layer z	$cm^3\ cm^{-3}$
ψ_l	Leaf water potential	MPa
$\psi_{l\ day}$	Leaf water potential during day (LED panel on)	MPa
$\psi_{l\ night}$	Leaf water potential during night (LED panel off)	MPa
$\psi_{soil\ \mathrm{eq}}$	Soil water potential sensed by the plant	MPa

Chapter 1

Introduction

1. Impact of extreme drought on grasslands

The term drought is heavy with meaning. It is used to refer to precipitation deficits (meteorological drought) or streamflow deficits (hydrological drought). If a causation dimension is considered, we have agricultural and ecological drought, defined as "period with abnormal soil moisture deficit, which results from combined shortage of precipitation and excess evapotranspiration (water flux from soil and vegetation as evaporation and plant transpiration, respectively), and during the growing season impinges on crop production or ecosystem function in general" (IPCC, 2021). In the efforts to predict and mitigate the detrimental effects of climate change, these last two definitions of drought have gained especial attention.

Since 1950, human-induced climate change has been the main driver of the increase in frequency and intensity of hot extremes. It has contributed to an increase in agricultural and ecological droughts – through increased land evapotranspiration – as well as in compound extreme events such as concurrent heatwaves and drought on the global scale (IPCC, 2021). The upward trend in frequency and intensity of ecological drought is especially worrying, since it "drives ecosystems beyond thresholds of vulnerability, impacts ecosystem services, and triggers feedbacks [sic] in natural and/or human systems" (Crausbay et al., 2017). Drought and heatwaves can affect directly the regional carbon cycle through alteration of the structure, composition, and function of ecosystems turning a particular area from a carbon sink into a source (Frank et al., 2015). Furthermore, land-atmosphere coupling (i.e., positive feedback between both high temperatures and precipitation deficits and soil moisture depletion) could intensify these climate-related extreme events (Bastos et al., 2013; Seneviratne et al., 2006). Drought effects in plant performance are evidenced in changes in their morphological, physiological, biochemical, and ecological traits (Seleiman et al., 2021) and this response to water deficits will depend on the drought intensity and duration and on the plants' growth stage, age, and species (Gray & Brady, 2016).

Vegetation may significantly influence the local climatic conditions (i.e., air humidity, temperature, rainfall, and wind) (Sheil, 2014) as well as the infiltration properties of the soil, especially in water limited ecosystems (Thompson et al., 2010). Therefore, the ecophysiological and hydrological processes at the plant-atmosphere and soil-plant interfaces have a preponderant role in ecosystem water cycling (Dubbert & Werner, 2019). Productivity in semi-arid and sub-humid regions, where ecosystems are dominated by herbaceous species (e.g., grasslands), depends strongly on water availability (i.e., from precipitation due to shallow rooting systems) (Knapp & Smith, 2001; Ponce Campos et al., 2013; Yang et al., 2016). In grasslands, adaptive plant physiological processes are set in motion during water scarcity to maintain ecosystem-level productivity (Jentsch et al., 2011).

Grasslands cover 40% of the terrestrial surface and are found in every continent. These biodiverse ecosystems provide forage for livestock and store large amounts of carbon in above- and below-ground biomass (White et al., 2000). On a regional scale, European temperate semi-natural grasslands host habitats with extreme species richness (e.g., up to 80 plant species per square meter; Biodiversity Information Sytem

for Europe, 2024), which has declined in the last decades due to land use change, invasive species, and pollution alongside climate change (IPBES, 2018). Allen et al. (2011) defined semi-natural grasslands as a "managed ecosystem dominated by indigenous or naturally occurring grasses and other herbaceous species". Most semi-natural grasslands originated from human activity, replacing forested areas at the beginning of the agriculture era (Hejcman et al., 2013). The projected rise of heatwaves, drought, and wildfires in Europe (Forzieri et al., 2016) and compounded detrimental effects (e.g., together with nutrient loading; Harpole et al., 2007; Kübert et al., 2019) will further contribute to biodiversity and service loss in these ecosystems.

In dry conditions, variations in evapotranspiration are not only linked to changes in precipitation patterns (Wever et al., 2002) but to the water use strategies of its plant community (Leitinger et al., 2015) dependent on species-specific strategies (Kübert et al., 2021). For example, a grass dominated plant community (poor in forb species) resulting from extreme drought at the beginning of a growing season is more vulnerable to a later summer drought, due to a lower ecosystem water use efficiency, weaker drought adaptations, and shallow rooting depths (Kübert et al., 2019; Stampfli et al., 2018; Zeiter et al., 2016). Thus, ecosystem productivity is affected on the short-term (above-ground dieback) (Kübert et al., 2019) and the long-term (reduced reproductive outcome) (Zeiter et al., 2016) turning a grassland from a carbon sink into a source (Kübert et al., 2019). Moreover, fertilization further promotes grass abundance and loss of species-richness, and even though it was linked to increased productivity by Harpole et al. (2007), they also linked it to earlier leaf senescence and Kübert et al. (2019) found that it increased ecosystem respiration probably via an increase in microbial decomposition in the soil. Species-rich grasslands are more resistant to and recover better from drought (Tilman & Downing, 1994; Tilman & El Haddi, 1992), for example, by allocating more carbon below-ground (Kahmen et al., 2005), preserving ecosystem productivity and functioning. Most importantly, water-use strategies of plant communities in grasslands could be used as "predictors" of the impacts of drought on resource cycling and maintenance of ecosystem services in grasslands (Leitinger et al., 2015).

Drought resistance of forbs positively influences that of plant biomass in grasslands (Mackie et al., 2019), enabled by their higher rooting depths (Craine et al., 2002), short-term water uptake dynamics (i.e., plasticity), and ability to maintain contact with dry soil by withstanding very low leaf water potential values (Kübert et al., 2021). The ecological adaptability of some native forb species in European semi-natural grasslands could be rooted in their genetic variability. For example, *Centaurea jacea* L. (brown knapweed) has many subspecies difficult to distinguish from each other. This ubiquitous perennial forb can be found in Europe, North Asia, and Northwest Africa, can grow up to 120 cm (Hegi, 1954) and its roots can reach a depth of over 2 m (Kutschera & Lichtenegger, 1992), potentially allowing it to extract water and nutrients from soil zones inaccessible to shallow-rooted species, like grasses. However, plant-level strategies of forbs might not be as effective in prolonged

extreme drought, especially when the described drought effects at the ecosystem-level reduce their abundance and survival.

A mechanistic understanding of the dynamic relationship between hydrological and biogeochemical processes (especially the less known ones below-ground; Kübert, 2019) in the soil-plant-atmosphere continuum is pursued (Dubbert, Piayda, et al., 2014; Newman et al., 2006). Because the links between biotic and abiotic phenomena control processes at the plant (e.g., plant water use), community (e.g., vegetation structure) and ecosystem level (e.g., water and carbon cycles and productivity). Such a mechanistic understanding would enable predictions of the response and resilience of ecosystems to climate change. This is pivotal for (semi-natural) grasslands due to their higher vulnerability as well as their societal and economic importance: they constitute around 30% of the agricultural land in Europe (Eurostat, 2022).

2. Water stable isotopic monitoring in ecohydrological studies

Investigating root water uptake (RWU) and plant transpiration patterns usually entails an ecohydrological exploration of the processes at the plant-atmosphere and soil-plant interfaces. The interplay between species-specific regulation of root conductivity and resource availability in the soil determine RWU patterns (e.g., Caldeira et al., 2014; Lobet et al., 2014), whereas the interplay between species-specific structural and functional water use strategies and atmospheric conditions determine plant transpiration (e.g., Blum, 2011; Dubbert & Werner, 2019). Measurable differences in the isotopic composition of water (i.e., ratio of the heavy, rare hydrogen or oxygen isotope to the light, common one – $^{2}H/^{1}H$ and $^{18}O/^{16}O$ – relative to the ratio in a standard in per mille: $\delta^{2}H$ and $\delta^{18}O$) in the different "compartments" of soil-plant-atmosphere the continuum (Fig. 1-1a) enable tracking of water movements (see section 3 in this chapter). The heterogeneous distribution of isotopes is due to physical or chemical processes and is referred to as isotopic fractionation. Insights into resource partitioning (Rothfuss et al., 2021) and plant competition (e.g., Meinzer et al., 1999), plant-mediated soil water redistribution (i.e., hydraulic lift; e.g., Meunier et al., 2017; Sun et al., 2014) and rooting depths and their role in water uptake dynamics (Beyer et al., 2016) have been possible with water stable isotopic analysis.

RWU is generally assumed a non-fractionating process (e.g., Thorburn et al., 1993; L. Zhao et al., 2016; Zimmermann et al., 1967). That is, the isotopic composition of the water entering the leaves (commonly computed from the isotopic composition of vapor transpired by the plant in steady-state) is assumed equal to that of xylem water and of the water mixture from the soil layers where the extraction took place. The contribution of the considered soil water sources to plant transpiration is commonly estimated with probabilistic multi-source linear mixing models (e.g., Asbjornsen et al., 2007; Prechsl et al., 2015; Volkmann et al., 2016a), like the one embedded in a Bayesian framework proposed by Parnell et al. (2010). Kühnhammer et al. (2020) list three conditions to improve the predictive power of these mixing models: steep and

monotonic soil water isotopic profiles (i.e., uniqueness of each sources' isotopic composition), decoupled information from the water isotopes, and elimination of soil sources based on water availability from an ecophysiological perspective. Attending to the last condition would be taking an ecohydrological approach to RWU quantification. That is, assessing the dynamics of both abiotic and biotic parameters. The first and second conditions in laboratory and field experiments can be realized with isotopic labelling: addition of water with different δ^2H or $\delta^{18}O$ than naturally occurring in soil water.

Observations of some studies of differences in δ^2H of soil water and xylem water have called into question the non-fractionation nature of RWU (e.g., Evaristo et al., 2017; Geris et al., 2015, 2017; Oerter & Bowen, 2019). This was first observed in xerophytic and halophytic species (Ellsworth & Williams, 2007; Lin & Sternberg, 1993) and attributed to a dominance of symplastic (i.e. through the cytoplasm) over apoplastic (i.e. through the cell walls) water transport. Because water aggregates dissociate into single molecules in the symplastic transport, isotopologue ($^1H_2{}^{16}O$, $^1H_2{}^{18}O$, $^1H^2H^{16}O$) discrimination (more apparent for $^1H^2H^{16}O$) occurs. Isotopic fractionation could even be taking place at the soil-root interface, where soil water vaporizes in air-filled soil pores and moves to the roots in the vapor phase (Allison & Hughes, 1983). This last phenomenon might be especially relevant in arid or semi-arid ecosystems. Furthermore, isotopic fractionation of soil water due to root decomposition (Allison et al., 1984) or the associated microbial activity (Poca et al., 2019) has also been described.

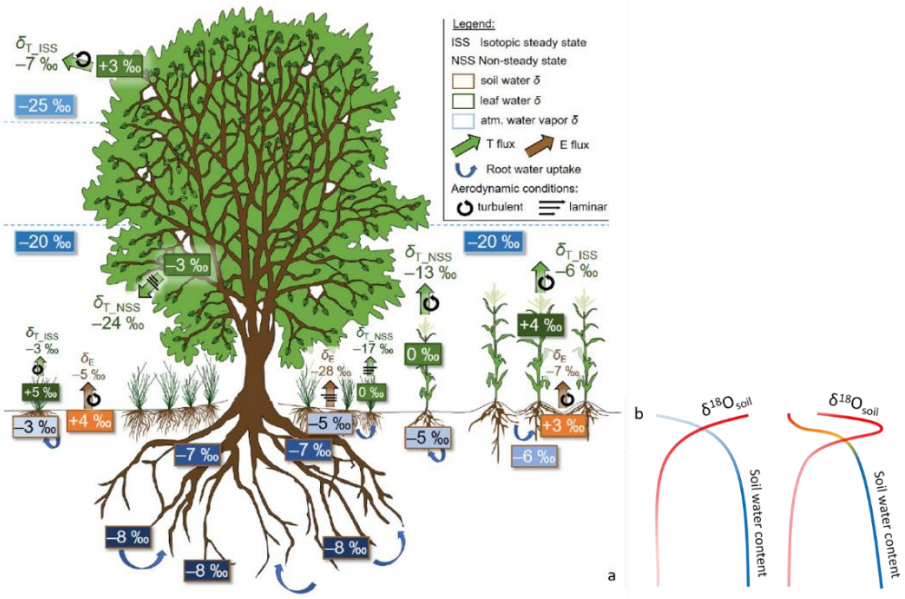

Figure 1-1: a) Schematic representation of water fluxes in the soil-plant-atmosphere continuum and approximated $\delta^{18}O$-values of the different compartments (Rothfuss et al., 2021) and b) $\delta^{18}O$ and soil water content vertical profile in the soil under saturated (left) and unsaturated conditions (right).

Moreover, deviations of the xylem isotopic composition from that of the source can happen inside the plant stem caused by mixing with storage water, which has been experimentally observed as well as modelled (Barbeta et al., 2020; Bariac et al., 1989; Knighton et al., 2020). Alternatively, these deviations can be explained by a water transport delay between the root system and sampling point in the stem (Gaines et al., 2016; Marshall et al., 2020; Meinzer et al., 2006; Mennekes et al., 2021), which is commonly not accounted for in multi-source mixing models. Finally, heterogeneities in soil water isotopic composition at the soil-pore scale emerge from (complex) interactions between water and soil when the former permeates the latter.

The aforementioned processes introduce biases and uncertainties to probabilistic isotope-based RWU quantification, already challenging due to the temporal and spatial variations of RWU (Rothfuss & Javaux, 2017), a situation occasionally leading to reductive associations of RWU distribution to root density and water availability profiles (Schymanski et al., 2008; Varado et al., 2006). Moreover, low spatio-temporal resolution and representativeness of established isotopic methodologies result in further estimation biases and uncertainties.

In the liquid phase, water isotopic fractionation has been mainly attributed to salinity and to contact with surfaces, not to transfer characteristics, as is the case in the gaseous phase. The fractionating processes related to salinity (e.g., Burgess, 1978; Michot et al., 2002; O'Neil & Truesdell, 1991; Phillips & Bentley, 1987; Sofer & Gat, 1972) or confinement in small pores (e.g., Chen et al., 2016; Hillel, 2003; Lin & Horita, 2016; Richard et al., 2007) in controlled experimental settings are well understood. However, there is no consensus yet on the overall or compounded fractionating effect in the soil (potentially traced back to texture, moisture, and moisture history) or how to systematically account for it. Based on the observations in several studies of soil-texture- and water-content-related fractionating effects on soil water, defined co-existing but rather isolated "water pools" in the soil with distinct isotopic compositions has been theorized. These are "mobile water", which is easily extractable, and "bound water", which remains in the soil at high water tensions and is not easily extractable (e.g., Sprenger et al., 2018).

The isotopic-centric mobile and immobile water separation in some studies overlooks exchange phenomena between these water pools or defines them solely based on the extraction capabilities of destructive isotopic techniques or of vegetation (e.g., Brooks et al., 2010; Evaristo et al., 2015; McDonnell, 2014) not entirely corresponding to the view in soil physics. The mobile-immobile axe in soil physics is based on differences in flow velocity in the two pore systems in structured soils resulting in a stagnant water fraction that however exchanges in the liquid and vapor phase with the mobile fraction (De Smedt & Wierenga, 1979; Gaudet et al., 1977; Gerke & van Genuchten, 1993). The isotopic exchanges between mobile and immobile water have been observed (e.g., Vargas et al., 2017) and modelled (Sprenger et al., 2018). Even with exchanges, the presence of isotopic heterogeneities at the pore-scale of soil water make the investigation of the overall fractionating effect of a particular soil with a particular isotopic technique a prerequisite for probabilistic isotope-based RWU quantification.

Another significant challenge resulting in biases and uncertainties in isotopic determinations is of a methodological nature. Most established isotopic techniques rely on offline measurement and destructive sampling, during which soil or plant water evaporation or incomplete water extraction negatively impact the accuracy of the determinations, leading ultimately to over- or underestimations of water uptake (e.g., Beyer & Penna, 2021; Duvert et al., 2022; He et al., 2023; Santos Pires et al., 2022; Zuecco et al., 2022). Through a comparison of the most commonly used lab-based water extraction methodologies Orlowski, Pratt, et al. (2016) found that the measured isotopic composition of extracted water from methods involving significant phase changes or distillation processes (i.e., cryogenic vacuum extraction, microwave extraction, and direct vapor equilibration) was not the same as the isotopic composition of the reference water. Moreover, they observed that soil type had a direct effect on distillation processes, whereas mechanical processes rendered comparable results. Gilg et al. (2004) also reported a lower fractionation effect from physical techniques of water extraction (e.g., ultracentrifugation and high pressure squeezing) but noted that these techniques may not allow a complete water extraction. Hence, standardization of isotopic techniques to overcome these methodological constraints has gained attention in later years (e.g., Ceperley et al., 2024). Finally, temporal heterogeneities in the studied systems might be difficult to capture with destructive techniques (Beyer & Penna, 2021).

Several studies have used in situ "non-destructive" continuous water stable isotopic monitoring in soil and vegetation in laboratory and field experiments (Beyer et al., 2020; Kühnhammer et al., 2022; Oerter et al., 2017; Rothfuss et al., 2013, 2015; Volkmann, Kühnhammer, et al., 2016; Volkmann & Weiler, 2014), sometimes in combination with "destructive" methods. Non-destructive isotopic soil water monitoring not only allows for isotopic measurements at a higher temporal resolution while removing the influence of lateral variability, it possibly accounts better for potential soil-related isotopic fractionation. In this novel technique soil water vapor in equilibrium with soil liquid water diffuses into a gas-permeable (polypropylene) tubing, is carried in a stream of dry air and its isotopic composition is determined online with laser-based spectroscopy (Fig. 1-2). The isotopic composition of soil water is computed from the isotopic composition of the sampled water vapor and the soil temperature at the respective sampling location. This continuous measurement of water vapor has also been used to determine directly the isotopic composition of plant transpiration (Dubbert, Cuntz, et al., 2014; Wang et al., 2012). Rothfuss et al. (2013, 2015) concluded after a thorough testing and calibration, that the setup displayed in Fig. 1-2 can be used in saturated and unsaturated soils, that it can perform at any level of water vapor mixing ratios of the sampling stream and that it can also be used in the field and laboratory at different depths of a soil profile.

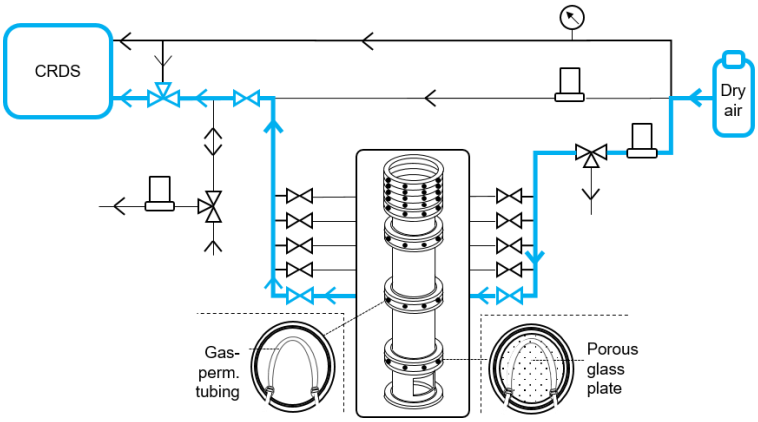

Figure 1-2: Diagram of the laboratory setup for the in situ non-destructive isotopic monitoring method. The blue line shows the sampling process of soil water vapor with dry air at different depths and the determination of its isotopic composition in a cavity ring-down spectrometer (CRDS), a type of laser-based spectrometer. Image modified from Rothfuss et al. (2015).

3. Isotopic terminology and fractionating processes in soil and plant water

The stable isotopic composition in water is expressed by convention and in order to produce comparable results in (eco)hydrological studies as the difference of the ratios (R) of the heavy, rare isotope to the light, common one (i.e. $^{18}O/^{16}O$ and $^{2}H/^{1}H$) in a water sample and a standard relative to the ratio in the standard (Eq. 1-1). This relative difference, referred to as delta value (δ-value) (Gat & Gonfiantini, 1981), is normally small and so, it is expressed in per mille (‰).

$$\delta = \frac{R_{sample} - R_{standard}}{R_{standard}} = \frac{R_{sample}}{R_{standard}} - 1$$

Equation 1-1

The international standard in water stable isotopic monitoring is the second sample of the Vienna Standard Mean Ocean Water (V-SMOW2) prepared in the International Atomic Energy Agency (IAEA) in 2006. The isotopic composition of V-SMOW2 is similar to that of the original sample, prepared in 1966 by Prof. H. Craig of the University of California also commissioned by the IAEA. Two other important international standards are the Standard Light Antarctic Precipitation 2 (SLAP2) and Greenland Summit Precipitation (GRESP) (Gat & Gonfiantini, 1981; IAEA, 2019). Samples with a greater $\delta^{2}H$ or $\delta^{18}O$ relative to other samples are considered "enriched" in the respective heavy isotope, whereas samples with a lower $\delta^{2}H$ or $\delta^{18}O$ are considered "depleted" in the heavy isotope.

Oxygen or hydrogen isotopic substitution in the water molecule causes the properties controlled by molecular mass (e.g., specific gravity and molecular

diffusivity) to differ among isotopologues. These differences in physical properties lead to discrimination against the heavier isotopologues during phase changes and this results in their heterogeneous distribution, a process called isotopic fractionation (Gat & Gonfiantini, 1981). When fractionation occurs due to the difference in saturated vapor pressures of water isotopologues, we are referring to equilibrium fractionation. Kinetic fractionation is caused by the difference in diffusivities of the isotopologues in the gaseous phase (Mathieu & Bariac, 1996).

Craig & Gordon (1965) proposed a model for calculating the isotopic composition of evaporation from a free water surface, which was later adapted for evaporating water in the soil and plant leaves. Their model proposes a gas-liquid interface over the surface of a water body where evaporation and equilibrium fractionation occur. Over (gas phase) and under (liquid phase) this interface are two discrete laminar layers where molecular diffusion of water is the dominant transport mechanism and kinetic fractionation occurs (calculations by Merlivat & Coantic (1975) validated the existence of the discrete gaseous layer above the interface). Eddy diffusion or turbulent transport to the atmosphere dominates beyond the upper gaseous discrete laminar layer, where no further fractionation occurs.

In the Craig & Gordon model, the isotopic composition of evaporated water is a function of the isotope ratio at the interface, of the isotope ratio of ambient water vapor, of kinetic and equilibrium fractionation factors (α_k and α_{eq}, respectively), and of relative humidity normalized to the temperature at the evaporating site (Dubbert, Piayda, et al., 2014). α_{eq} is temperature-dependent and the equations of this dependency have been experimentally tested (Horita & Wesolowski, 1994; Majoube, 1971). α_k is assumed equal to the ratio of the molecular diffusivities of the light and heavy isotopic species elevated to a factor n describing the nature of the transport through the layer above the evaporating surface (i.e., $0.5 \leq n \leq 1$ with $n = 1$ for fully molecular diffusion and $n = 0.5$ for fully turbulent conditions) (Ehhalt & Knott, 1965; Merlivat, 1978; Münnich et al., 1978).

The linear correlation between δ^2H and $\delta^{18}O$ in meteoric waters (i.e., rivers, lakes, rain, and snow) not having undergone evaporation ($\delta^2H = 8 \cdot \delta^{18}O + 10$), referred to as Global Meteoric Water Line (GMWL) (Craig, 1961), is the result of a single fractionation source: condensation of atmospheric water vapor. Thus, a change in the slope of this linear correlation (i.e., different from 8) is an indication of the existence of additional kinetic effects (Mathieu & Bariac, 1996). For example, when evaporation dominates the isotopic relationship the slope ranges between ~2 and 5 (Craig, 1961; Rothfuss et al., 2015).

Zimmermann et al. (1967) applied successfully Craig & Gordon's model to describe the isotopic profile in the saturated zone in steady-state in a drying sand column and this approach was later adapted for an unsaturated soil in steady-state isothermal and non-isothermal conditions (Barnes & Allison, 1983, 1984). A modification for the parameter n (now nk) to account for an additional diffusive component in the dry zone below the soil surface added to the total atmospheric resistance was proposed by Mathieu & Bariac (1996). Under saturated conditions, the isotopic transfer is

controlled by the atmosphere ($nk = 0.5$), whereas, under unsaturated conditions, the transfer is soil-controlled (i.e., dominated by molecular diffusion through the dry layer with $nk = 1$). Under saturated conditions, there is a maximum isotopic enrichment at the soil surface and an exponential decrease of both δ^2H and $\delta^{18}O$ with increasing soil depth (left side of Fig. 1-1b). Under unsaturated conditions, the isotopic composition at the soil surface is that of the atmospheric water vapor and it increases exponentially to a maximum a few centimeters under the soil surface. Beyond this point of maximum enrichment or of maximum change in isotopic composition relative to a close point in the soil profile (i.e., $d(\delta)/dz$; Rothfuss et al., 2015) (i.e., evaporating front), δ^2H and $\delta^{18}O$ decrease with increasing depth (right side of Fig. 1-1b).

The model of Craig & Gordon has also been used to estimate the isotopic composition of leaf water. It seemed to overestimate δ^2H and $\delta^{18}O$ of leaf water, probably because experimentally extracted and analyzed leaf water is a mixture of isotopically distinct pools inside the leaf and the modelled values are of the "evaporating pool" (Dongmann et al., 1974; Leaney et al., 1985; Yakir et al., 1989). In this regard, the model of Farquhar & Lloyd (1993), considering a continuous isotopic gradient inside the leaf, has been deemed a more realistic approach by Yakir & Sternberg (2000). In this model, the isotopic composition of leaf water is expressed as a function of the isotopic composition of the water entering the plant, of the isotopic composition of leaf water at steady-state, and of the ratio between the rate of advection and diffusion of leaf water (i.e., Péclet number). Despite water isotopic fractionation taking place in the leaf, the isotopic composition of plant transpiration (water vapor) at steady-state equals that of the water entering the leaves, in the plant xylem, and the mix taken up by the plant across the soil profile. This is why, by measuring the isotopic composition of plant transpiration in steady-state, it is possible to estimate indirectly the isotopic composition of xylem water and quantify RWU, assuming no fractionation happens during water uptake or transport by the roots (see section 2 in this chapter).

4. Probabilistic and physically-based root water uptake quantification

Water flow at the soil-plant interface of the continuum is described as a response to a negative gradient of water potential through a network of hydraulic resistances (Van Den Honert, 1948) (usually) from the bulk soil into the roots and reaching the leaves. Flow from the roots into the soil, referred to as "hydraulic lift" or plant-mediated water redistribution, is also possible, if the water potential outside the roots is lower than inside (i.e., if the soil is dry).

Hydraulic conductivity in the soil depends on soil texture and saturation state (Mualem, 1976; van Genuchten, 1980). Hydraulic conductivity inside the plant depends on numerous factors with rather complex interdependencies responding to biotic (e.g., hormones) and abiotic (e.g., water stress, nutrient deficiency or day-night cycles) stimuli (Tardieu et al., 2011) conferring the plant plasticity, especially in challenging environmental conditions. Aquaporin regulation seems to play a

significant role in short-term changes in root hydraulic conductivity (e.g., Javot & Maurel, 2002). Plant conductivity changes through stomatal aperture or closure wich seems to response to both chemical and hydraulic signaling from the root system (e.g., Christmann et al., 2007). Furthermore, vegetation can modify the hydraulic conductivity of the soil near the roots (i.e., inside the rhizosphere) via exudation of mucilage to hydraulically isolate sections of the root system or keep contact with dry soil (Carminati et al., 2016; Carminati & Vetterlein, 2013). Finally, the facilitating role of root hairs and mycorrhizal fungi for water and nutrient uptake is less understood (M. F. Allen, 2007; Vetterlein et al., 2022). Still, effects of root traits or even hydraulic properties on resource uptake and conflicting resource use strategies (e.g., water vs. nutrient uptake) are rarely considered in water and heat transfer models, commonly used in hydrological studies, or broader models coupling water, nutrient, and carbon cycling, commonly used in plant or ecosystem ecology (Dubbert et al., 2023).

The dependency of RWU along a root on radial and axial resistances (the former due to transport trough the root wall and the latter, through the xylem) and their spatio-temporal dynamics was first mathematically described by Landsberg & Fowkes (1978). Since then, several microscopic (3D) models quantifying RWU from the root system architecture accounting for root hydraulic properties or root hydraulic architecture (Couvreur et al., 2012; Doussan et al., 2006; Draye et al., 2010; Javaux et al., 2008; Schröder et al., 2009) and their upscaled macroscopic (1D) versions have also contributed to the mechanistic understanding of soil-root interactions. The advantage of 1D models over 3D ones is that they are less computationally costly and require only average estimates of radial and axial root conductivities along a soil profile. The latter is relevant, since both radial and axial conductivities are dependent not only on plant physiology but on environmental factors (Bouda et al., 2018; Vetterlein & Doussan, 2016). Accordingly, the estimation of a root system hydraulic conductance (K_{rs}), a whole-root system parameter dependent not only on root hydraulic properties but also on those of the soil, is required in these mechanistic physically-based models.

In later years, the spatio-temporal dynamics of water potential near the roots have been investigated with both micro- and macroscopic mechanistic approaches. A steep soil water tension gradient near the root surface appears in drying soils limiting RWU and its caused by the non-linear relationship between the resistance to water flow in the soil-root interface and soil hydraulic conductivity (e.g., Schröder et al., 2008; Vanderborght et al., 2023). The effect of this emerging resistance in a plant's response to water stress (e.g., stomatal closure or mucilage secretion) is now subject of intense investigation.

Improving the accuracy, precision, and reproducibility of isotopic techniques, especially the destructive ones, would further contribute to the understanding of the interactions in the soil-plant-atmosphere continuum underlying water, nutrient and carbon cycling. Additionally, it would increase the predictive power of existing isotope-enabled process-based soil-vegetation-atmosphere transfer models, like

SiSPAT-Isotope from Braud et al. (2005) or HYDRUS as used by Zhou et al. (2021) and Schneider et al. (2024).

Moreover, integration of probabilistic isotope-based mixing models and deterministic physically-based transfer models – e.g., R-SWMS (Javaux et al., 2008), the implicit model of the root system hydraulic architecture of Couvreur et al., (2012) or the one of Meunier, Couvreur, et al. (2017) – could also enable more realistic insights into water use and drought resistance strategies from the single plant to the community scale. Water sources in probabilistic mixing models are already excluded from the analysis in some studies based on soil-plant hydraulic properties and interesting novel approaches of "full integration" are available: the probabilistic (Bayesian) hydrodynamic approach incorporating advection-diffusion modelling of water isotopologues of De Deurwaerder et al. (2021) or the process-based mixing model of Ogle et al. (2014). In these novel isotope-enabled physically-based approaches, additional data (such as root traits or environmental covariates) could be incorporated, allowing for a holistic mechanistic understanding of the processes underlying water, carbon, and nutrient cycling (Dubbert et al., 2023; Ogle et al., 2014), as well as predictions on potential interactions between these cycles and extreme weather events.

5. Main and specific objectives of the thesis

The doctoral project described here was part of the research program "Assessing ecohydrological responses from single plant to community scale using a stable isotope approach" (RO-5421/1-1 and DU-1688/1-1) aiming at quantifying ecohydrological responses of a grassland ecosystem to extreme drought from single plant to community scale. This program also sought to further a mechanistic understanding of the link between ecohydrology on the one hand and plant community structural responses on the other. The ecohydrological assessment (response to drought and nitrogen loading) at the community scale was addressed in a series of experiments in a semi-natural temperate grassland in the vicinity of the University of Freiburg in the southwest of Germany (Kübert et al., 2019, 2020, 2021).

The main objective of this doctoral project was to:

Assess the ecohydrological response to drought of the forb species Centaurea jacea L. at the single plant scale in controlled laboratory conditions.

The forb species was selected, and not one of the grass species also present in the studied temperate grassland by Kübert et al. (2019, 2020, 2021), because of the observed replacement of this species by grasses in the field experiments and its positive and significant role in the drought response of the temperate grassland (see section 1 in this chapter).

The ecohydrological assessment at the plant scale was to be pursued via continuous non-destructive monitoring of plant physiology and of water stable isotopes in the soil (via the in situ online method; Rothfuss et al., 2013, 2015) and of plant transpiration. Thus, potential soil-mediated fractionating processes (i.e., caused by the soil matrix or soil water tension) influencing the accuracy and precision of soil water isotopic determinations via the in situ online method had to be quantified, to ensure reliable

isotope-based estimations of RWU (see section 2 in this chapter) from these isotopic determinations in wet and dry soil. Additionally, we aimed at designing a methodological framework enabling testing and cross-comparing a range of destructive and non-destructive isotopic techniques to quantify inaccuracies and uncertainties in the determinations (see section 2 in this chapter). Could potential changes in soil water isotopic composition be traced back to soil texture or saturation? Thus, the first specific objective and corresponding hypothesis were:

O.1. Determine the fractionating effect of soil texture and soil water tension on the measured values of soil water isotopic composition using destructive and in situ online isotopic monitoring.

H.1. No dependency of soil water isotopic composition to soil tension or soil texture is observed when using a range of destructive and in situ online isotopic techniques.

The specific question in the ecohydrological assessment of the response to drought of a single plant individual of the species *Centaurea jacea* L. was: how do the water extraction patterns of *Centaurea jacea* L. change in dry conditions compared to those in wet conditions? The second specific objective and corresponding hypothesis were:

O.2. Assess the ecohydrological response of Centaurea jacea L. to drought in controlled laboratory conditions at the single plant scale with an isotopic approach.

H.2. Centaurea jacea L. displays efficient water use in dry conditions and dynamic water extraction patterns (i.e., plasticity).

Finally, we aimed at broadening our insight into the biotic and abiotic interactions at the soil-plant interface and at the single plant scale by comparing the probabilistic isotope-based RWU quantification to a hydraulic modeling approach (see section 4 in this chapter). Would the simulated RWU patterns be different if we consider the influence of soil and root hydraulic properties? The third specific objective and corresponding hypothesis were:

O.3. Describe the interplay between soil-root and plant-atmosphere processes in Centaurea jacea L. from a hydraulic perspective during drought and compare probabilistic and physically-based modelled RWU patterns.

H.3. Decreases in hydraulic conductance at the soil-root interface and in the leaves are linked, causing changes in RWU patterns likely not observed in an probabilistic isotope-based framework.

To achieve O.1 (test H.1), a comparison of soil water isotopic monitoring methods was conducted in custom-made acrylic vessels using quartz sand and a loamy sand. Measurements from the in situ non-destructive online method described and standardized by Rothfuss et al. (2013, 2015) were compared against those of three offline, punctual, destructive methodologies – direct water vapor equilibration, centrifugation and cryogenic vacuum distillation – and one offline, non-destructive pressure-mediated water extraction method. This published study is presented (with some modifications) in chapter 2.

Deseano Diaz, P., Nong, T., Brüggemann, N., Dubbert, M., Javaux, M., Orlowski, N., Vereecken, H., & Rothfuss, Y. (2023). Insights into tension-mediated and antecedent water effects on soil water isotopic composition. *Vadose Zone Journal*, *22*(6), 1–19. https://doi.org/10.1002/vzj2.20288

To achieve O.2 (test H.2), plant physiological parameters (i.e., root density, leaf water potential, canopy conductance, water use efficiency, and CO_2 assimilation) and above- and below-ground environmental conditions (i.e., temperature, relative humidity, and soil water content) were monitored under varying hydroclimatic conditions. Daily RWU profiles were estimated with soil water and plant transpiration isotopic determinations using the multi-source mixing model embedded in a Bayesian statistical framework of Parnell et al. (2010), Stable Isotope Analysis with R (SIAR). This published study is presented (with some modifications) in chapter 3.

Deseano Diaz, P., van Dusschoten, D., Kübert, A., Brüggemann, N., Javaux, M., Merz, S., Vanderborght, J., Vereecken, H., Dubbert, M., & Rothfuss, Y. (2023). Response of a grassland species to dry environmental conditions from water stable isotopic monitoring: no evident shift in root water uptake to wetter soil layers. *Plant and Soil*, *482*(1–2), 491–512. https://doi.org/10.1007/s11104-022-05703-y

In this second study the improvement and extension of the system described in Kühnhammer et al. (2020) for semi-automated plant physiology and environmental measurements under controlled laboratory conditions (Fig. 1-3) allowed measurements with an increased spatio-temporal resolution. The isotopic determinations of soil water vapor at different soil depths and of plant transpiration were done using a setup consisting of a custom-made acrylic column incorporating gas-permeable tubing and a custom-made acrylic chamber enclosing the plant, both connected to a cavity ring-down spectrometer. Daily flux and isotopic measurements were conducted under constant air temperature and humidity in a climate chamber. Root density could also be monitored in a non-destructive manner with magnetic resonance imaging (MRI) at different developmental stages in several plant individuals.

To achieve O.3 (test H.3), we used the 1D mechanistic hydraulic model of Vanderborght et al. (2021, 2023) to estimate the hydraulic parameters (i.e., root system hydraulic conductance, standard sink fraction, and soil water potential at the soil-root interface) of *Centaurea jacea* L. during the drought experiment done in the second study and detailed in chapter 3. Additionally, RWU patterns were estimated with this physically-based approach and compared to the profiles obtained with the probabilistic isotope-based approach described also in chapter 3. This unpublished study is described in chapter 4.

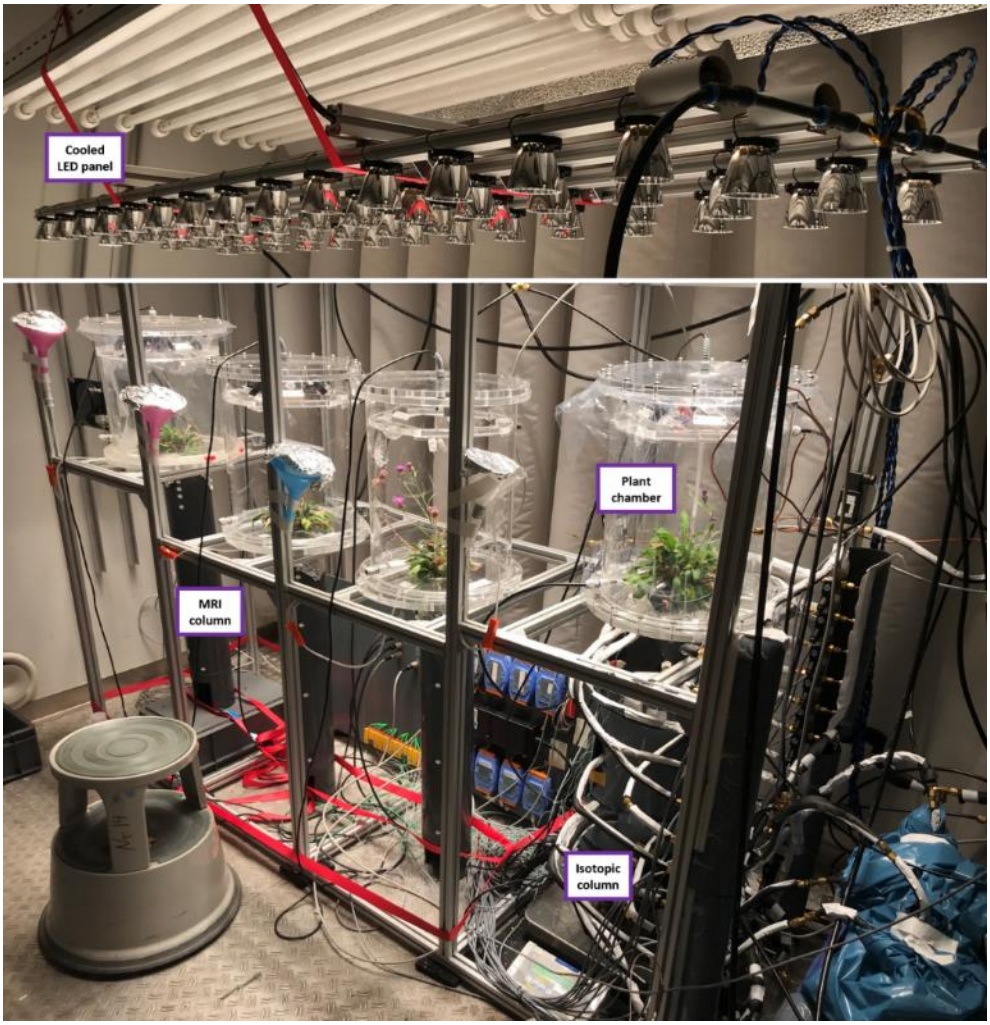

Figure 1-3 : Experimental setup for the semi-automated monitoring of plant physiological and environmental (above- and below-ground) parameters in a climate chamber under fully controlled laboratory conditions.

6. Author contributions

Youri Rothfuss (YR) and Maren Dubbert (MD) acquired the funding for and administrated the research program, in which this doctoral project was embedded. YR, MD, Mathieu Javaux (MJ), and Nicolas Brüggemann (NB) provided continuous supervision and support to the doctoral candidate, author of this thesis (PDD) in all research and administrative tasks. Additionally, MJ, Sarah Garré (SG), Jean-Thomas Cornelis (JTC), and Bernard Longdoz (BL) in their role as members of the thesis committee and Harry Vereecken (HV) and Jan Vanderborght (JV) in their role as institute directors in the research center where the project was done supervised yearly

the progress of the doctoral project. They provided written and verbal feedback on the reports and presentations prepared by PDD.

For the study described in chapter 2, YR, Thai Nong (TN), and PDD planned and designed the experiments. PDD and TN conducted the experiments and collected the laboratory data. MD, Natalie Orlowski (NO), YR, and PDD discussed and analyzed the data, as well as its visualization. PDD wrote the original manuscript and HV, MD, MJ, NB, NO, and YR reviewed and edited the manuscript.

For the study described in chapter 3, YR, MD, MJ, NB, Dagmar van Dusschoten (DvD), Steffen Merz (SM), and PDD planned and designed the experiment. DvD, SM, and YR designed the components of the setup. PDD and DvD constructed and assembled some of them. DvD, YR, and PDD conducted the experiment and collected the laboratory data. Angelika Kübert (AK), MD, YR, and PDD analyzed the data and prepared its visualization. AK, DvD, MD, NB, JV, and YR helped with data interpretation. PDD wrote the original manuscript and YR, MD, MJ, NB, DvD, SM, HV, AK, and JV reviewed and edited the manuscript.

For the study described in chapter 4, Valentin Couvreur (VC), JV, MJ, YR, and PDD contributed to conceptualization, methodology, and formal analysis. YR and PDD worked out the visualization of the results. PDD wrote the manuscript and VC, JV, MJ, and YR reviewed and edited the manuscript.

Chapter 2

Insights into tension-mediated and antecedent water effects on soil water isotopic composition

In this chapter, a slightly modified version of the study of Deseano Diaz et al. (2023) on potential soil-mediated isotopic fractionation is included. As stated in chapter 1 section 5, the objective of this first study (O.1) was to determine the fractionating effect of soil texture and soil water tension on the measured values of soil water isotopic composition using destructive and in situ online isotopic monitoring. This potential soil-mediated isotopic fractionation, observed and described in other studies (see chapter 1 section 2), would result in inaccuracies and uncertainties in soil water isotopic determination and in the probabilistic isotope-based RWU quantification we conducted in the second study (chapter 3). The results in this first study helped determine if further corrections to the estimations of soil water δ-values via the in situ online method described by Rothfuss et al. (2013, 2015) with a loamy sand had to be implemented.

Section 1 contains a short overview of the increasing evidence of methodological issues in established destructive isotopic techniques mainly observed in "spike experiments", as well as the influence of soil texture, soil water tension, and mixing of newly added and precedent water on soil water δ-values.

Section 2 contains a detailed description of the methodological framework used to compare soil water δ-values in two chemically inert soils, quartz sand and a loamy sand, contained in custom-made acrylic vessels. δ-values of soil water determined offline from samples extracted under pressure, via cryogenic vacuum distillation, centrifugation, and direct water vapor equilibration, and online via the in situ method (Rothfuss et al., 2013, 2015) were compared.

Based on the results and discussion in section 3 and the conclusions in section 4, H.1 was partially rejected: no dependency of soil water δ-values to soil texture was observed but a dependency to soil tension was observed. Nevertheless, methodological issues (i.e., evaporative enrichment) in our experiments and intrinsic to the destructive methods caused this apparent soil tension dependency. Consequently, no further corrections of the estimations of soil water δ-values via the in situ online method in the loamy sand had to be implemented. An improved version of our experimental setup, eliminating the interference of evaporative enrichment, could assist in future comparisons of isotopic techniques or investigations of soil-mediated fractionation. However, it is more suited to make a reference to the thorough and collaborative analysis in Ceperley et al., (2024) to achieve standardization of water stable isotopic monitoring overarching "experimental design and isotopic analysis to minimize biased estimates of the relative contribution of different water sources to plant water uptake".

1. Introduction

Using the hydrogen and oxygen isotopic composition (δ^2H and $\delta^{18}O$) of soil water to determine the spatial distribution of vegetation water use relies on a series of important assumptions (Rothfuss & Javaux, 2017) and is affected by non-negligible uncertainties (Millar et al., 2022). One of the main sources of uncertainties when quantifying spatio-temporal patterns of water use by comparing the isotopic composition of soil and xylem water is associated with the step of water extraction. This is typically done retrospectively in the laboratory using a range of methods including cryogenic vacuum extraction (Orlowski et al., 2013), centrifugation (Walker et al., 1994), or direct water vapor equilibration (Wassenaar et al., 2008). The isotopic composition of soil water may not be conserved during extraction because of, e.g., an incomplete water recovery or occurrence of disequilibrium phase change (evaporation). One of the most popular experiments to identify and quantify the uncertainty associated with one particular water extraction method are so-called "spike experiments". These experiments consist of adding water of known isotopic composition (i.e., spike water) to a dry soil sample, extract water from the sample using one of the aforementioned methods, and analyze its isotopic composition to determine if it is conserved, i.e., if it is equal to that of the spike water.

In the majority of the methodologically diverse spike experiments – the study of Goebel & Lascano (2012) being an exception – the isotopic composition of extracted soil water differs from the isotopic composition of the spike water (e.g., Bowers et al., 2020; Figueroa-Johnson et al., 2007; Newberry, Nelson, et al., 2017; Orlowski et al., 2013; Orlowski, Pratt, et al., 2016; Thielemann et al., 2019; Walker et al., 1994). Even small amounts of residual soil water – very difficult to eliminate, likely heavily fractionated and therefore isotopically different from the spike water – potentially mix with the newly added water, resulting in an observed isotopic mismatch (e.g., Thielemann et al., 2019; Wen et al., 2021), or as Newberry, Prechsi, et al. (2017) called it, an "isotopic memory effect".

Partly as a result of this observation, some have investigated the mixing of and equilibrium time between isotopically distinct soil water pools that may co-occur in the soil (e.g., Sprenger et al., 2018) held at different tension values (e.g., Gaj & McDonnell, 2019; Orlowski & Breuer, 2020). In structured soil, it has been shown that water fluxes could be conceptualized as flow in and between two fractions of water: an immobile one located in finer pores within aggregates, having a significantly lower velocity than the other, and the mobile pool in larger pores between aggregates (De Smedt & Wierenga, 1979; Gaudet et al., 1977; Gerke & van Genuchten, 1993). More recently, researchers using water stable isotopes have proposed this concept as a mechanism for preferential flow at larger scales (on the watershed and global scale, e.g., Bowling et al., 2017; Brooks et al., 2010; Evaristo et al., 2015). The spatially heterogeneous distribution of soil water isotopic composition has been explicitly linked to the "moisture history" (Newberry, Prechsi, et al., 2017), that is, the contribution of "new" and "old" water (i.e., antecedent) to the mobile and immobile water pools. In addition to the effect of an incomplete mixing of water within the soil

pore space, the nature of soil particles and the chemical properties of the liquid phase may result in isotopic fractionation and lead to a heterogeneous distribution of the isotopic composition of soil water at the pore scale (e.g., Meißner et al., 2014; Orlowski, Breuer, et al., 2016; Richard et al., 2007).

Describing mixing or fractionating processes in the soil is a prerequisite for quantification of root water uptake using water stable isotopic monitoring. Nevertheless, the above-mentioned methodological uncertainties make the interpretation of the results of experiments, aiming at determining soil-related fractionating effects, challenging. If water isotopic fractionation is observed, is it a result of the extraction technique or can it be traced undoubtedly to soil physicochemical properties and processes that should be considered in root water uptake quantification studies?

Our research questions were: i) how well does antecedent and newly added water mix within a soil sample?; ii) excluding soil-chemistry-related processes, is the isotopic composition of soil water mainly a function of soil water tension?; and iii) does the isotopic composition of extracted soil water match that of spike water? Our null hypotheses were: a) two isotopically distinct water sources successively added to an isotopically inert soil (i.e., a soil, the properties of which do not lead to any quantifiable isotopic effect on pore space water) mix completely; b) the isotopic composition of extracted soil water is independent from soil water tension in that same inert soil and equals that of the added (spike) water; and c) the isotopic composition of water extracted using a range of techniques is comparable (i.e., the differences observed are < 1‰ in δ^2H and < 0.5‰ in $\delta^{18}O$).

To test null hypothesis a), we compared the measured isotopic composition of soil water in a pure quartz sand after two successive saturation-desaturation cycles (one with deionized tap water and one with isotopically enriched water) with the theoretical value of perfectly mixed soil water. To test null hypothesis b), we compared the isotopic composition of soil water in a standard soil classified as a loamy sand near saturation, at pF ≈ 1.8, and near residual water content (pF = 3) with the isotopic composition of the added water. Finally, to test null hypothesis c), we compared the isotopic composition of soil water recovered with four methods: cryogenic vacuum distillation, centrifugation, direct water vapor equilibration, and a non-destructive in situ online method (Rothfuss et al., 2013), which is similar in its prerequisites and assumptions to the direct water vapor equilibration method.

2. Materials and Methods

The experiments were conducted in custom-made acrylic glass vessels (Fig. 2-1a) (301.6 cm^3 inner volume), each consisting of one upper and one lower part attached together. The upper part, in which the soil was placed, was equipped with two 1/8 inch openings, one inlet and one outlet, both connected to a 19 cm-long piece of gas-permeable polypropylene tubing (0.155 cm wall thickness, 0.55 cm i.d., 0.86 cm o.d., 0.2 μm pore size; Katmaj Filtration, Poland) for the sampling of the soil water vapor. The lower part of the vessel included a membrane of regenerated cellulose (diameter = 33.02 cm; pore size = 24 Å; Soilmoisture Equipment Corp., USA) supported by a

stainless steel mesh. Underneath the steel mesh, a hollow space connected to one stainless steel outlet was designed to collect liquid soil water. In the center of the vessel lid, a 1/8 inch opening allowed the soil pore air to exit the vessel during the saturation with water through the membrane (Fig. 2-1a).

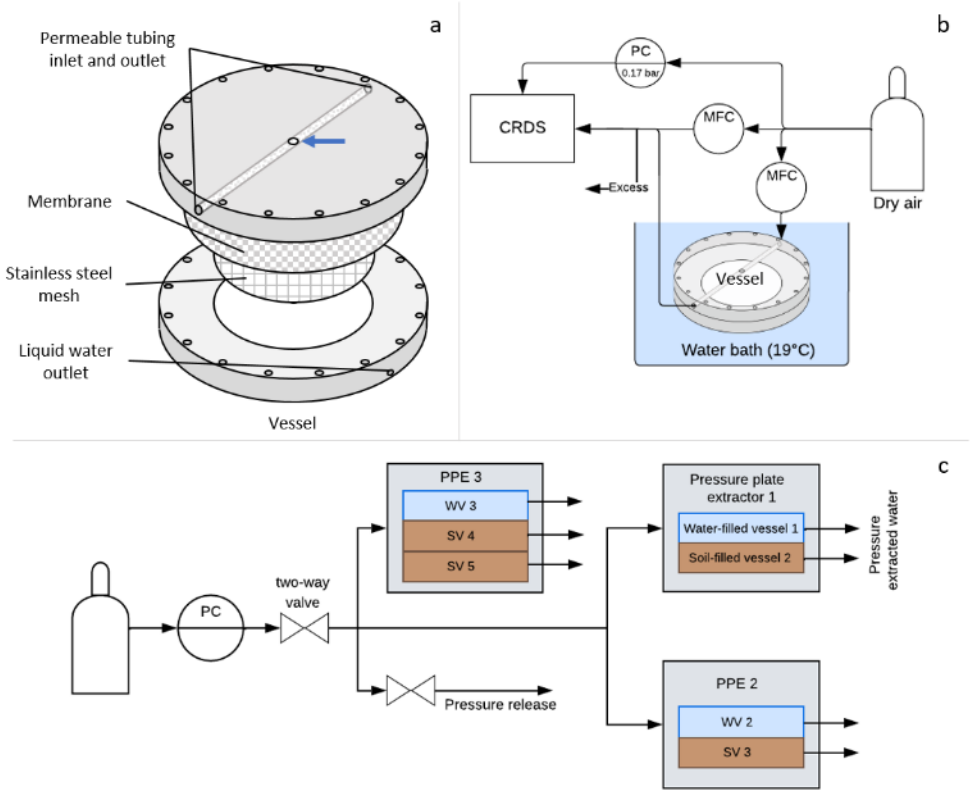

Figure 2-1 : a) Elements of the custom-made acrylic glass vessel, b) principle of the in situ online method, and c) scheme of the system to extract soil water by increasing the soil water tension (ψ, pF) inside the vessels with two types of pressure plate extractors. A blue arrow in a) indicates the opening in the upper part of the vessels, allowing increasing the soil tension. CRDS stands for cavity ring-down spectrometer; MFC, for mass flow controller; PC, for pressure controller (pressure range during the experiments: 0.01 to 0.1 MPa); PPE, for pressure plate extractor; and SV and WV, for soil- (brown) and water-filled (blue) vessels. The 2-way valve marked as pressure release in c) was closed during the water extraction and was opened once equilibrium between the pressure applied and soil water tension was reached to release the dry air inside the extractors and be able to open them.

2.1. Continuous isotopic monitoring: pressure-extraction of water

With this method (Fig. 2-1c), soil water from the vessels was pushed through the membrane by applying pressure inside the extractor with dry synthetic air (20.5% O_2 in N_2 with approximately 20–30 ppmv water vapor, Air Liquide, Germany). The method is based on the principle that, at equilibrium, the water potential inside and outside the vessel equilibrate and therefore the soil water tension reaches a value equal to the opposite of the pressure set inside the extractor and water collection ends. For this, two types of pressure plate extractors were used: two 5 bar pressure and two 15 bar extractors (Soilmoisture Equipment Corp., USA). Custom-designed polypropylene pierced screws were used to seal the three vessel openings (center of the lid, inlet, and outlet of the permeable tubing, Fig. 2-1a) during pressure-mediated extraction. These pierced screws allowed the pressure inside the vessel to equilibrate with that outside the vessel (i.e., inside the plate extractor), while minimizing soil water evaporation. The stainless steel tubing connecting the hollow space underneath the membrane with the outside of the vessel was attached inside the extractor with one of the outlets of the extractor (the 5 bar extractors had two and the 15 bar extractors had four). The extractor plate outlet, through which the extracted water was transferred, was equipped with a 1/16 inch diameter needle, which perforated a piece of Parafilm® covering a glass beaker, in which extracted soil water was collected.

2.2. Discrete isotopic measurements

The hydrogen and oxygen isotopic compositions (δ^2H and $\delta^{18}O$) of soil water extracted under pressure (section 2.1 in this chapter) were compared to those determined in situ online (i.e., non-destructively) and with the following destructive techniques: cryogenic vacuum distillation (CVD), centrifugation (CF), and direct water vapor equilibration (DVE).

2.2.1. In situ online isotopic analysis (IS)

Prior to the in situ isotopic measurement, the vessel with soil and added moisture was placed in a water bath at a constant temperature of 19°C for four days to ensure thermodynamic equilibrium between soil water and its vapor (Fig. 2-1b). The in situ isotopic measurement was then conducted three times on three different days. Each time, the water vapor inside the gas-permeable tubing in each vessel was flushed at a low flow rate (approx. 100 ml min^{-1}) with synthetic dry air (20.5% O_2 in N_2 with approximately 20–30 ppmv water vapor, Air Liquide, Germany) and directed to a cavity ring-down spectrometer (CRDS, L2130-*i*; Picarro, Santa Clara, USA). The soil water vapor was sampled until constant δ^2H and $\delta^{18}O$ readings were observed (standard deviations < 0.7% and < 0.2% for δ^2H and $\delta^{18}O$, respectively; Rothfuss et al., 2013), which was usually the case after ~30 min. The δ-value of soil liquid water in the vessel was calculated from that of the soil water vapor averaged over the last 5.5 min of online measurements (yielding exactly 330 measurements with the aforementioned standard deviation), the soil temperature (assumed to be 19°C, i.e.,

that of the water bath) considering thermodynamic equilibrium between the liquid and gas phase, and calibrated against measurements of two soil water vapor standards. These standards consisted of acrylic glass vessels, different in design from those used in the water extraction (see Rothfuss et al. (2013)), also incorporating the gas-permeable tubing, and filled with the same soil type as the vessels. One standard was saturated with isotopically depleted water (i.e., melted ice; δ^2H = -78.8 ± 0.4‰ and $\delta^{18}O$ = -18.9 ± 0.1‰) and the other, with isotopically enriched water (i.e., evaporated water; δ^2H = 7.7 ± 0.6 ‰ and $\delta^{18}O$ = 10.4 ± 0.1‰). The soil water vapor in the standards was sampled and measured twice before and twice after the vapor in the vessels.

2.2.2. Cryogenic vacuum distillation (CVD)

Soil samples (20 g each) were processed in two locations, namely the Chair of Ecosystem Physiology at University of Freiburg (extraction temperature = 95-98°C; duration = 1.5 h) and the Institute for Landscape Ecology and Resources Management at the Justus Liebig University Giessen, according to Orlowski et al. (2013) (extraction temperature > 90°C; duration = 4 h). The isotopic composition of the extracted water was determined offline via CRDS (L2120-*i*, Picarro; long-term precision = 1 and 0.5‰ for δ^2H and $\delta^{18}O$, respectively) at the Institute for Bio- and Geosciences Agrosphere (IBG-3) at Forschungszentrum Jülich. The extraction efficiency in all but three samples was above 98% (Araguás-Araguás et al., 1995).

2.2.3. Centrifugation (CF)

Soil samples (40 g each) were placed in custom-made polyvinyl chloride (PVC) centrifuge tubes, sealed with plastic plugs to avoid soil water evaporation, placed in a centrifuge (6K15; Sigma Laborzentrifugen GmbH, Germany) and spun at 10,000 g-forces (equivalent to a soil tension of ~2.1 MPa) for 20 min at 20°C together with water-filled tubes used as controls. The isotopic composition of the water used for the controls was measured before and after centrifugation to ensure that, no isotopic fractionation occurred during the handling and centrifugation of the samples. Isotopic analyses were performed via CRDS (L2120-*i*, Picarro).

2.2.4. Direct water vapor equilibration (DVE)

Soil samples (100 g each) were placed in stand-up pouches (i.e., sample pouches) with zip-seal locks (152 x 98 x 229 mm; WEBER Packaging GmbH, Germany). Additionally, six pouches were filled each with 10 mL of deionized local tap water (δ^2H = -51.8 ± 0.4‰ and $\delta^{18}O$ = -7.8 ± 0.1‰) and six, with 10 mL of evaporated water (δ^2H = 7.7 ± 0.6 ‰ and $\delta^{18}O$ = 10.4 ± 0.1‰) and were used as isotopic standards (i.e., standard pouches). Sample and standard pouches were inflated with dry air and their tops sealed with hot pliers (WEBER Packaging GmbH, Germany). A small amount of silicon (transparent sanitary silicon; OBI, Germany) was placed on an upper section of each sample and standard pouch to serve as septum. All pouches were then stored for four days so that isotopic equilibrium between (soil) water and the headspace water vapor was reached. On the day of measurement, the pouches were pierced trough the silicon septum with a needle attached to a piece of 1/8 inch polytetrafluoroethylene

(PTFE) tubing connected to a CRDS (L2130-*i*, Picarro) for online isotopic analysis for approximately 15 min. The δ-value of the soil water in the sample pouches was calculated using the last 2 min of recorded raw soil water vapor δ-data considering thermodynamic equilibrium at the observed laboratory temperature (Sprenger et al., 2015; Wassenaar et al., 2008) and calibrated against the δ-values of the standard pouches. The mean standard deviation of the water vapor measurements in the standard pouches was 0.4 ± 0.2‰ for δ^2H and 0.1 ± 0.0‰ for $\delta^{18}O$. In the sample pouches, these values were 0.5 ± 0.1‰ for δ^2H and 0.1 ± 0.0‰ for $\delta^{18}O$.

2.3. Experimental protocols: "memory effect" and "tension effect" experiments

2.3.1. Memory effect experiment

The memory effect experiment consisted of two consecutive saturation/pressure-extraction steps (stages A and B, left panel Fig. 2-2). In stage A step I, five custom-made vessels (numbered 1 to 5) were filled and packed with quartz sand (grain size distribution between 0.72 mm and 0.18 mm; Quarzwerke Frechen, Germany; mean dry bulk density = 1.67 ± 0.01 g cm^{-3}) and saturated from the bottom through the membrane with deionized local tap water (δ^2H = -51.8 ± 0.4‰ and $\delta^{18}O$ = -7.8 ± 0.1‰) to a mean volumetric soil water content (θ) of 0.35 ± 0.01 cm^3 cm^{-3}. Following saturation, the isotopic composition of soil water in vessels 1-5 was determined with the in situ online method (IS, step II), and a total of nine samples intended for the destructive water recovery techniques (i.e., three for cryogenic vacuum distillation, CVD; three for centrifugation, CF; and three for direct water vapor equilibration, DVE) were taken from vessel 1. Subsequently, the four remaining vessels (2 to 5) were placed in pressure plate extractors with three vessels containing 100 mL of tap water each (step III). These water-filled vessels served as controls to verify that water was extracted free of fractionation. An air pressure of 0.01 MPa (corresponding to a soil water tension pF value of 2) was applied to extract (soil) liquid water. At this pressure, almost all soil water should have been extracted (discontinuous line, Fig. 2-3). After 47 days, equilibrium was reached, and no more water was collected from the vessels. After this first extraction, mean θ across vessels was 0.04 ± 0.01 cm^3 cm^{-3} (determined gravimetrically). In step IV, the soil water isotopic composition in vessels 2-5 was measured with IS. Soil from vessel 2 was then sampled for destructive isotopic determinations.

In stage B of the experiment, vessels 3-5 were re-saturated (mean θ = 0.33 ± 0.01 cm^3 cm^{-3}) with isotopically enriched water (step V; δ^2H = 29.0 ± 0.5‰ and $\delta^{18}O$ = 15.7 ± 0.0‰). After four days, the isotopic composition of the soil water in these vessels was determined with IS and the soil in vessel 3 was destructively sampled (step VI). Vessels 4 and 5 were then placed again in the extractors with two control vessels, one containing 100 mL and the other 180 mL of the isotopically enriched water (step VII). The same air pressure (i.e., 0.01 MPa, pF = 2) was applied, and the time to reach equilibrium and the final mean θ were 35 days and 0.04 ± 0.00 cm^3 cm^{-3}, respectively. Finally, the isotopic composition of soil water in

vessels 4-5 was measured with IS, and the soil in vessel 4 was destructively sampled (step VIII).

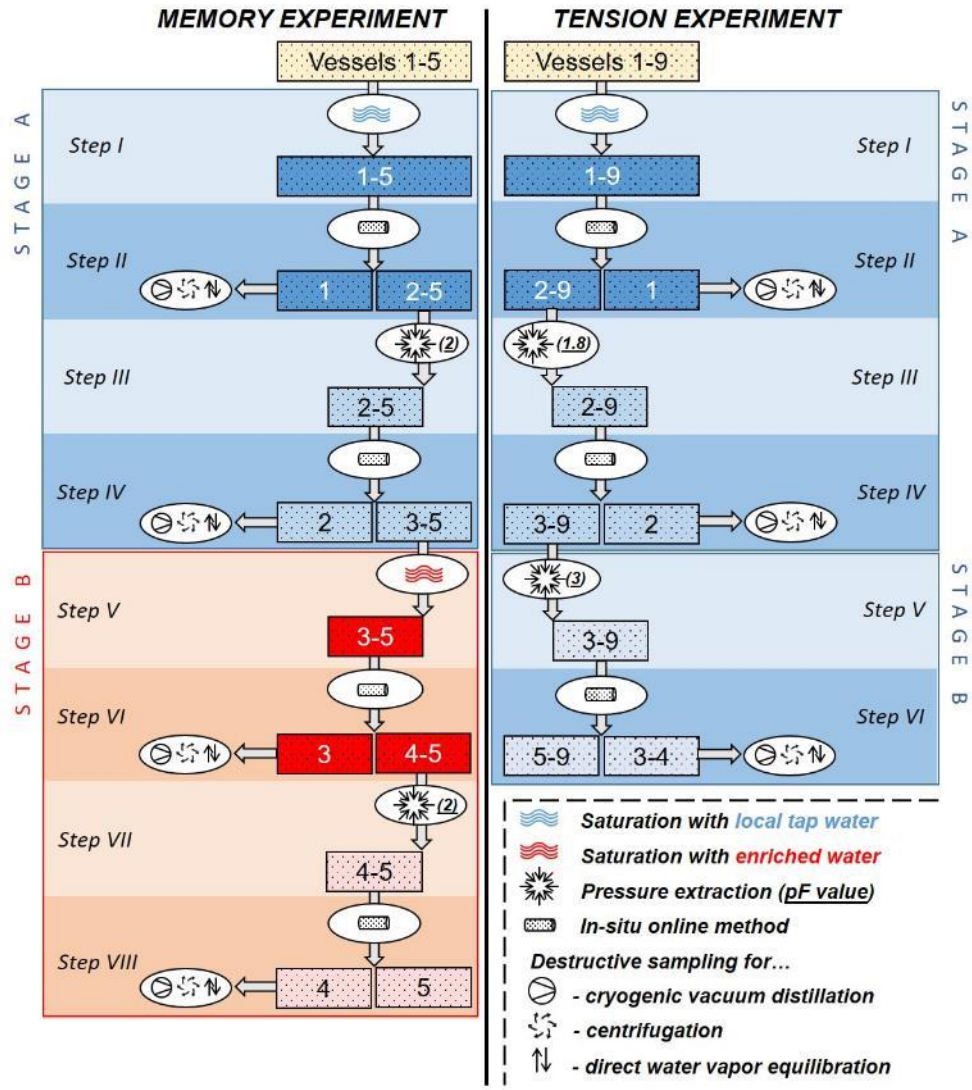

Figure 2-2 : Stages and steps of the memory effect and tension effect experiments. Numbers in boxes refer to the vessels, while symbols in circles refer to the action performed (i.e., water saturation, pressure-extraction of water, in situ online isotopic analysis, and sampling for destructive water recovery techniques). The background color refers to the isotopic composition of the water in the vessels: blue shades for tap water and red shades for isotopically enriched water.

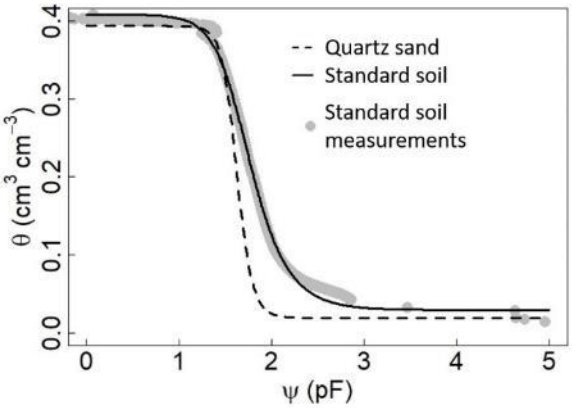

Figure 2-3 : Water retention curve for quartz sand (discontinuous line), fitted water retention curve for the standard soil classified as a loamy sand (continuous line) and measurements with the standard soil (gray filled circles).

2.3.2. Tension effect experiment

Possible tension-mediated isotopic effects were investigated using a two-step pressure-extraction process (stages A and B, right panel Fig. 2-2), but in contrast to the memory effect experiment without re-saturation at the end of stage A. The experiment was conducted using a soil classified as a loamy sand (standard soil 2.1, particle size distribution = 84.7% 2–0.063 mm, 11.4% 0.063–0.002 mm, 3.9% < 0.002 mm; LUFA Speyer, Germany). In step I, nine custom-made vessels (numbered 1 to 9) were filled and packed with air-dried and homogenized loamy sand (dry bulk density = 1.53 ± 0.02 g cm^{-3}) and saturated with deionized local tap water (θ = 0.39 ± 0.03 cm^3 cm^{-3}, δ^2H = -51.0 ± 0.4‰ and $\delta^{18}O$ = -7.7 ± 0.1‰). The isotopic composition of the soil water in vessels 1-9 was measured with IS and the soil in vessel 1 was sampled for the different water recovery techniques in triplicates (step II), similar to the memory effect experiment. The remaining eight vessels (2 to 9) were placed in pressure plate extractors, and 0.006 MPa pressure was applied (step III). This pressure corresponded to a soil tension pF of ~1.8 and was necessary to extract 50% of the soil water inside the vessels (continuous line, Fig. 2-3). Two control vessels containing 100 mL of deionized tap water (δ^2H = -51.0 ± 0.4‰ and $\delta^{18}O$ = -7.7 ± 0.1‰) were also placed in the extractors. Equilibrium was reached after 30 days of extraction with a final mean θ of 0.29 ± 0.03 cm^3 cm^{-3}. The isotopic composition of the soil water in vessels 2-9 was determined with IS and the soil in vessel 2 was destructively sampled (step IV). In stage B, vessels 3 to 9 were placed again in the pressure plate extractors with two control vessels containing 200 mL of deionized tap water and a pressure of 0.1 MPa (pF = 3) was applied (step V). Since more water was extracted from the control vessels at a higher pressure, more water had to be added to these so that the extraction period of the controls was as long as that of the soil vessels. After 14 days, equilibrium was reached (θ = 0.09 ± 0.08 m^3 m^{-3}), the isotopic composition of soil

water in vessels 3 to 9 was determined with IS, and the soil in vessels 3 and 4 was destructively sampled (step VI).

For stages A and B of the memory effect experiment and for stage A of the tension effect experiment (soil saturated or partly filled with local tap water of isotopic composition $\delta_{tap\ water}$), we express the isotopic composition of the water extracted ($\delta_{extracted\ water}$, determined either non-destructively with the pressure plates and IS or destructively) relative to $\delta_{tap\ water}$ using the Δ notation (Eq. 2-1):

$$\Delta = \delta_{extracted\ water} - \delta_{tap\ water}$$

Equation 2-1

For stage B in the memory effect experiment (i.e., re-saturation with isotopically enriched water, steps V-VIII), the measured $\delta_{extracted\ water}$ value was compared to the result of a two-end-member mixing equation (δ_{mix}), considering in a first approximation perfect mixing between tap water remaining after stage A extraction (step III) and the added isotopically enriched water ($\delta_{enriched\ water}$) in stage B, step V (Eq. 2-2):

$$\Delta = \delta_{extracted\ water} - \delta_{mix}$$

Equation 2-2

with δ_{mix} defined as:

$$\delta_{mix} = \delta_{tap\ water} * x_{tap\ water} + \delta_{enriched\ water} * (1 - x_{tap\ water})$$

Equation 2-3

where $x_{tap\ water}$ (-) is the fraction of tap water in the soil water mixture after re-saturation:

$$x = \frac{w_{tap\ water}}{w_{mix}}$$

Equation 2-4

$w_{tap\ water}$ (g) is the amount of deionized tap water remaining in the vessels after the extraction in stage A and w_{mix} (g) is the sum of remaining tap water and added isotopically enriched water amounts.

2.4. Intercomparison of discrete isotopic measurements

We compared in pairs the different discrete isotopic determinations with so-called Bland-Altman plots (Altman & Bland, 1983). This statistical approach was proposed for comparing the measurements obtained using an "established" method A with those of a "new" method B to ultimately decide whether method B rendered reliable results, as method A was assumed to do. First, the repeatability of IS and of the three destructive methods (i.e., CVD, CF, and DVE) was assessed for the two soil types to rule out a dependency of the within-subject standard deviation (s_w) and the magnitude of the measurement that could produce misleading results. The significance of the correlation between the mean δ-values and s_w associated with the mean of each

method was tested by calculating Kendall's rank correlation coefficient (Bland & Altman, 1996).

Then, a repeatability coefficient (RC, ‰) was calculated using Eq. 2-5 (Bland & Altman, 1996):

$$RC = 1.96 * \sqrt{2} * s_w$$

Equation 2-5

The RC-value is the expected difference between two measurements done with a certain method for the same subject (vessel in our study) for 95% of subjects. In other words, the lower the RC, the better the repeatability of the method.

Afterwards, the difference between the δ-values of the soil water extracted from vessel *j* measured with method A and method B ($\delta_{(A-B)j}$) and the mean of the δ-values obtained with both methods A and B ($\bar{\delta}_{A,Bj}$) were calculated using Eq. 2-6 and Eq. 2-7, respectively, for the method pairs IS/CF, IS/DVE, IS/CVD, CF/DVE, CF/CVD, and DVE/CVD (Altman & Bland, 1983):

$$\delta_{(A-B)j} = \delta_{Aj} - \delta_{Bj}$$

Equation 2-6

$$\bar{\delta}_{A,Bj} = \frac{\delta_{Aj} + \delta_{Bj}}{2}$$

Equation 2-7

In each Bland-Altman plot (or method pair), $\bar{\delta}_{A,Bj}$ is expressed as a function of $\delta_{(A-B)j}$ and the dependency between these two variables was assessed by calculating a Kendall's rank correlation coefficient (as done for the measurements of each method). Then, the lower (LL) and upper limits of agreement (UL), between which we expect to find 95% of the differences, were calculated using Eq. 2-8 and Eq. 2-9, respectively:

$$LL = \bar{\delta}_{A-B} - 1.96 * \hat{s}_{diff}$$

Equation 2-8

$$UL = \bar{\delta}_{A-B} + 1.96 * \hat{s}_{diff}$$

Equation 2-9

where $\bar{\delta}_{A-B}$ is the mean of the δ-value differences between methods A and B, and $\hat{s}_{diff}$ is a corrected standard deviation for these differences. This corrected standard deviation is employed when repeated measurements of the same subject for each method were performed (n = 3 in our study; Bland & Altman, 1999).

$$\hat{s}_{diff} = s_{diff} + \left(1 - \frac{1}{n_A}\right) s_{wA} + \left(1 - \frac{1}{n_B}\right) s_{wB}$$

Equation 2-10

where s_{diff} is the standard deviation of the δ-value differences between method A and method B, n_A and n_B are the numbers of observations of each subject in method A and method B, respectively, and s_{wA} and s_{wB} are the within-subject standard deviations in method A and method B, respectively.

3. Results and Discussion

The results of the memory and tension effect experiment are presented and discussed in section 3.1 and 3.2. The comparison of the three destructive isotopic techniques and the in situ online method is detailed in section 3.3. Finally, a broader discussion about the isotopic methodologies used, co-existing water pools in the soil, and their relation to soil texture and saturation is offered in section 3.4.

3.1. Time-evolution in isotopic composition and evaporative enrichment during pressure-extraction of water

A continuous increase in the Δ-values (up to 13.3 and 3.8‰ in Δ^2H and $\Delta^{18}O$, respectively) of the water extracted under pressure from the soil- and water-filled (i.e., control) vessels was observed during stage A of the memory effect experiment (step III, Fig. 2-4). Such increase was strongest in the last 15 days of the extraction (day of the experiment – DoE – 30 to 45). This was also reflected in the higher Δ-values determined with the destructive and in situ methods before (up to 3.8 and 1.2‰ in Δ^2H and $\Delta^{18}O$, respectively) and after (up to 11 and 3‰ in Δ^2H and $\Delta^{18}O$, respectively) stage A pressure-extraction (steps II and IV, Fig. 2-4). Noticeably, such a Δ-increase was not observed during stage B extraction (i.e., after re-saturation of the soil vessels with isotopically enriched water; step VII, Fig. 2-4). The maximum Δ-values determined destructively and in situ before and after stage B pressure-extraction (steps VI and VIII, Fig. 2-4) did not differ as greatly as they did in stage A (2.5 against 4‰ in Δ^2H and 1.3 against 1.5‰ in $\Delta^{18}O$). It is important to note that stage B extraction was shorter than stage A extraction and that the results from centrifugation (CF) and cryogenic vacuum distillation (CVD) after the extractions were not included in our analysis. It was not possible to collect soil water via CF after each pressure-extraction (steps IV and VIII) due to very low θ in the soil samples and the extraction of water via CVD in the same steps was incomplete (i.e., extraction efficiency below 98%; Araguás-Araguás et al., 1995).

The Δ-values calculated based on isotopic results of the destructive and in situ methods and the variation among methods seemed to be higher in vessels with lower θ compared to the Δ-values in vessels close to water saturation. The average absolute Δ^2H ($\Delta^{18}O$) value in the vessel sampled in step II ($\theta = 0.34$ cm^3 cm^{-3}, Fig. 2-4) and step VI ($\theta = 0.33$ cm^3 cm^{-3}) was 2.7 and 0.9‰ (0.6 and 0.5‰), respectively, whereas in the vessel sampled in step IV ($\theta = 0.05$ cm^3 cm^{-3}) and step VIII ($\theta = 0.04$ cm^3 cm^{-3}) was 9.2 and 3.5‰ (2.8 and 0.8‰).

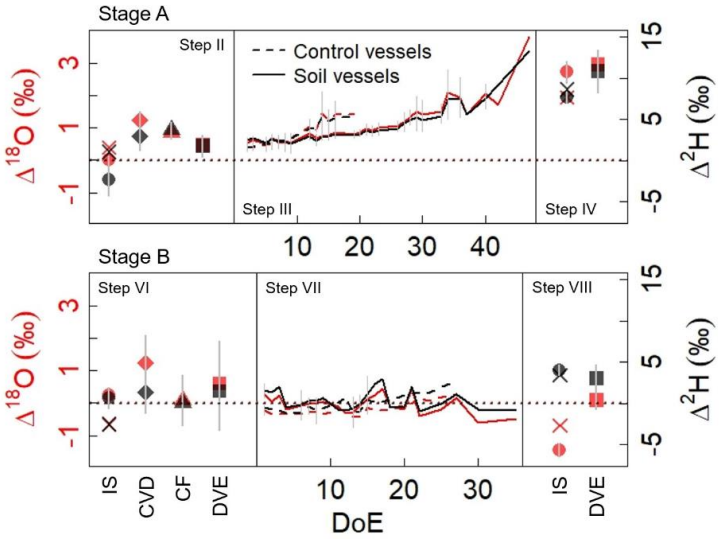

Figure 2-4 : Time series (days of experiment - DoE) of Δ (‰) recorded during the memory effect experiment. Δ is the difference between the δ-value of the water measured destructively or in situ and the δ-value of the spike water (stage A) or the theoretical δ-value of a perfect mix between remaining tap water and added enriched water (stage B). Continuous and discontinuous lines refer to soil- and water-filled (used as controls) vessels, respectively. The Δ-values from in situ determinations (circle, IS) or following destructive sampling via cryogenic vacuum distillation (diamond, CVD), centrifugation (triangle, CF) or direct water vapor equilibration (square, DVE) before and after the pressure-extraction in stage A (step III) are presented in the panels labeled step II and step IV, respectively. Likewise, the Δ-values of soil water measured destructively or in situ before and after the pressure-extraction in stage B (step VII) are presented in the panels labeled step VI and step VIII, respectively. In steps II, IV, VI, and VIII, the mean Δ-value measured with IS in all vessels (not only in the vessel destructively sampled) is indicated with the symbol 'x'.

As for the tension effect experiment, a smaller (compared to the memory effect experiment) increase in Δ-value (up to 7.7‰ in Δ^2H and 1.8‰ in $\Delta^{18}O$) was observed in the soil vessels and controls during stage A pressure-extraction (step III, Fig. 2-5), but not during stage B extraction (step V, Fig. 2-5). Like in the memory effect experiment, the second extraction step was considerably shorter. The Δ-values calculated based on results of the in situ and destructive techniques after stage A pressure-extraction (up to 9.5‰ in Δ^2H and 2.3‰ in $\Delta^{18}O$; step IV, Fig. 2-5) were greater than those calculated before stage A pressure-extraction (up to 3.7‰ in Δ^2H and 0.9‰ in $\Delta^{18}O$; step II, Fig. 2-5).

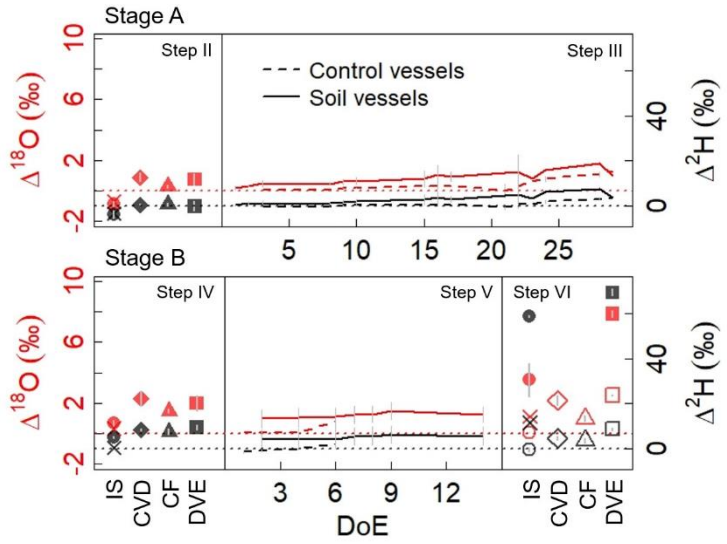

Figure 2-5 : Time series (days of experiment – DoE) of Δ (‰) recorded during the tension effect experiment. Δ is the difference between the δ-value of the water measured destructively or in situ and the δ-value of the spike water. Continuous and discontinuous lines refer to soil- and water-filled (used as controls) vessels, respectively. The Δ-values from in situ determinations (circle, IS) or following destructive sampling via cryogenic vacuum distillation (diamond, CVD), centrifugation (triangle, CF) or direct water vapor equilibration (square, DVE) before the pressure-extraction in stage A (step III) are presented in the panel labeled step II. Likewise, the Δ-values of soil water measured destructively or in situ before and after the pressure-extraction in stage B (step V) are presented in the panels labeled step IV and step VI, respectively. Empty and full symbols in step VI refer to two different vessels, one with wet soil (empty symbols) and one with dry soil (full symbols). In steps II, IV, and VI the mean Δ-value measured with IS in all vessels (not only in the vessel destructively sampled) is indicated with the symbol 'x'.

Again, the increase in Δ-values and the variation among methods seemed to be higher in the vessel with the driest soil. The average absolute Δ^2H ($\Delta^{18}O$) value in the vessels destructively sampled in steps II and IV (θ = 0.42 and 0.27 cm^3 cm^{-3}, respectively) and one of the vessels sampled in step VI (θ = 0.24 cm^3 cm^{-3}, empty symbols) was below 4.4‰ (1.3‰), whereas in the other vessel sampled in step VI (θ = 0.01 cm^3 cm^{-3}, filled symbols, Fig. 2-5) the average absolute Δ^2H ($\Delta^{18}O$)-value was 63.9‰ (5.7‰).

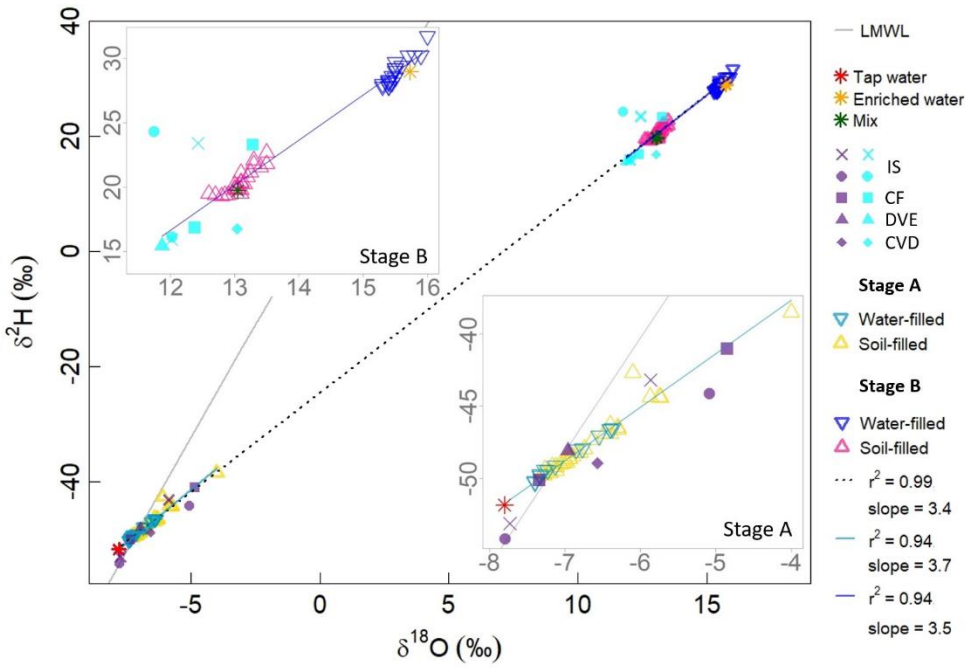

Figure 2-6 : Dual isotope plot of the water extracted under pressure from the soil vessels (empty triangles) and the (water-filled) control vessels (empty inverted triangles) in stages A and B during the memory effect experiment. Soil water δ-values obtained before and after stage A extraction using the in situ online method (circles, IS), via centrifugation (CF, filled triangles), direct water vapor equilibration (DVE, squares), and cryogenic vacuum distillation (CVD, diamonds) are presented as purple symbols. The results determined before and after stage B extraction are presented as cyan symbols. The mean δ-values measured with IS in all vessels (not only in the destructively sampled vessel) is indicated with an 'x'. The δ-values of the water used to saturate the soil vessels and to fill the controls are presented as asterisks in red (extraction stage A) and orange (stage B). The calculated mean δ-value of the soil water inside the re-saturated vessels is shown as a green asterisk. Linear regression models of $\delta^{18}O$ vs $\delta^{2}H$ were fitted to the data obtained during both extraction steps (black dotted line) and separately for each extraction step (light and dark blue continuous lines). All correlations were significant ($p < 0.05$). The local meteoric water line (i.e., LMWL - gray line, $\delta^{2}H = 7.9*\delta^{18}O + 6.9$) is included as a reference.

Based on the small difference between the δ-values of the pressure-extracted water in stage B in the memory effect experiment and the reference, we could accept our null hypothesis a): complete mixing between the remaining local tap water after step III and added isotopically enriched water in step V. Nevertheless, we cannot definitely assert this at this point, since the zigzagging pattern in the time series of the extraction and the bigger Δ-values observed in the destructive and in situ measurements in step VI point towards spatial heterogeneities (see section 3.2). In section 3.2, we also discuss in more detail the results of the tension effect experiment to either accept or

reject null hypothesis b) dependency of the soil water isotopic composition on soil tension.

The increase in Δ described in the previous paragraphs in the extractions in both the memory and tension effect experiments was very likely the consequence of water having evaporated from the soil vessels and controls inside the pressure plate extractors. In the memory effect experiment, the conditions (air temperature and relative humidity) prevailing in the extractors and driving the isotopic enrichment seemed to have been comparable during the extractions in stages A and B as evidenced by the similar values of the slopes of the δ^2H-$\delta^{18}O$ linear models fitted separately (3.7 vs. 3.5, $p < 0.05$; light blue vs. dark blue continuous lines, Fig. 2-6).

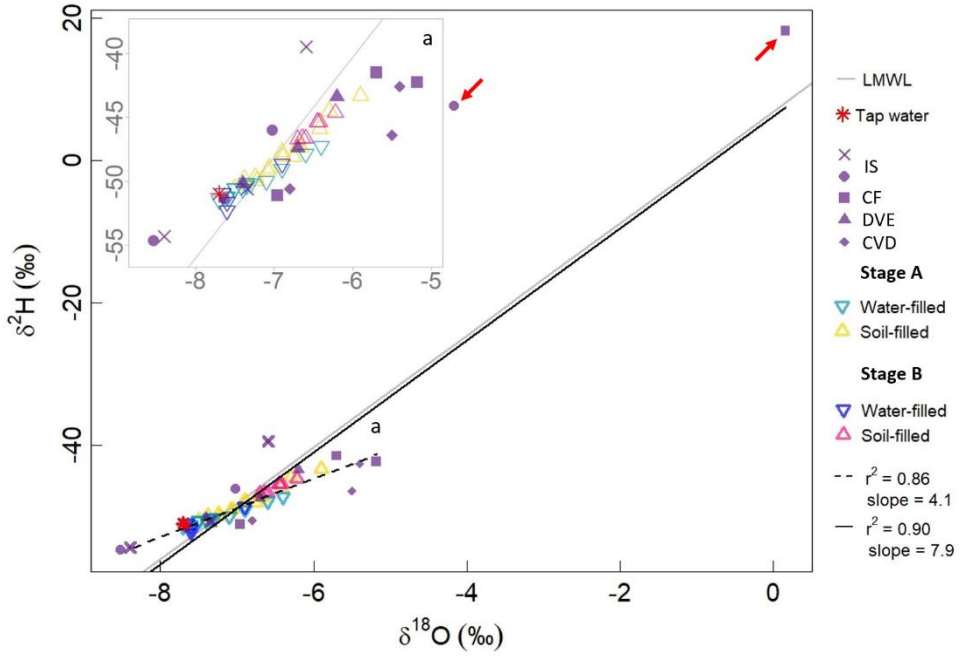

Figure 2-7 : Dual isotope plot of the water extracted under pressure from the soil vessels (empty triangles) and the (water-filled) control vessels (empty inverted triangles) in stages A and B during the tension effect experiment. Soil water δ-values obtained from the in situ online method (circles, IS), via centrifugation (CF, filled triangles), direct water vapor equilibration (DVE, squares), and cryogenic vacuum distillation (CVD, diamonds) are presented as purple symbols. The mean δ-values measured with IS in all vessels (not only in the destructively sampled vessel) is indicated with an 'x'. The δ-values of the water used to saturate the soil vessels and to fill the controls is presented as a red asterisk. Linear regression models of $\delta^{18}O$ vs δ^2H were fitted to the data obtained during both extraction steps (black continuous line) and excluding the data points measured in the vessel with dry soil (marked with red arrows; discontinuous black line). Both relationships were significant ($p < 0.05$). The local meteoric water line (i.e., LMWL - gray line, $\delta2H = 7.9*\delta18O + 6.9$) is included as a reference.

Furthermore, regardless of the stage, the isotopic enrichments observed in water extracted under pressure from the soil vessels and controls were comparable, which points towards no soil-texture-related isotopic fractionation of soil water.

The δ-values measured with the discrete isotopic techniques (i.e., IS, CVD, CF, and DVE) deviated more from those obtained continuously under pressure and from the δ-values of the reference water during stage B than during stage A. This is most likely because there were differences in the amount of tap water remaining in the soil vessels after the extraction in stage A and in the amount of isotopically enriched water added in the re-saturation.

In the tension effect experiment, the slope of the correlation between the $\delta^{18}O$- and $\delta^{2}H$-values of the non-destructive and destructive water samples during the extractions in stages A and B was 7.9 ($p < 0.05$, continuous black line in Fig. 2-7). This value was 4.1 ($p < 0.05$, discontinuous black line) when the paired δ-values associated to an extremely high standard deviation or that deviated considerably from the cluster of points shown in the lower left side of Fig. 2-7 were excluded from the analysis. These data points, indicated by a red arrow, are those of soil water in the vessel with dry soil after extraction stage B measured via DVE (square) and IS (circle).

Alternatively, the increase in Δ could have been related to the amount of pressure-extracted water. To explore this possibility, we expressed Δ as a function of the amount of water (w, g) collected daily from the pressure plate extractors from each control and soil vessel in the memory and tension effect experiments (Fig. 2-8). $\Delta^{2}H$ and $\Delta^{18}O$ in the memory effect experiment during stage A extraction in the soil vessels (yellow triangles, left panels Fig. 2-8) and controls (light blue inverted triangles) seemed to be higher the lower the amount of pressure-extracted water was. This trend is also observed in the tension effect experiment in both extraction steps (right panels Fig. 2-8). However, no clear trend was observed between $\Delta^{2}H$ and $\Delta^{18}O$ and the amount of pressure-extracted water (pink triangles and dark blue inverted triangles) in stage B extraction in the memory effect experiment (bottom left panel Fig. 2-8).

The parameters of a fitted exponential model (Eq. S2-1) for the data points of stage A extraction in the memory and in the tension effect experiment were very similar (Table S2-1) and they were both statistically significant (i.e., $p < 0.05$), albeit with a low r^2 (< 0.21). Likewise, the parameters of the models fitted to the data of both extractions (stage A and B) in the memory and tension effect experiment were very similar (Table S2-1) and statistically significant. However, the r^2 in these cases was below 0.15. The results presented in Fig. 2-6, 2-7, and 2-8 led us to conclude that the isotopic effect of water evaporation in both memory and tension effect experiments was comparable and that this evaporation could have happened both inside and outside of the pressure plate extractors. Furthermore, the fact that the parameters of the model fitted to the data in the memory and in the tension effect experiment were similar and that the trend for the Δ in the controls was the same as that of Δ in the soil vessels, was an indication of no soil-texture-related isotopic effect on soil water.

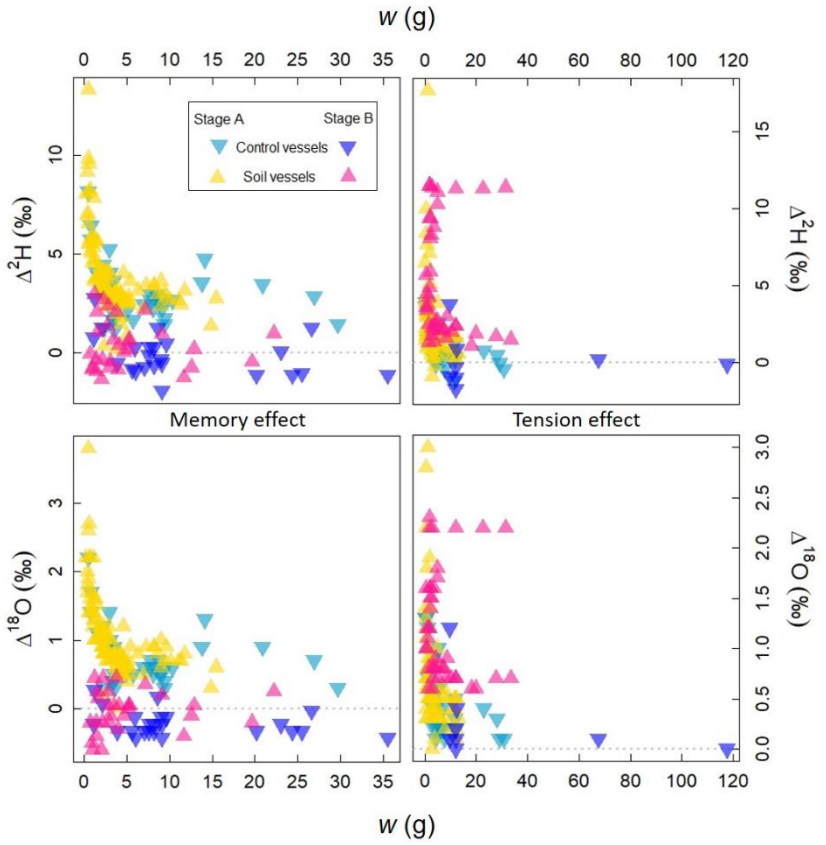

Figure 2-8 : The difference between the δ-value of the water extracted daily from the pressure plate extractors and the δ-value of the reference water (i.e., Δ, ‰) in the soil vessels (triangles) and (water-filled) control vessels (inverted triangles) during stage A (yellow and light blue, respectively) and stage B extraction (pink and dark blue, respectively) as a function of the amount of water extracted under pressure (w, g) in the memory (left panels) and tension (right panels) effect experiment. The δ-value of the reference water in stage A in the memory effect experiment and in stage A and B in the tension effect experiment was that of tap water. For stage B extraction in the memory effect experiment, the reference water δ-value was that of a perfect mixture between remaining tap water in the soil vessels after stage A extraction and the isotopically enriched water added in the second saturation (i.e., step V). A gray dotted line at Δ = 0 (no difference between extracted and reference water) is included as reference.

3.2. Analysis of the memory and tension effects

Regarding our research question i), we observed the so-called “memory effect” (Newberry, Prechsi, et al., 2017) in the isotopic composition of soil water after two isotopically distinct water sources were sequentially added to the same soil sample in the memory effect experiment. Like in the study of Newberry, Prechsi, et al. (2017),

the isotopic composition of extracted water after re-saturation differed from (in our case, was lower than) that of the reference water (in our study, isotopically enriched water, Fig. 2-6). Thus, the extracted water was a mixture of isotopically enriched water and remaining tap water from the previous wetting event. Thielemann et al. (2019) reported that this memory effect could still be observed even after several re-wetting events (three in their case).

Interestingly, there seemed to be spatial heterogeneity in the degree of mixing in the soil-filled vessels, since we recorded a zigzagging trend of the difference to reference water (i.e., Δ) during stage B extraction in the memory effect experiment (i.e., step VII, Fig. 2-4). The mean δ-value of soil water measured across vessels with the IS method before the extraction (i.e., step VI, Fig. 2-4) was lower than that of the reference water (i.e., δ-value of a perfect mixture), which may support the previous statement. Of course, this could also have a methodological explanation: the perfectly mixed soil water had not yet completely replaced the depleted tap water around the permeable tubing (Rothfuss et al., 2013). However, we do not believe this was the case, since no significant differences were observed between the IS measurements performed on three different days after a four-day equilibration time. Bowers et al. (2020) reported a mixing and equilibration time for isotopically distinct and sequentially added water of little more than four days. We believe our results support the conclusion of Gaj et al. (2016) that the well-documented spatial heterogeneity of soil water content and differences in the degree of equilibration between different water pools (Hsieh et al., 1998) in the unsaturated zone naturally leads to spatial differences in the distribution of soil water stable isotopes.

To draw a conclusion to our research question ii), we fitted a linear and exponential model to the function between Δ and soil water potential (ψ, pF) (Eq. S2-2). The linear correlation was positive and significant ($p < 0.05$) for both the tension (left panels Fig. 2-9, Table S2-1) and the memory effect experiments (right panels Fig. 2-9, Table S2-1) for the data points measured in both extractions. However, all calculated correlations had very low r^2 values (≤ 0.15, Table S2-1). The r^2 of the correlation of the data in the tension effect experiment following an exponential trend was slightly higher than that of the linear correlation, but it was still low (≤ 0.20). An exponential correlation for the data points in the memory effect experiment was not statistically significant. The slope of the linear correlations in the tension effect experiment were lower (up to ~60%) than those obtained in the memory effect experiment.

It seemed that the isotopic fractionation of soil water in the memory effect experiment – in which quartz sand was used – was stronger than in the tension effect experiment – in which a loamy sand with a finer texture was used – as shown by a lower evaporation line slope in the former (Fig. 2-6) than in the latter (Fig. 2-7). This result is contrary to the conclusions of Gaj & McDonnell (2019), who found that the slope of the evaporation line is lower for soils with a finer structure. Although this effect might have also been related to the higher clay content in their soil samples with a finer structure.

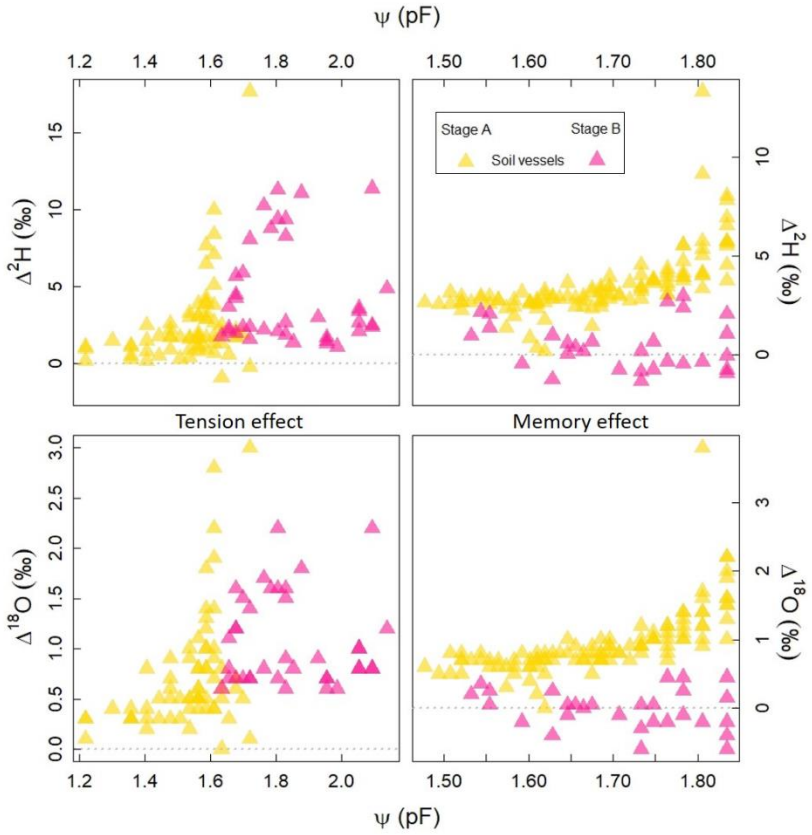

Figure 2-9 : The difference between the δ-value of the water extracted daily from the pressure plate extractors and the δ-value of the reference water (i.e., Δ; ‰) in the soil vessels during stage A extraction (yellow) and stage B extraction (pink) as a function of the soil water potential (ψ, pF) in the tension (left panels) and memory (right panels) effect experiment. The δ-value of the reference water in stage A extraction in the memory effect experiment and in both extractions in the tension effect experiment was that of tap water. For stage B extraction in the memory effect experiment, the reference water δ-value was that of a perfect mixture between remaining tap water in the soil vessels after stage A extraction and the isotopically enriched water added in the second saturation (i.e., step V). A gray dotted line at Δ = 0 (no difference between extracted and reference water) is included as reference.

The low r^2 of the correlations between Δ and the amount of pressure-extracted water and between Δ and soil tension, as well as the observed evaporative enrichment of the pressure-extracted water in both memory and tension effect experiments hindered a more conclusive and quantitative assessment of a soil tension fractionating effect (e.g., calibration equations like the ones presented by Oerter et al. (2017) or Newberry, Prechsi, et al. (2017)). However, we observed a higher standard deviation associated with isotopic measurements (e.g., Gaj et al., 2016; Meißner et al., 2014; Oerter & Bowen, 2017), greater differences between the results of the different methods (e.g.,

Tsuruta et al., 2019; Walker et al., 1994), and between the extracted soil water and the reference water (e.g., Orlowski, Pratt, et al., 2016; Sprenger et al., 2015) when soil tension was high (i.e., at low soil water content). In our study, the highest mean isotopic differences to the reference water not attributable to methodological issues (e.g., incomplete water extraction via CVD) were 9.5 ± 1.2‰ in δ^2H and 2.5 ± 0.0‰ in $\delta^{18}O$ measured via DVE in the tension effect experiment. In the memory effect experiment, the highest mean differences were 10.8 ± 2.5‰ in δ^2H and 3.0 ± 5.0‰ in $\delta^{18}O$ determined via DVE in a vessel sampled in step VIII (θ < 4%). Sprenger et al. (2015) summarized the discrepancies between the isotopic composition of soil water extracted via CVD and the reference water in several studies: up to ~15‰ in δ^2H (clay; Walker et al., 1994) and ~2‰ in $\delta^{18}O$ (clayey silt; Orlowski et al., 2013).

We could not explain the observed isotopic differences only by methodological artifacts or shortcomings. We reject then our null hypothesis ii): we observed isotopic differences in the soil water when the soil was close to saturation, at a pF of 1.8 and close to residual water content. However, we could not establish a clear relationship between soil tension and isotopic changes, since these changes could also have been caused exclusively or simultaneously by evaporation of soil water during the extraction process. Furthermore, we believe that our experimental setup with some improvements (aiming at quantifying evaporation) could be used to further test soil-texture-related isotopic fractionation, because there is already numerous studies that have found such an effect (e.g., Gaj et al., 2019; Koeniger et al., 2011; Meißner et al., 2014; Orlowski & Breuer, 2020).

3.3. Intercomparison of discrete isotopic measurements

The mean soil water δ-values and standard deviation obtained with the discrete methods are summarized in Table 2-1. The IS and CF methods showed to be the most reproducible, with a mean standard deviation of 1.0‰ (0.3‰) and 1.3‰ (0.3‰) for δ^2H ($\delta^{18}O$), respectively, compared to the direct water vapor equilibration (DVE, 1.9‰ (0.4‰)) and cryogenic vacuum distillation (CVD, 2.3‰ (0.9‰)).

No dependency between the within-subject standard deviation measured with the IS or destructive methods and the magnitude of the measurement was found in the memory or tension effect experiments ($p > 0.05$ of the Kendall's rank correlation coefficient). This meant that no transformation of the isotopic determinations from the discrete methods was necessary to analyze visually their agreement in the Bland-Altman plots.

With a few exceptions, the repeatability coefficients (RC, Table 2-2) of all methods at the different experimental stages were higher than the long-term precision of the CRDS: 1‰ and 0.5% in δ^2H and $\delta^{18}O$, respectively. Only for IS, it was possible to calculate RC-values considering isotopic determinations in several vessels (values in parenthesis in Table 2-2) and not only in the destructively sampled ones. These values were in some cases smaller than the ones calculated with only the isotopic determinations in the destructively sampled vessels.

The IS method had a lower mean RC (2.7 ± 1.0‰ and 0.6 ± 0.2‰) compared to the destructive methods (6.0 ± 1.6‰ and 1.5 ± 1.1‰ for CVD; 4.7 ± 5.6‰ and 1.4 ±

1.7‰ for CF; and 7 ± 4.2‰ and 1.6 ± 1.5‰ for DVE) in δ^2H and $\delta^{18}O$, respectively. In other words, the expected difference in δ-values between two measurements of the same soil water sample in 95% of all soil water samples was smaller using IS. The RC of CF was very close to that of IS and even smaller in some vessels.

The mean upper and lower limits in the method pairs including CF (±7.5 and ±1.8‰ in δ^2H and $\delta^{18}O$, respectively, Fig. 2-10) and IS (±8.5 and ±1.8‰ in δ^2H and $\delta^{18}O$, respectively) were slightly higher than the mean values in the pairs including CVD (±6.9 and ±1.8‰ in δ^2H and $\delta^{18}O$, respectively). The highest values were in the pairs including DVE (±9.5 and ±2.3‰ in δ^2H and $\delta^{18}O$, respectively). We highlight here the fact that for the pairs including CF and CVD less data points were included, due to zero or incomplete water extraction in dry soil samples.

In general, the agreement between measurements with the different methods shown in Fig. 2-10 was not good, since the observed differences were higher than the long-term precision of the CRDS (1 and 0.5‰ in δ^2H and $\delta^{18}O$).

Table 2-1: Mean δ^2H and $\delta^{18}O$ ($\bar{\delta}^2H$ and $\bar{\delta}^{18}O$, ‰) and standard deviation (s_w) in soil water measured in four vessels filled with quartz sand in steps II, IV, VI, and VIII of the memory effect experiment and four vessels filled with a loamy sand in steps II, IV, and VI of the tension effect experiment with the discrete isotopic measurement methods: in situ online (IS), cryogenic vacuum distillation (CVD), centrifugation (CF), and direct water vapor equilibration (DVE).

	Description	**IS**	**CVD**	**CF**	**DVE**
		$\bar{\delta}^2H \pm s_w$ $\bar{\delta}^{18}O \pm s_w$			
		‰			
Memory effect experiment	Stage A / Step II	-54.2 ± 1.9 -7.8 ± 0.1	-49.0 ± 1.7 -6.6 ± 0.3	-48.1 ± 0.9 -7.0 ± 0.2	-50.1 ± 1.3 -7.3 ± 0.2
	Stage A / Step IV	-44.2 ± 0.7 -5.1 ± 0.3	NA NA	NA NA	-41.0 ± 2.5 -4.9 ± 0.5
	Stage B / Step VI	16.1 ± 1.3 12.0 ± 0.2	16.8 ± 2.6 13.0 ± 0.8	15.5 ± 2.8 11.9 ± 0.8	16.9 ± 4.7 12.4 ± 1.3
	Stage B / Step VIII	24.3 ± 0.7 11.8 ± 0.2	NA NA	NA NA	23.3 ± 1.7 13.3 ± 0.3
Tension effect experiment	Stage A / Step II	-54.7 ± 1.7 -8.5 ± 0.2	-50.6 ± 0.4 -6.8 ± 0.3	-50.2 ± 0.6 -7.4 ± 0.1	-51.1 ± 2.1 -7.0 ± 0.4
	Stage A / Step IV	-46.0 ± 0.4 -7.0 ± 0.2	-42.6 ± 0.4 -5.4 ± 0.5	-43.4 ± 1.1 -6.2 ± 0.1	-41.5 ± 1.2 -5.7 ± 0.5
	Stage B / Step VI (wet soil)	-51.4 ± 0.8 -7.6 ± 0.0	-46.4 ± 0.7 -5.5 ± 0.3	-47.4 ± 1.0 -6.7 ± 0.2	-42.3 ± 0.6 -5.2 ± 0.0
	Stage B / Step VI (dry soil)	7.7 ± 0.23 -4.2 ± 1.1	NA NA	NA NA	18.2 ± 1.4 0.2 ± 0.2

Table 2-2 : Repeatability coefficient (RC, ‰) for the in situ online (IS), cryogenic vacuum distillation (CVD), centrifugation (CF), and direct water vapor equilibration (DVE) methods in each of the vessels where the isotopic composition (i.e., δ^2H and $\delta^{18}O$) of soil water was measured: steps II, IV, VI, and VIII in the memory effect experiment and steps II, IV, and VI in the tension effect experiment. For IS, RC-values (in parenthesis) considering the isotopic determinations in all vessel and not only in those destructively sampled could be calculated.

	Description	**IS**	**CVD**	**CF**	**DVE**
		RC δ^2H RC $\delta^{18}O$			
		‰			
Memory effect experiment	Stage A / Step II	5.4 (4.0) 0.3 (0.5)	4.8 0.7	0.7 0.2	3.6 0.6
	Stage A / Step IV	1.9 (1.7) 0.9 (0.8)	NA NA	NA NA	7.0 1.2
	Stage B / Step VI	3.5 (2.7) 0.7 (0.4)	7.1 2.3	8.6 2.6	12.9 3.7
	Stage B / Step VIII	1.8 (2.5) 0.6 (0.8)	NA NA	NA NA	4.6 0.7
Tension effect experiment	Stage A / Step II	4.7 (3.0) 0.4 (0.3)	1.1 0.9	1.7 0.3	5.8 1.0
	Stage A / Step IV	1.0 (1.7) 0.5 (0.5)	5.4 1.3	1.7 0.3	3.4 1.4
	Stage B / Step VI (wet soil)	2.2 (2.5) 0.0 (1.1)	1.9 0.9	2.4 0.7	1.6 0.1
	Stage B / Step VI (dry soil)	0.7 3.0	NA NA	NA NA	3.9 0.7

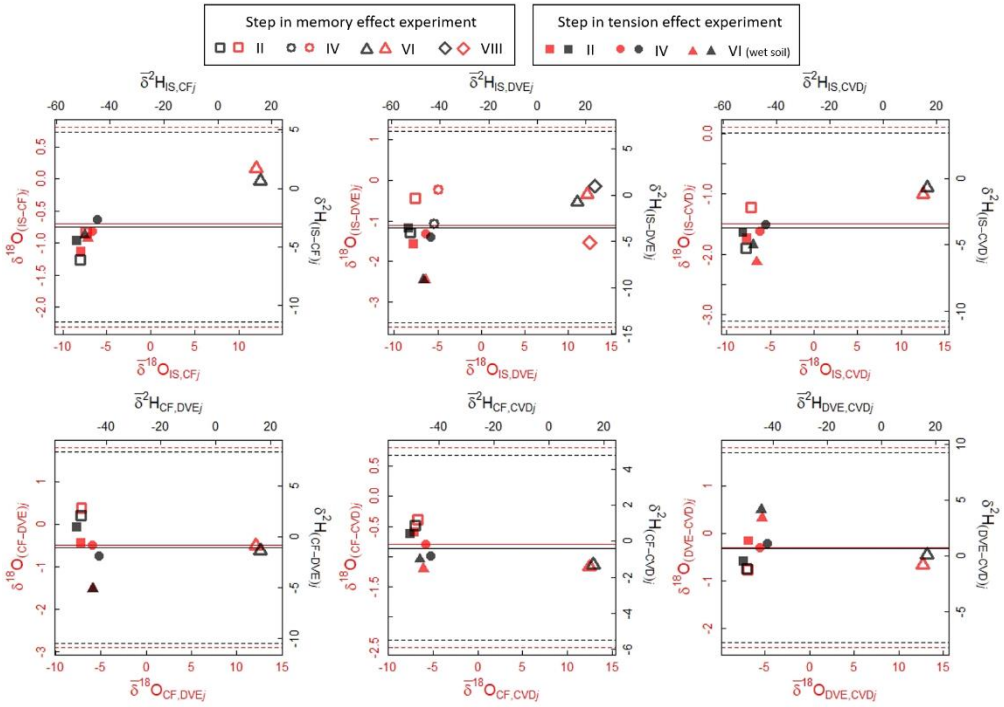

Figure 2-10 : Bland-Altman plots for the comparison in pairs of the four discrete isotopic methods (in situ online, IS; cryogenic vacuum distillation, CVD; centrifugation, CF; and direct water vapor equilibration, DVE) used to measure the δ-value (‰) of water at different steps (II, IV, VI, and VIII) during the memory and tension effect experiment (steps II, IV, and VI)**.** In each plot, the difference between the δ-value calculated with method A and method B (i.e., $\delta_{(A-B)j}$, ‰) is displayed as a function of the mean δ-value calculated with method A and method B (i.e., $\bar{\delta}_{A,Bj}$, ‰). The continuous horizontal line represents the mean $\delta_{(A-B)j}$ (i.e., $\bar{\delta}_{(A-B)j}$, ‰). The discontinuous horizontal lines are the upper (UL, above $\bar{\delta}_{(A-B)j}$, ‰) and lower limits (LL, below $\bar{\delta}_{(A-B)j}$, ‰) calculated with the corrected standard deviation of $\bar{\delta}_{(A-B)j}$ (i.e., $\hat{s}_{diff}$, ‰).

3.4. Different water pools sampled with different extraction methods?

Since the differences we observed between the isotopic determinations from the discrete methods were greater than 1‰ in δ^2H and 0.5‰ in $\delta^{18}O$, we reject our null hypothesis c): the isotopic composition of soil water measured or extracted using IS, CF, CVD, and DVE was not comparable. Considerable isotopic differences between methods, like the ones we present here, have been reported. Tsuruta et al. (2019) reported differences of up to 17.5 and 1.8‰ in δ^2H and $\delta^{18}O$, respectively, between determinations via CF and CVD. Kübert et al. (2020) reported isotopic differences between IS and CVD of up to 152.2‰ in δ^2H and 14.2‰ in $\delta^{18}O$ rooted mainly in

spatial heterogeneity in the field following isotopic labelling. Oerter & Bowen (2017) reported a difference of up to 30‰ in δ^2H and 4‰ in $\delta^{18}O$ between IS and CVD in natural samples (spatial heterogeneity could have contributed greatly to the observed differences). In our controlled laboratory study, the highest absolute difference in δ^2H and $\delta^{18}O$ were 15.4‰ and 4.1‰, respectively, between IS and CVD.

In both the memory and tension effect experiments, the following trend of the Δ-values was observed: IS < CF < DVE < CVD. It could be hypothesized that we determined the isotopic composition of different soil water pools with different degrees of mixing (e.g., Adams et al., 2020; Geris et al., 2015; Landon et al., 1999; Oerter & Bowen, 2017) or equilibration (e.g., Hsieh et al., 1998) with each method, a conclusion presented in several studies. For example, Figueroa-Johnson et al. (2007) explained that there was a concentration gradient of the water stable isotopes around the soil particles after extracting isotopically enriched water with CF (water held at low soil water tension or "mobile water") and depleted water with azeotropic distillation (water held at high soil water tension or "immobile water"). Likewise, Adams et al. (2020) concluded that soil water extracted via CF was biased (i.e., isotopically more similar) towards the mobile pool, whereas soil water extracted via CVD was biased towards the immobile pool. Moreover, Orlowski et al. (2018) call cryogenic vacuum distillation a "brute force technique" with which water held at a wide range of soil tensions can be extracted. Geris et al. (2015) found the following trend in the isotopic composition of extracted soil water in the field: porous rhizon samplers > CF > CVD, matching the decreasing ability of the methods to extract water at increasing soil tensions.

The two main water pools in the soil in our study would be tap water and enriched water in the memory effect experiment, and residual water in the dry soil and tap water in the tension effect experiment. The isotopic composition of the mobile water (theoretically sampled via CF) in stage A extraction in the memory effect experiment and in the tension effect experiment would be close to that of tap water, whereas in stage B extraction in the memory effect experiment, it would be closer to that of enriched water. This means that Δ measured via CF before stage B extraction in the memory effect experiment (step VI, Fig. 2-4) would have been higher (i.e., closer to the isotopic composition of recently added enriched water) than that measured via DVE or CVD. Likewise, the isotopic composition of soil water (mobile and immobile) measured via DVE and CVD would be closer to the mixture of depleted and enriched water. However, this is not what we observed. Additionally, we did not observe comparable results from the IS method and DVE, even though both methods are based on measurements of the isotopic composition of soil water vapor.

The presence of isotopically distinct soil water pools that incompletely mix (Sprenger et al., 2018; Thielemann et al., 2019), spatial heterogeneity (both in soil water content and soil water isotopes), and methodological issues (that led to soil water evaporation) together, allow us to explain the "disagreement" between the isotopic measurements from each method. A disagreement clearly reflected in the important span between the upper and lower limits in the Bland-Altman plots (Fig. 2-10). Regarding spatial heterogeneity, isotopic measurements of all discrete methods

might have been similarly representative at near-saturation conditions: Quade et al. (2019) reported representative soil volumes between CVD and IS of the same order of magnitude. However, they also reported a ten-fold increase of the representative soil volume for IS in dry conditions while the representative soil volume for CVD decreased. Regarding the methodological issues, the preponderance of isotopic fractionation during collection and handling of the soil samples followed the same trend as the isotopic measurements (IS < CF < DVE < CVD).

We believe that the above-presented order of the methods in the observed trend in the isotopic measurements might not have changed if we had used a soil with a higher clay content. However, the differences between methods and with the spike water might have been higher. Additionally, water extraction with certain methods might have been more challenging: no water extracted via CF or incomplete water extraction via CVD at relatively higher soil water contents.

As explained in several studies, there are isotopic exchanges happening among the different water pools in the soil. We observed this during stage B extraction in the memory effect experiment, in the overall match between the isotopic composition of the pressure-extracted water and the theoretical δ-value of a perfect mix between remaining tap water and added enriched water. Sprenger et al. (2018) compared experimental data with a two-pore domain model and found a better match when using a conceptualization of co-existing and interacting (i.e., isotopic exchange via water vapor) water pools in the soil. Thielemann et al. (2019) considered the idea that the water pools in the soil are not in isotopic equilibrium as unlikely. The extracted soil water in their study differed from the spike water due to exchanges with residual soil water.

Since elimination of residual water content might require drying the soil at very high temperatures (>~200°C; Thielemann et al., 2019; Wen et al., 2021) changing its physicochemical properties in the process, the suitability of spike experiments to investigate soil-related isotopic fractionation could be questioned. Considering the collected evidence so far, pointing towards spatial and temporal heterogeneity of the isotopic composition of water in the soil, spike experiments might be just part of an experimental strategy when studying soil-related isotopic fractionation.

Finally, it could be argued that certain methods might not be suitable for root water uptake studies since plants might access water held at higher soil tensions (McDonnell, 2014) not extractable with these methods (e.g., centrifugation). Since the debate regarding soil-related isotopic fractionation and the role of moisture history in the interactions of isotopically distinct soil water pools is still open, we agree with the statement of Penna et al. (2020): “it is important to sample potential soil source water that is held across the variability of soil water tensions and at multiple times”. That is, we might be able to describe better the spatial and temporal variability of soil water isotopic composition and of root water uptake if we use several isotopic methods in the same study.

4. Conclusions

Soil water fractionation during water extraction or resulting from physicochemical interactions with the soil matrix are two intertwined phenomena that add significant uncertainties to quantification and spatio-temporal distribution analysis of root water uptake and of soil water isotopes. Disentangling these processes and measuring their impact in soil water isotopic analysis would contribute to a better understanding and description of water fluxes in the soil-plant-atmosphere continuum. By using "isotopically inert" soils, we aimed at exploring soil water mixing processes, soil-tension-related isotopic fractionation and methodological constrains of some of the established water extraction techniques. We partially accepted null hypothesis a), that is, remaining tap water in the soil did mix with the newly added, isotopically enriched water. However, the observed zigzagging pattern in the time series of the stage B extraction in the memory effect experiment pointed towards a certain degree of incomplete mixing in some areas. We rejected null hypothesis b): the isotopic composition of soil water changed as a function of the estimated soil water potential value (i.e., from saturation to residual water content). The explanation for these differences was of a methodological nature and potentially caused or enhanced by low soil water potential values. No quantitative assessment of a soil tension fractionating effect could be done. Likewise, we rejected hypothesis c): there were considerable differences between the measurements from three destructive methods (centrifugation, direct water vapor equilibration, and cryogenic vacuum distillation) and the in situ online method. The in situ online method had the best repeatability, followed by centrifugation. However, we could not extract soil water via centrifugation from dry soil samples (i.e., soil water content < 4%). The discrepancies in the isotopic determinations (either among methods or with reference water) were mostly related to moisture history, spatial heterogeneity, and potential methodological issues than to soil texture or soil tension fractionating effects. Spike experiments, comparison between isotopic methodologies (especially between those relying on destructive sampling and in situ ones), and complementary use of these techniques for the characterization of (soil-texture- and -tension-related) isotopic fractionation can enhance the accuracy of soil water isotopic measurements. Ultimately, this will contribute to the validation and standardization of water stable isotopic monitoring in (eco)hydrological studies.

5. Supplementary material

We calculated the parameters of a linear and an exponential model fitted to our data points: difference between the δ-value of the water extracted daily from the pressure plate extractors and the δ-value of the reference water (Δ, ‰) as a function of amount of pressure-extracted water (w, g) (Eq. S2-1 for the exponential model) and as a function of soil water potential (ψ, pF) (Eq. S2-2 for the exponential model). The values of the parameters of the fitted models are summarized in Table S2-1.

$$\ln \Delta = \ln a + \omega * \ln b$$

Equation S2-1

$$\ln \Delta = \ln a + \psi * \ln b$$

Equation S2-2

Table S2-1 : Values of the parameters (a, b, and r^2 or ln a, ln b, and r^2) of the linear (a + b*w = Δ; a + b*ψ = Δ) and exponential (ln a + ln b*w = ln Δ ; ln a + ln b*ψ = ln Δ) models fitted to our data. All sets of parameters were statistically significant (i.e., $p < 0.05$).

	Memory effect experiment		**Tension effect experiment**	
Description	**^{2}H**	**^{18}O**	**^{2}H**	**^{18}O**
Δ as a function of soil water potential (ψ, pF) during stage A extraction	a = -18.15 b = 12.90 r^2 = 0.49 ln a = -4.41 ln b = 3.30 r^2 = 0.39	-5.22 3.66 0.53 -5.73 3.32 0.63	-9.25 8.45 0.11 -1.31 1.59 0.08	-1.92 1.94 0.14 -2.49 1.59 0.16
Δ as a function of soil water potential (ψ, pF) during stage A and B extraction	-12.82 9.22 0.14 NA NA NA	-3.64 2.58 0.15 NA NA NA	-5.35 5.18 0.10 -0.18 0.99 0.13	-0.88 1.05 0.13 -1.50 0.96 0.19
Δ as a function of the amount of extracted water (w, g) during stage A extraction	4.39 -0.17 0.16 1.34 -0.04 0.11	1.18 -0.05 0.17 0.07 -0.05 0.21	4.13 -0.16 0.13 1.25 -0.05 0.19	1.19 -0.4 0.17 0.08 -0.04 0.20
Δ as a function of the amount of extracted water (w, g) during stage B extraction	NA NA	NA NA	NA NA	1.21 -0.01

	NA	NA	NA	0.10
	NA	NA	NA	0.11
	NA	NA	NA	-0.03
	NA	NA	NA	0.31
Δ as a function of the amount of extracted water (w, g) during stage A and B extraction	3.46	0.90	3.16	0.86
	-0.17	-0.05	-0.05	-0.01
	0.15	0.15	0.02	0.05
	1.58	0.40	1.40	0.08
	-0.04	-0.03	-0.01	-0.01
	0.09	0.08	0.05	0.09

Chapter 3

Response of a grassland species to dry environmental conditions from water stable isotopic monitoring

In this chapter, a slightly modified version of the study of Deseano Diaz, van Dusschoten, et al. (2023) is presented. The conclusion reached in the first study (chapter 2) that no soil texture, soil tension or soil water mixing processes affected the isotopic determinations in a loamy sand via the in situ online method, both used in this second study, meant that no additional correction steps in the estimation of soil water δ-values were necessary. The specific objective in this second study (O.2) was to conduct an ecohydrological assessment of the response to drought of *Centaurea jacea* L. at the single plant scale in controlled laboratory conditions from an isotopic perspective (see chapter 1 section 5). Kübert et al. (2019, 2020, 2021) observed a decline in abundance of this forb species and described a positive link between the plant- and ecosystem-level water use strategies in a semi-natural temperate grassland in the southwest of Germany during experiments conducted in the framework of the research program this doctoral project was embedded in. We hypothesized (H.2) that the drought resistance at the single plant scale and in controlled conditions of *C. jacea* L. would be related to efficient water use and RWU plasticity.

In section 1, the contribution of water stable isotopic monitoring to the ultimate goal of (eco)hydrological studies is described: advance a mechanistic understanding of the biotic and abiotic interactions in the soil-plant-atmosphere continuum underlying water, nutrient, and carbon cycles. Thanks to advances in non-destructive in situ isotopic, root system imaging, and plant physiology monitoring, RWU dynamics and the driving mechanisms can be investigated with data sets with a high spatio-temporal resolution.

In section 2, a detailed description of the semi-automated experimental setup, in which plant physiological, as well as above- and below-ground environmental conditions were concurrently and non-destructively monitored, is offered. Moreover, the probabilistic isotope-based estimation of RWU profiles with a multi-source mixing model in a Bayesian statistical framework is detailed.

The results and discussion from the 87 days of semi-automated concurrent monitoring are presented in sections 3 and 4. As hypothesized (H.2), *Centaurea jacea* L. displayed efficient water use: leaf gas exchange could be maintained, even in moderate dry conditions, because leaf water potential could drop to low values. Canopy conductance decreased at a relatively high soil water content, evidencing an active control of the plant to water loss and ultimately, hydraulic failure. RWU profiles were similar in varying hydroclimatic conditions but short-term water uptake dynamics were observed.

In section 5, the main conclusions of this study are presented in short. Namely, there was an apparent reliance of the studied forb species on water in shallow depths, partly linked to water availability and root distribution. The strategies of *Centaurea jacea* L. to maintain high water use efficiency and cope with dry conditions might not ensure its survival or competitiveness in terminal or extended drought periods.

To broaden the insights enabled by the isotopic approach of this second study, RWU was estimated in a third study (see chapter 4) also from a hydraulic perspective, that is, considering the dynamics of plant and soil hydraulic properties in plant water use

and, more specifically, their link to canopy conductance. Non-destructive continuous monitoring of biotic and abiotic parameters in varying hydroclimatic conditions could provide highly spatio-temporally resolved data sets, as well as insights into the links in the soil-plant continuum to test, improve, and extend soil-vegetation-transfer models. This could ultimately result in more accurate and precise predictions of the impacts of climate change across spatial scales.

1. Introduction

In recent years, some researchers aim at investigating the strategies and mechanisms plants use to cope with dry soils and high temperatures from an ecohydrological perspective. That is, understanding the dynamic relationship between hydrological and biogeochemical processes within the plant community and between soil and vegetation (e.g., Newman et al., 2006; Dubbert, Piayda, et al., 2014; Chitra-Tarak et al., 2021) and how these links are impacted by climate change. Grasslands are a popular subject in ecohydrological studies due to the marked dependency of biological processes to changes in hydroclimatic conditions in these ecosystems (Yang et al., 2016; Zwicke et al., 2015) and their rapid response to these changes by setting in motion ecosystem-regulating processes (Jentsch et al., 2011). *Centaurea jacea* L. (brown knapweed), an ubiquitous forb native to grasslands, meadows and open well-lit spaces in Europe, North Asia, and Northwest Africa (Hegi, 1954) is well adapted to dry conditions and therefore a feasible study species for getting a mechanistic understanding of the interactions in the soil-plant-atmosphere continuum in an environment highly dependent on water from precipitation.

The difference between water potential in the soil and in the surrounding environment drives RWU and the magnitude of this difference depends on the rate of plant transpiration (Carminati & Javaux, 2020). Plants actively control transpiration rate by opening or closing the stomata to "limit the variation in plant water potential with soil moisture and evaporative demand" (Sperry et al., 2002). It is an established belief that plant species in drying soil either set a relatively high leaf water potential limit by an "early" closing of the stomata (i.e., isohydricity) or display a less strict stomatal control and much lower leaf water potential values (i.e., anisohydricity) (Maseda & Fernández, 2006; Tardieu & Simonneau, 1998). The magnitude and timing of stomata closure is pivotal, because through this process plants avoid hydraulic failure (i.e., xylem embolism) but it also causes the reduction of photosynthetic activity (Cowan & Farquhar, 1977).

Evaluating stomatal control and quantifying RWU assist in the assessment of the role of water and nutrient availability, root distribution, radiation, temperature, relative humidity, among other factors, in the response of plants to dry conditions. Because many of these factors vary constantly in time and space, both stomatal control and RWU are highly dynamic processes. A single plant species might display iso- or anioshydric behavior depending on the environmental conditions and describing water uptake patterns might be challenging (Rothfuss & Javaux, 2017), when relying on destructive sampling of soil and plant material at low spatio-temporal resolution. Non-destructive water stable isotopic monitoring coupled with laser-based spectroscopy has shown its potential in helping to overcome this challenge. In this method, the isotopic composition of soil water – that is, the relative ratio between the least abundant, ^{2}H and ^{18}O, and most abundant isotopes, ^{1}H and ^{16}O, i.e. $\delta^{2}H$ and $\delta^{18}O$, expressed in per mille (‰) – is computed from the measured isotopic composition of sampled water vapor. This method can be used in saturated and unsaturated soils in

both the lab and the field at different depths of the soil profile (Quade et al., 2018; Rothfuss et al., 2013).

According to Rothfuss & Javaux (2017), several methods exist to quantify RWU using the isotopic composition of different soil layers or depths ("sources") and the isotopic composition of plant transpiration ("product"). Multi-source (MS) mixing models with a Bayesian statistical approach do seem to outperform the graphical inference method and the two-end-member mixing model. The most popular MS mixing model embedded in a Bayesian framework is the one developed by Parnell et al. (2010). The authors developed the Stable Isotope Analysis with R (SIAR) for dietary source partitioning, but it has proven quite suitable for RWU quantification (e.g., Prechsl et al., 2015; Volkmann et al., 2016; Beyer et al., 2018). This tool coupled with non-destructive isotopic monitoring allows the calculation of RWU profiles with a 1-cm spatial and daily temporal resolution.

Since RWU is a process that depends on both above- and below-ground processes, it is essential to obtain comprehensive data sets in which both environmental and plant-related variables are simultaneously monitored. Comparing the evolution of these two types of variables can help in understanding the role of soil and leaf water status, and of root distribution on RWU, especially during drought. Moreover, this comparison can also help in describing the direction and magnitude of the links between environmental demand and soil water status, and stomatal conductance and leaf gas exchange. Therefore, our main purpose was to assess the performance of the drought-resistant grassland species *Centaurea jacea* L. under varying above- and below-ground environmental conditions. More specifically, we aimed at i) linking leaf water status (i.e., leaf water potential) and gas exchange (i.e., CO_2 assimilation rate, canopy conductance, transpiration rate) with changes in environmental conditions (i.e., vapor pressure deficit and soil water content) and ii) describe the role of root length density in RWU in both wet and dry environmental conditions in the soil and the atmosphere.

2. Materials and methods

In the following subsections, our experimental setup is described in detail (a schematic view is presented in Fig. 3-1), as well as the measurement sequences and calculations used to determine and monitor above- and below-ground conditions and plant physiological variables. All calculations were done using the software R (R Core Team, 2020).

2.1. Soil columns and soil water isotopic measurements

Three columns made of PVC and one acrylic column (11 cm diameter, 60 cm length, 5.7 l volume) were filled with loamy sand (standard soil 2.1, particle size distribution: 84.7% 2–0.063 mm, 11.4% 0.063–0.002 mm, 3.9% < 0.002 mm; LUFA Speyer, Germany) from which the largest ferromagnetic particles were removed. This was done in a semi-automated custom-made system, in which the soil is spread in a thin layer and passes under a set of rare earth magnets (NdFeB, 9 x 4 x 1 cm^3 size) on a conveyor belt (van Dusschoten et al., 2016). The removal of large ferromagnetic

particles is a critical step to avoid interferences in root observations with MRI. The standard soil was used to be able to observe a higher percentage of roots measured with MRI in the PVC columns, referred to as “MRI columns” from this point onwards (Pflugfelder et al., 2017).

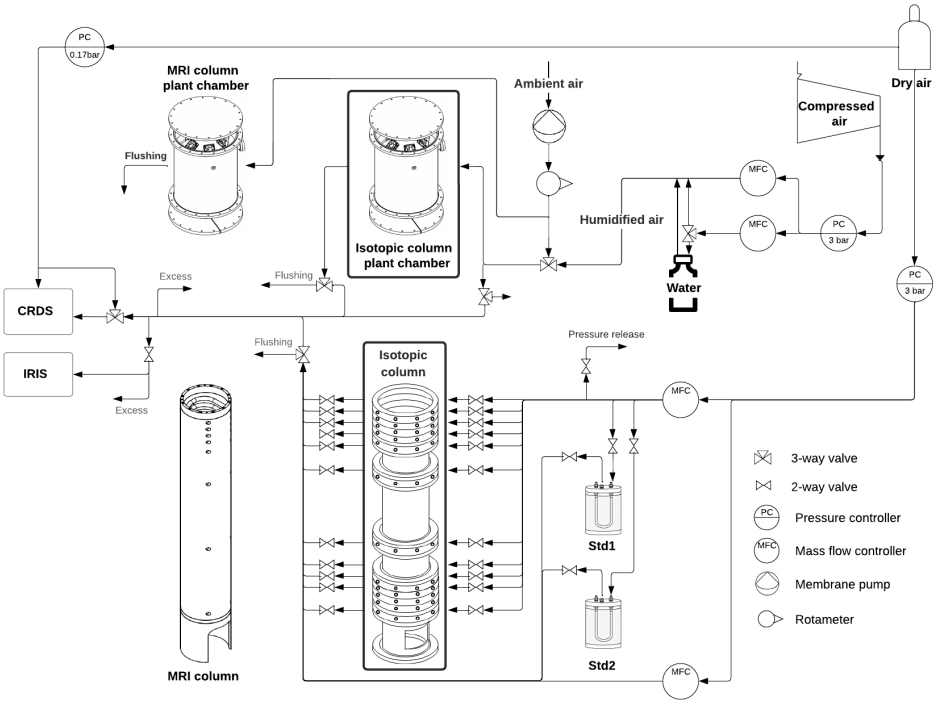

Figure 3-1 : Piping and instrumentation diagram (PID) of the experimental setup placed in a climate chamber (temperature = 19 ± 0.22°C and relative humidity = 64.7 ± 1.3%): one isotopic column (framed by a black empty polygon), three magnetic resonance imaging (MRI) columns (only one is depicted next to the isotopic column), and a plant chamber over each column (a total of four, the isotopic column plant chamber framed by a black empty polygon and only one MRI column plant chamber are depicted). The relative humidity inside the isotopic column plant chamber was changed by increasing or decreasing the amount of water vapor saturated air from a water bottle mixed with compressed air (upper right section) entering the plant chamber. All soil water vapor isotopic measurements were done online with a cavity ring-down spectrometer (CRDS) in the isotopic column and the rate and isotopic composition of plant transpiration was measured using the isotopic column plant chamber. The isotopic standards used were labeled Std1 and Std2. CO_2 mixing ratio determinations in the isotopic column plant chamber were conducted with an Isotope Ratio Infrared Spectrometer (IRIS). The MRI columns were used to monitor root distribution on day after seeding (DaS) 237 and 307. The MRI columns and their respective plant chambers were not connected to the semi-automated water vapor sampling system and the MRI column plant chambers were flushed with air circulating in the climate chamber using a membrane pump and a rotameter.

The dry bulk density was determined at 1.54 and 1.47 g cm^{-3} for the MRI columns and acrylic column, referred to as "isotopic column" from this point onwards, respectively (Fig. 3-1).

The soil water vapor was sampled using the method described in Rothfuss et al. (2013) at eleven depths (1, 3, 5, 7, 10, 20, 40, 50, 53, 55, and 59 cm) in the isotopic column through a 17.5 cm-long gas-permeable polypropylene tubing (Accurel® PV8/2HF, 0.155 cm wall thickness, 0.55 cm i.d., 0.86 cm o.d., 0.2 µm pore size; 3M, USA). Temperature was recorded at the aforementioned depths using thermocouples (type K, 0.01°C precision; Greisinger electronic GmbH, Regenstauf, Germany). θ, (cm^3 cm^{-3}) was recorded at depths of 1, 10, 50, and 59 cm with frequency domain sensors (EC-5, 0.001 m^3 m^{-3} precision; Decagon Devices, USA). According to Bogena et al. (2007), the accuracy of this sensor is lower, around 1-2 % volume, when temperature, electric conductivity, and supply voltage effects on the readings are taken into account. θ was recorded at depths 15, 25, and 34 cm with fixed capacitor sensors, similar to the ones used in the soil water profiler (SWaP, accuracy of 0.002 cm^3 cm^{-3}) described in van Dusschoten et al. (2020). A calibration curve for each and one of the sensors was obtained at the same temperature, supply voltage, and with the same soil used in our experiments by recording the sensors' readings in soil with known volumetric water content.

The water vapor inside the tubing in each soil depth was sampled two times a day for 30 min with synthetic dry air (20.5% O_2 in N_2 with approximately 20–30 ppmV water vapor; Air Liquide, Germany) at low flow rate (approximately 70 ml min^{-1}). The mixture of dry air and water vapor was carried to a CRDS (L2130-i; Picarro, Santa Clara, USA) for online isotopic measurements. The δ^2H- and $\delta^{18}O$-value was calculated from the last 330 readings of the plateau (representing approximately the last 5 min and 30 seconds out of the 30 min of measurements). The corresponding liquid water δ-value was calculated using the equations given by Majoube (1971) at the temperature measured at the observation depth, assuming a thermodynamic equilibrium between soil liquid water and water vapor. To account for the water vapor mixing ratio dependency of the CRDS measurements, the liquid water mean δ-value was recomputed to a value of water vapor mixing ratio of 17,000 ppmV. Finally, this recomputed value was calibrated on the V-SMOW scale using two soil water vapor standards, as described in Rothfuss et al. (2015) (Std1 and Std2 in Fig. 3-1). Each standard consisted of a smaller acrylic glass vessel filled with the same type of soil as the four columns containing a piece of gas-permeable tubing. The soil in one of the vessels was saturated with isotopically enriched water (δ^2H = 102.4 ± 1.4‰ and $\delta^{18}O$ = 30 ± 0.3‰), whereas the soil in the second vessel was saturated with isotopically depleted water (δ^2H = -78.4 ± 0.6‰ and $\delta^{18}O$ = -18.8 ± 0.1‰).

2.2. Plant chamber and leaf measurements

A custom-made cylindrical plant chamber (29 cm diameter, 35.5 cm length, 23 l volume) was used to determine the isotopic composition and rate of plant transpiration and CO_2 assimilation of the plant growing in the isotopic column. The plants in the MRI columns were also enclosed each in a plant chamber with the same dimensions

and were continuously flushed with ambient air using a membrane pump (Fig. 3-1). However, no isotopic or plant transpiration measurements were performed there. Each chamber was equipped with an air relative humidity (rh) and temperature (T) sensor (RFT-2, rh = 2% and T = 0.1°C precision; METER Group, Munich, Germany) and enclosed a single plant individual. The soil surface of each column was covered with aluminum foil to avoid soil water evaporation. The air entering the plant chamber over the isotopic column (i.e., inlet airstream) was a mixture of ambient air and water vapor from a dew point generator (i.e., a water bottle equipped with an air diffuser, see Fig. 3-1). The outlet airstream from the plant chamber was a mixture of inlet airstream and plant transpiration. The inlet and outlet airstream were kept constant during each experimental period (Table 3-1) and were sampled six and three times per day for 31 min, respectively. The inlet airstream was sampled directly before and after each outlet airstream measurement. The isotopic composition and mixing ratio of the water vapor in the inlet and outlet airstream were measured using the CRDS, and the mixing ratio of CO_2 was determined using an Isotope Ratio Infrared Spectrometer (IRIS, Delta Ray™; Thermo Scientific™, USA). These measurements were done five, eight, and eleven hours after a fully programmable water-cooled LED panel (4 x 14 LED lamps à 20 W, 3200K; Cree LED, USA) was switched on.

Table 3-1 : Measured mean values of air temperature (T, °C), relative humidity (rh, %), light intensity (mmol s^{-1} m^{-2}), soil water content (θ, cm^3 cm^{-3}), and computed values of vapor pressure deficit (vpd, kPa) and transpiration rate (Tr, mmol s^{-1} m^{-2}) inside the isotopic column plant chamber for the different experimental periods in days after seeding (DaS). Values of vpd and Tr were calculated using Eq. 3-1 and 3-3**.**

Period (DaS)	**T (°C)**	**rh (%)**	**vpd (kPa)**	**Light intensity (mmol s^{-1} m^{-2})**	**θ (cm^3 cm^{-3})**	**Tr (mmol s^{-1} m^{-2})**
231 - 232	21.8 ± 0.0	73.2 ± 0.2	0.7 ± 0.0	~500	0.22 ± 0.01	3.5 ± 0.1
234 - 235	21.8 ± 0.1	65.9 ± 1.7	0.9 ±0.0	~500	0.21 ± 0.01	4.2 ± 0.1
237 - 240	22.4 ± 0.2	70.5 ± 0.3	0.8 ± 0.0	~500	0.21 ± 0.02	2.8 ± 0.4
243 - 248	22.5 ± 0.1	62.7 ± 1.4	1.0 ± 0.0	~500	0.18 ± 0.01	3.4 ± 0.2
250 - 253	22.3 ± 0.2	43.0 ± 1.1	1.5 ± 0.0	~500	0.15 ± 0.01	4.1 ± 0.3
256 - 267	22.4 ± 0.2	67.1 ± 0.6	0.9 ± 0.0	~500	0.19 ± 0.02	2.9 ± 0.1
269 - 278 (HTr-I)	23.1 ± 0.5	50 ± 2.7	1.4 ± 0.1	~1000	0.17 ± 0.02	6.5 ± 0.5
280 - 290 (HTr-II)	24.5 ± 0.0	67.4 ± 0.7	1 ± 0.0	~1000	0.14 ± 0.01	4.7 ± 0.3
292 - 316 (LTr-I)	22.6 ± 0.2	68.8 ± 1.1	0.9 ± 0.0	~500	0.17 ± 0.03	2.9 ± 0.1
318 - 323 (HTr-III)	24.4 ± 0.1	42.4 ± 2.2	1.8 ± 0.1	~1000	0.10 ± 0.02	4.7 ± 0.5
325 - 327 (LTr-II)	22.7 ± 0.0	50.3 ± 2.5	1.4 ± 0.1	~500	0.06 ± 0.00	1.3 ± 0.2

Leaf water potential (ψ_l, MPa) of the plant in the isotopic column was monitored every 30 min using a psychrometer (PSY1, 0.1 MPa precision; Armidale, NWS, Australia). A broad leaf was selected and the surface over the midrib was carefully rubbed with sandpaper to expose the xylem. Afterwards, the leaf was rinsed with distilled water and the excess water was wiped. Then, the chamber of the psychrometer with greased edges was placed over the exposed midrib and fixed with a leaf clamp. The psychrometer was re-installed in this manner several times, because the leaf it was attached to had withered.

The vapor pressure deficit (vpd, kPa) inside the plant chamber was computed using Eq. 3-1 (Murray, 1966).

$$vpd = \frac{100 - rh'}{100} 0.61078 e^{\frac{17.27 \times T_{leaf}}{T_{leaf} + 237.3}}$$

Equation 3-1

where T_{leaf} (°C) is the leaf temperature measured with the psychrometer and rh' (%) is the air relative humidity normalized to T_{leaf} calculated using Eq. 3-2.

$$rh' = rh\left(\frac{P_{air}}{P_{leaf}}\right)$$

Equation 3-2

where rh (%) is the air relative humidity, and P_{air} and P_{leaf} are the vapor saturation pressure at the air and leaf temperature (kPa), respectively. The plant transpiration rate (Tr, mmol s^{-1} m^{-2}) was calculated using Eq. 3-3 (von Caemmerer & Farquhar, 1981).

$$Tr = \frac{u_{in}(w_{out} - w_{in})}{s(1 - w_{out})}$$

Equation 3-3

where w_{in} (-) and w_{out} (-) are the mixing ratio of the water vapor in the inlet and outlet airstream of the plant chamber, respectively; u_{in} (mmol s^{-1}) is the molar flow of air into the plant chamber and s (m^2) is the soil surface area of the column (0.0095 m^2). The isotopic composition of plant transpiration (δ_{Tr}) was calculated using Eq. 3-4 (Dubbert, Cuntz, et al., 2014).

$$\delta_{Tr} = \frac{w_{out}\delta_{out} - w_{in}\delta_{in}}{w_{out} - w_{in}} - \frac{w_{in}w_{out}(\delta_{out} - \delta_{in})}{w_{out} - w_{in}}$$

Equation 3-4

where δ_{in} and δ_{out} are the isotopic composition of the water vapor in the inlet and outlet airstream of the plant chamber, respectively. The CO_2 assimilation rate (A, μmol s^{-1} m^{-2}) was calculated according to von Caemmerer and Farquhar (1981) (Eq. 3-5).

$$A = \frac{u_{in}}{s}\left[c_{in} - c_{out}\frac{(1 - w_{in})}{(1 - w_{out})}\right]$$

Equation 3-5

where c_{in} (-) and c_{out} (-) are the CO_2 mixing ratio in the inlet and outlet airstream of the plant chamber, respectively. The canopy conductance (G_s, mmol s^{-1} m^{-2}) was calculated using Eq. 3-6.

$$G_s = \frac{Tr}{vpd_l}$$

Equation 3-6

where vpd_l (kPa kPa^{-1}) is the air-to-leaf vpd obtained dividing vpd by ambient pressure in kPa. The instantaneous and intrinsic water use efficiency (WUE and iWUE, µmol CO_2 $mmol^{-1}$ H_2O, respectively) were calculated using Eq. 3-7 and Eq. 3-8, respectively.

$$WUE = \frac{A}{Tr}$$

Equation 3-7

$$iWUE = \frac{A}{G_s}$$

Equation 3-8

Finally, the standard error in the calculation of Tr and A was computed using a first order Taylor series.

The average conditions inside the plant chamber are summarized in Table 3-1. The temperature inside the plant chamber was modified by i) increasing or decreasing the light intensity of the LED panel and ii) increasing or decreasing its vertical distance to the columns. The relative humidity was changed by increasing or decreasing the amount of vapor saturated air (from the dew-point generator) in the plant chamber's inlet airstream. The flow of air into the plant chamber ranged from 4.3 to 11.9 l min^{-1}.

2.3. Isotopic labeling and drought experiment

The soil in the MRI and isotopic columns was saturated from the bottom with deionized tap water (δ^2H = -51.6 ± 0.6‰ and $\delta^{18}O$ = -7.7 ± 0.1‰) by applying a pressure head of around 1 m. Then, the columns were placed in a climate chamber (T = 19 ± 0.22°C and rh = 64.7 ± 1.3%) under the programmable water-cooled LED panel with a photoperiod of 14 h light and 10 h of darkness. The weight loss of the isotopic column was recorded (Plattformwaage DS, 0.2 g precision; Kern & Sohn GmbH, Germany) throughout the experiment to calculate the transpiration rate gravimetrically. *Centaurea jacea* L. was seeded shortly after saturation at a density of ~20 seeds per 95 cm^2. On day after seeding 6 (DaS 6), the first seedlings were

observed and on DaS 34, one individual was selected, while all other seedlings were removed.

The objective of our isotopic labeling strategy was i) to create differences in isotopic composition among the potential soil water sources for plant transpiration in order to constrain the results of the mixing model, and ii) to obtain complementary information from the δ^2H and $\delta^{18}O$ values by creating orthogonal profiles. The isotopic column was watered from the top using water low in δ^2H and high in $\delta^{18}O$ and from the bottom, using water high in δ^2H and low in $\delta^{18}O$ from DaS 256 to DaS 312 (Table 3-2). The plants in the MRI columns were watered using deionized tap water following the same protocol in terms of irrigation and timing. From DaS 313 to 327 no more water was added to the column in order to simulate a short drought period, during which vpd was modified by changing rh inside the plant chamber as explained at the end of section 2.2 of this chapter and by changing light intensity (Table 3-1).

2.4. Root distribution measurements

Before (DaS 237) and towards the end (DaS 307) of the isotopic labeling period, the root system of the plants in the three MRI columns was monitored using a 4.7 T MRI magnet (Magnex, Oxford, UK). It was determined that root segments with a diameter >~0.3 mm were visible. The root length in 2.5 cm-thick soil layers was obtained by processing the MRI images using the NMRooting software according to van Dusschoten et al. (2016).

Table 3-2 : Isotopic composition of labeled water used for the irrigation of the isotopic column and water amounts in the three labeling stages in days after seeding (DaS).

DaS	**Water added (mL)**		**Isotopic composition of labeled water**	
	Top	**Bottom**	**Top**	**Bottom**
256 - 261	-	15	Stage 1 $\delta^{18}O$ = 29.0‰ δ^2H = -78.4‰	Stage 1 $\delta^{18}O$ = -20.2‰ δ^2H = 104.7‰
263 - 269	60	-		
270	60	15		
271	60			
272 - 274	120	30		
276 - 278	200	60		
283	100	-		
285, 287, 290	100	15		
292	70	30	Stage 2 $\delta^{18}O$ = 29.0‰ δ^2H = -90.0‰	Stage 2 $\delta^{18}O$ = -20.2‰ δ^2H = 120.0‰
293 - 294	100	30		
296 - 298	50	30		
299 - 301	100	15		
305 - 308	100	30	Stage 3 $\delta^{18}O$ = 29.0‰ δ^2H = -90.0‰	Stage 3 $\delta^{18}O$ = -40.0‰ δ^2H = 220.0‰
310 - 312	40	-		

At the end of the experiment (DaS 327), the roots of the isotopic column were harvested from the soil layers 0-2, 2-4, 4-6, 6-8, 8-11, 11-21, 21-41, 41-51, 51-54, 54-56, 56-58, and 58-60 cm and scanned (Expression 10000XL Model J181A; EPSON, Japan). The images were analyzed using the WinRhizo™ (Regent Instruments Inc., Quebec, Canada) software package for the determination of the total root length in each of the aforementioned soil layers. The root length density (RLD, cm cm^{-3}) in each soil layer in the MRI columns and in the isotopic column was calculated using Eq. 3-9.

$$RLD_z = \frac{RL_z}{V_z}$$

Equation 3-9

where RL_z (cm) is the total root length in soil layer z and V_z (cm^3) is the soil volume of layer z.

Due to time and technical constrains, root distribution in the MRI columns was not measured with MRI at the end of the experiment (i.e., DaS 327), nor were the roots in these columns harvested and scanned. This decision did not limit the analysis of our results, since we did not aim at systematically comparing the scan and MRI methods.

2.5. Calculation of RWU profiles

The relative contribution to plant RWU from the different soil layers was calculated at a daily resolution using the Bayesian statistical model SIAR (Parnell et al., 2010) with the δ^2H and $\delta^{18}O$ of the soil and plant transpiration. The function used inside the SIAR package, i.e. *siarmcmcdirichletv4*, uses a Markov chain Monte Carlo algorithm to produce estimated proportions of the sources (i.e., $\delta_{soil\ water}$ in the different soil depths) in the observed mix or product (i.e., δ_{Tr}). The used prior distribution for the sources' proportions in this function is the Dirichlet. To obtain the sources' proportions or relative contributions of soil water at the eleven depths to plant transpiration we ran the function *siarmcmcdirichletv4* 1,000 times for each day from DaS 270 to 312. The number of iterations and values for burn-in and thinning in each of the runs were set at 500,000, 50,000, and 15, respectively. That is, in each run, 30,000 iterations out of 500,000 were considered for calculating the vector of most frequent relative contribution value for each depth (i.e., mfv). Since the mfv vector did not add up to one as each and one of the iterations did, the iteration (i.e., "best iteration") with the "greatest probability of occurrence" (as defined by Couvreur et al., 2020) was identified. The "best iteration" (or *bi*) was the vector of relative contribution values with the lowest root mean square error (RMSE) when compared with the mfv vector. That is, the *bi* minimized the following objective function (OF) in Eq. 3-10 (Couvreur et al., 2020).

$$OF = \sqrt{\frac{\sum_{J=1}^{11}(mfv_J - bi_J)^2}{11}}$$

Equation 3-10

The aforementioned process was performed 1,000 times and a "best run" out of the 1,000 *bi* was identified. A new mfv vector from the 1,000 *bi* was calculated and the vector of relative contribution values for a particular day was identified as the one with the lowest RMSE when compared with this new mfv vector.

The absolute contribution of each soil layer or sink term (cm^3 water cm^{-3} soil day^{-1}) to plant transpiration, referred to as "RWU profile" from this point onwards, was calculated as the product of transpiration rate and the relative contribution for each analyzed day at each depth. This value is always positive and this is why RWU values in our study are a quantification of the amount of water flowing only from the soil via the roots to the leaves on a daily basis. That is, we did not quantify the overall uptake by the roots at a certain depth, which includes also the water uptake that may be redistributed via the root system to other soil layers (i.e., plant-mediated water redistribution).

Additionally, RWU daily profiles were calculated using only δ^2H- or $\delta^{18}O$-values and they were statistically compared to the RWU profiles calculated with both δ^2H- and $\delta^{18}O$-values. First, the Shapiro-Wilk normality test was applied to every profile and, according to the result; either a paired t-test or the non-parametric paired Wilcoxon-test was used to compare the RWU profiles (Table S3-1). The analyzed periods were DaS 270 to 278, 280 to 290, 292 to 316, 318 to 323 and 325 to 327 referred to as HTr-I (high transpiration rate I), HTr-II, LTr-I (low transpiration rate I), HTr-III, and LTr-II, respectively.

3. Results

A brief summary of the evolution of measured and calculated variables is presented in section 3.1, followed by a description of the obtained isotopic profiles during and after the isotopic labeling in section 3.2. The series of calculations to obtain RLD profiles in the isotopic column and MRI columns is detailed in section 3.3. In section 3.4, we report on the observed RWU patterns of *Centaurea jacea* L.

3.1. Dynamics of environmental conditions and plant-related variables

The temporal variation of directly measured (air temperature - T_{air}, T_{leaf}, rh, ψ_l, and θ) and calculated variables (vpd, Tr, WUE, iWUE, A, and G_s) are shown in Fig. 3-2. In Fig. 3-2a the temporal variation of daily mean T_{leaf}, T_{air}, and rh values are displayed. T_{leaf} was slightly higher than T_{air} in some periods (up to 0.8°C). Tr dynamics was similar to the dynamics of vpd for most DaS (Fig. 3-2b), whereas A dynamics was similar to that of G_s (Fig. 3-2d). Note that G_s, Tr, and A started dropping progressively to zero from DaS 319 onwards, a trend that will be discussed in depth in section 4.1 in this chapter. Until DaS 322, ψ_l was higher than -1.5 MPa and after this point it decreased more markedly compared to previous periods: it decreased from -1.49 MPa to -3.19 MPa during the last six days of the experiment (Fig. 3-2c). The WUE remained constant until the end of LTr-I (DaS 313), after which it decreased until around DaS 320 (mid-HTr-III) with an again constant period until the end of the experiment. On the other hand, iWUE values were constant during the experiment and

even increased slightly during the last days (Fig. 3-2e). θ in the bottom half of the isotopic column was higher compared to θ in the top half until DaS 265. Afterwards, θ became more homogeneous across the whole soil column, ranging from 0.07 ± 0.01 to 0.24 ± 0.08 cm^3 cm^{-3} (Fig. 3-2f).

3.2. Isotopic labeling

After the first labeling stage from DaS 270 to DaS 290 (Table 3-2), the differences in $\delta_{soil\ water}$ values among layers were considerable only in layer 7-50 cm (Fig. 3-3a). Increasing and decreasing the δ-value of the added labeled water (labeling stage 2 and 3 in Table 3-2) resulted in a progressively steeper isotopic gradient in layer 7-50 cm (Fig. 3-3b and c), while a steep gradient in layer 50-60 cm was reached until labeling stage 3 (Fig. 3-3c). Nonetheless, the isotopic profile in layer 0-7 cm remained homogeneous from the beginning of the labeling until DaS 318. That is, no gradient was observed during the three labeling stages.

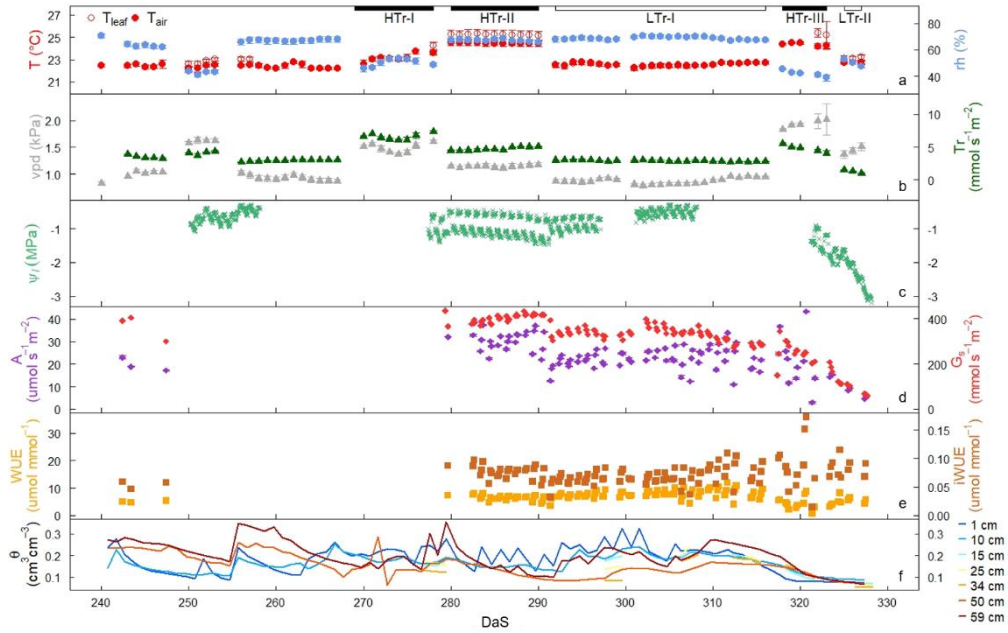

Figure 3-2 : Time series (DaS: days after seeding) a) of the daily measured air temperature (T_{air}, °C), leaf temperature (T_{leaf}, °C), and relative humidity (rh, %); b) of vapor pressure deficit (vpd, kPa) and transpiration rate calculated from the isotopic column plant chamber measurements (Tr, mmol s^{-1} m^{-2}); c) of leaf water potential (ψ_l, MPa); d) of CO_2 assimilation rate (A, umol s^{-1} m^{-2}) and canopy conductance (G_s, mmol s^{-1} m^{-2}); e) of instantaneous and intrinsic water use efficiency (WUE and iWUE, umol $mmol^{-1}$); and f) of volumetric soil water content (θ, cm^3 cm^{-3}) at different soil depths. Filled black polygons mark the periods with high transpiration rate (HTr-I, HTr-II, and HTr-III) and empty polygons, periods with low transpiration rate (LTr-I and LTr-II).

After DaS 318, when no more water was added to the column, the isotopic gradient in layer 20-60 cm remained steep, whereas the isotopic profile in layer 0-10 cm evolved in a heterogeneous manner. The δ^2H-values at 1, 5, and 10 cm increased faster than those at 3 and 7 cm. Simultaneously, the $\delta^{18}O$-values at 1, 5, and 10 cm decreased faster than those at 3 and 7 cm (Fig. 3-3d).

The highest and lowest δ^2H-values reached in the soil were 216.4 ± 0.7‰ at depth 59 cm (DaS 312) and -69.9 ± 0.6‰ at depth 3 cm (DaS 313), respectively. The highest and lowest $\delta^{18}O$-values were 24.5 ± 0.3‰ at depth 3 cm (DaS 313) and -39.5 ± 0.3‰ at depth 59 cm (DaS 312), respectively. That is, the minimum δ^2H- and the maximum $\delta^{18}O$-values in soil water at the top of the column were measured the last day where labeled water was added (i.e., DaS 312). The maximum δ^2H- and the minimum $\delta^{18}O$-values at the bottom were measured the following day (i.e., DaS 313). The $\delta_{soil\ water}$ values at 59 cm depth, were very similar to the δ-values of the labeled water added to the bottom (δ^2H = 220 ‰; $\delta^{18}O$ = -40‰, stage 3 in Table 3-2). A larger difference between the $\delta_{soil\ water}$ values at the top and the added labeled water (δ^2H = -90‰; $\delta^{18}O$ = 29‰, stage 3 in Table 3-2) was found. Most daily δ_{Tr} values plot over the $\delta_{soil\ water}$ values from the upper 10 cm of the column (Fig. 3-4b). From around DaS 310 onwards, the δ_{Tr} values progressively plot closer to the $\delta_{soil\ water}$ values in deeper soil layers (Fig. 3-4a). Since the labeling water was only enriched with one of the isotopologues at a time, δ^2H and $\delta^{18}O$ were negatively correlated (Fig. 3-4).

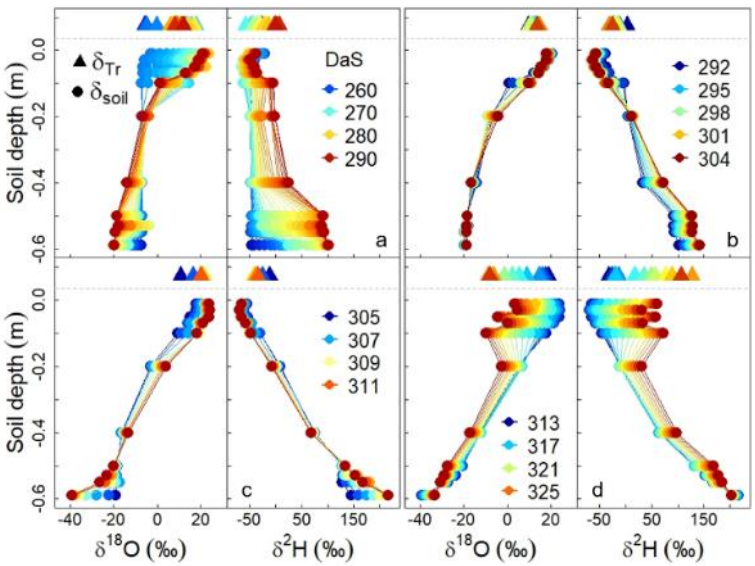

Figure 3-3 : Temporal changes in soil water (circles) and plant transpiration (triangles) δ^2H- and $\delta^{18}O$-values a) during the isotopic labeling stage 1 (day after seeding – DaS – 256-290), b) stage 2 (DaS 291-304), c) stage 3 (DaS 305-312), and d) when the soil was drying (DaS 313-327).

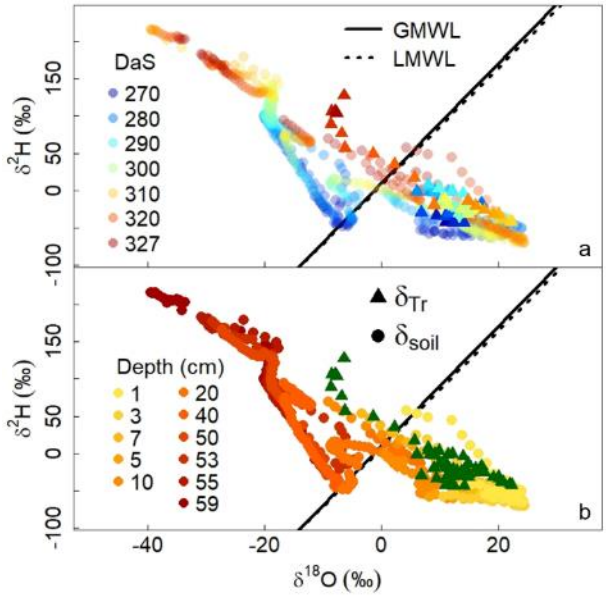

Figure 3-4 : a) Temporal and b) spatial dynamics in the relationship between δ^2H and $\delta^{18}O$ in soil water (circles) and plant transpiration (triangles) from day after seeding (DaS) 270 to 327. The global (solid black line) and local (dotted black line) meteoric water lines (GMWL and LMWL, respectively) are included as a reference. In panel a, the temporal dynamics of plant transpiration and soil water δ-values from DaS 270 to 327 are represented by a color scale from cold to warm tones. In panel b, the spatial dynamics of the soil water δ-values in eleven soil depths from the top to the bottom are represented by a color scale from yellow to red.

3.3. Root length distribution

The objective of the MRI measurements of the MRI columns on Das 237 and 307 was to non-destructively produce RLD profiles inside the isotopic column at these same dates. The comparison between the MRI pictures from the MRI columns and the scanning of the roots of the isotopic column at the end of the experiment (DaS 327) showed that root length measured with WinRhizo in the isotopic column was around ten times higher than root length measured with MRI in the MRI columns (compare x-axis of Fig. 3-5a and b). In order to assess the magnitude of this discrepancy, a ratio was calculated for five soil horizons (0-10, 10-20, 20-40, 40-50, and 50-60 cm). This ratio was obtained by dividing the scan-derived RLD values measured on DaS 327 in the isotopic column by the MRI-derived RLD values measured on DaS 237 and DaS 307 in each MRI column (Table 3-3). The mean of the ratios was 10.8 ± 2.9 and no systematic differences across soil layers or columns were identified.

Table 3-3: Calculated ratio between the root length density (RLD, cm^3 cm^{-3}) in the magnetic resonance imaging (MRI) columns determined with MRI and RLD in the isotopic column determined with root scans in the five sections of the soil column.

	Depth (cm)				
MRI column no.	**0 – 10**	**10 – 20**	**20 – 40**	**40 – 50**	**50 – 60**
1	13.8	11.06	13.08	7.14	6.19
	09.26	10.51	12.75	8.47	5.94
2	17.59	11.97	7.73	6.00	10.85
	10.91	11.00	7.54	7.24	17.23
3	14.23	11.26	10.04	10.36	41.48
	10.21	11.28	13.37	12.62	13.82

The maximum RLD on DaS 237, 307, and 327 was observed at depth 59 cm (3.0 ± 2.6 cm cm^{-3}, 3.7 ± 3.1 cm cm^{-3}, and 52.2 cm cm^{-3}, respectively). In all profiles, RLD values in layers 0-10 cm and 50-60 cm were higher than the RLD values in the middle section of the column (i.e., layer 10-50 cm). The higher RLD values at depth 59 cm are most likely the product of pot-bound roots, which could be a consequence of the extended time the plants grew in the columns.

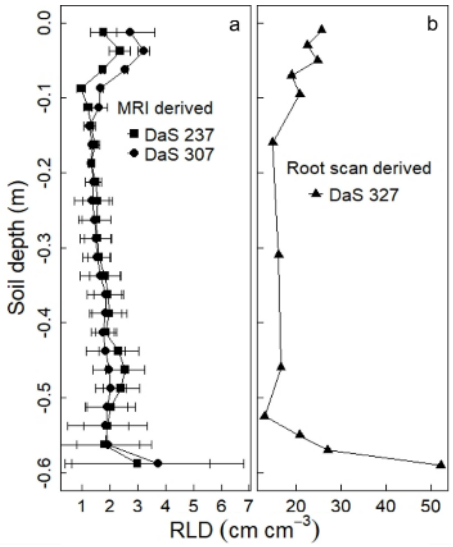

Figure 3-5 : a) Mean root length density (RLD, cm^3 root cm^{-3} soil) profile derived from the non-destructive magnetic resonance imaging (MRI) measurements on day after seeding (DaS) 237 (squares) and 307 (circles) in the MRI columns and b) RLD derived from the destructive root scan measurement at the end of the experiment on DaS 327 in the isotopic column.

3.4. Daily RWU profiles

The RWU profiles obtained using both δ^2H and $\delta^{18}O$ input data (referred to as "δ^2H-$\delta^{18}O$-derived") in days with high Tr (i.e., HTr-I, -II, and -III) compared to days with low Tr (i.e., LTr-I and -II) were very similar (Fig. 3-6a). RWU was highest in layer 0-15 cm, second highest in layer 45-60 cm, and lowest in the middle section of the column (i.e., 15-45 cm). In LTr-I and LTr-II, an average of 79 ± 4% and 44 ± 4% of the total RWU, respectively, was extracted in layer 0-15 cm, while 13 ± 4% and 44 ± 4% in the same respective periods was extracted in layer 45-60 cm. An average of 69 ± 5% in HTr-I and HTr-II, and 56 ± 9% in HTr-III of the total RWU was extracted in layer 0-15 cm, while around 22 ± 5% in HTr-I and HTr -II and 35 ± 8% in HTr-III was extracted in layer 45-60 cm. Note that, during the last two periods (i.e., HTr-III and LTr-II), RWU in layer 0-15 cm was lower and in layer 45-60 cm, higher compared to RWU in the same soil layers in previous periods.

The RWU profiles obtained using either δ^2H or $\delta^{18}O$ input data (referred to as "δ^2H-derived" and "$\delta^{18}O$-derived", Fig. 3-6b and c, respectively,) were not statistically different from the δ^2H-$\delta^{18}O$-derived RWU profiles (except between δ^2H- and δ^2H-$\delta^{18}O$-derived profiles in DaS 245, Table S3-1). In general, the RWU in layer 0-15 cm and 45-60 cm in the δ^2H- and $\delta^{18}O$-derived profiles was slightly lower than RWU in δ^2H-$\delta^{18}O$-derived profiles in the same layers. Consequently, RWU in layer 15-45 cm in the δ^2H- and $\delta^{18}O$-derived profiles was slightly higher than RWU in the δ^2H-$\delta^{18}O$-derived profile (Fig. 3-6a-c).

As already mentioned in section 3.1 in this chapter, θ was rather homogeneous along the column from DaS 265 onwards, that is, for all days where RWU profiles were calculated. However, some differences in the water saturation between soil layers are visible in Fig. 3-6d. For example, there was consistently less water in layer 30-55 cm than in the rest of the layers from around DaS 285 until around DaS 307. Afterwards, the θ profile was more homogeneous with a decreasing trend. Due to our labeling strategy, soil layers 0-5 cm and 55-60 cm were wetter than the rest of the layers from DaS 270 to DaS 312.

Daily changes in RWU profiles did not match those of θ for some periods. In LTr- I, the RWU was higher in layer 0-20 cm than deeper in the soil profile (Fig. 3-7a). However, θ in this layer did not decrease much faster than deeper in the soil profile (Fig. 3-7b). In HTr-III, θ in layer 10-60 cm decreased slightly faster than in layer 0-10 cm (Fig. 3-7d), even though the RWU in layer 0-10 cm was higher than in the rest of the column (Fig. 3-7c).

4. Discussion

In sections 4.1 and 4.2, we describe the response of *Centaurea jacea* L. to dry conditions through correlations of the environmental and plant-related variables and a simple hydraulic model. In section 4.3, we link RWU changes of *C. jacea* L. and the dynamics of above- and below-ground environmental conditions and root distribution. We observed a stricter control of the stomata by *C. jacea* L. when vpd was high and the soil was drying. The increasingly dry soil seemed to set off stomatal closure. Under

varying hydroclimatic conditions, most of the water extracted by *C. jacea* came from the soil layer 0-15 cm (up to 79%) and the second greatest contribution (up to 44%) came from the soil layer 45-60 cm. In most days, water availability and root distribution seemed to be the main drivers of RWU.

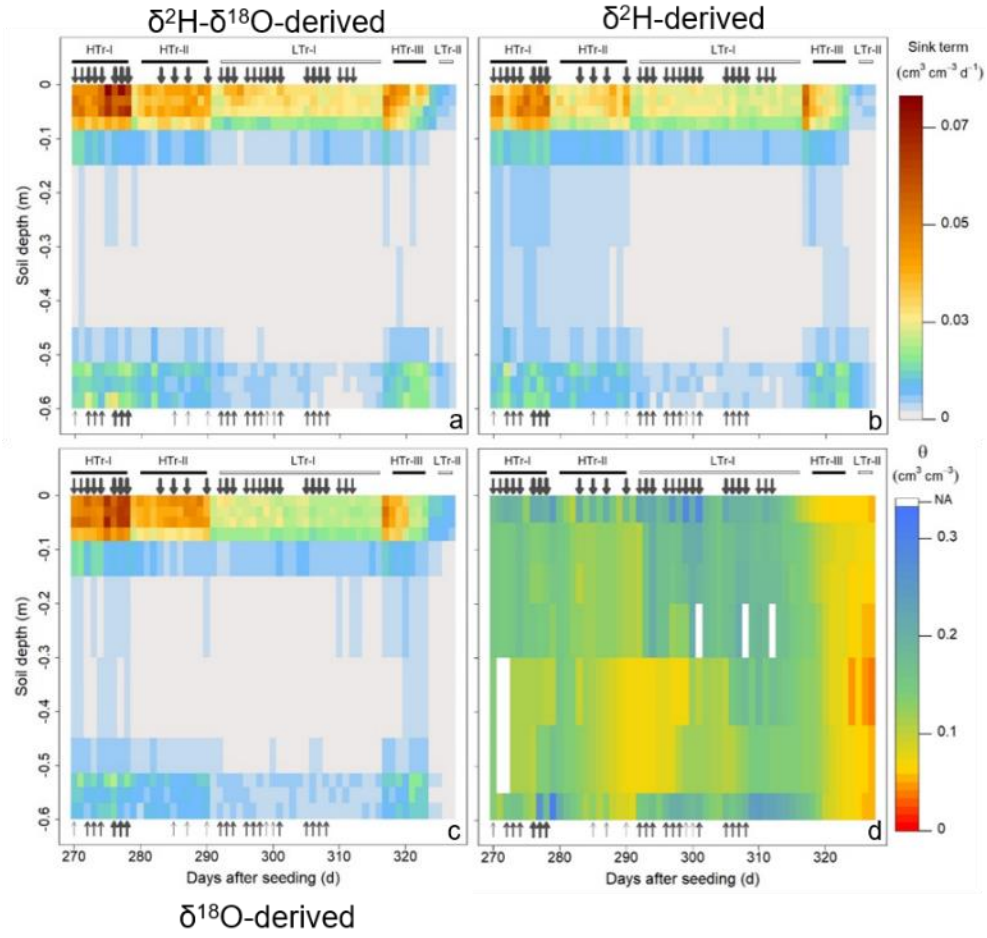

Figure 3-6 : a) Temporal changes in the sink term profiles (cm^3 water cm^{-3} soil day^{-1}) in the isotopic column calculated with both soil water δ^2H and $\delta^{18}O$ profiles (δ^2H-$\delta^{18}O$-derived), b) with δ^2H profiles only (δ^2H-derived) and c) with $\delta^{18}O$ profiles only ($\delta^{18}O$-derived) during isotopic labeling and until the end of the experiment. The temporal changes in volumetric soil water content profiles (θ, cm^3 cm^{-3}) during the experiment is shown in panel d. Filled black polygons mark the periods with high transpiration rate (HTr-I, HTr-II, and HTr-III) and empty polygons, periods with low transpiration rate (LTr-I and LTr-II). The gray downward arrows represent water added to the top of the column and the upward gray arrows, water added to the bottom. Thicker arrows represent a higher amount of water added.

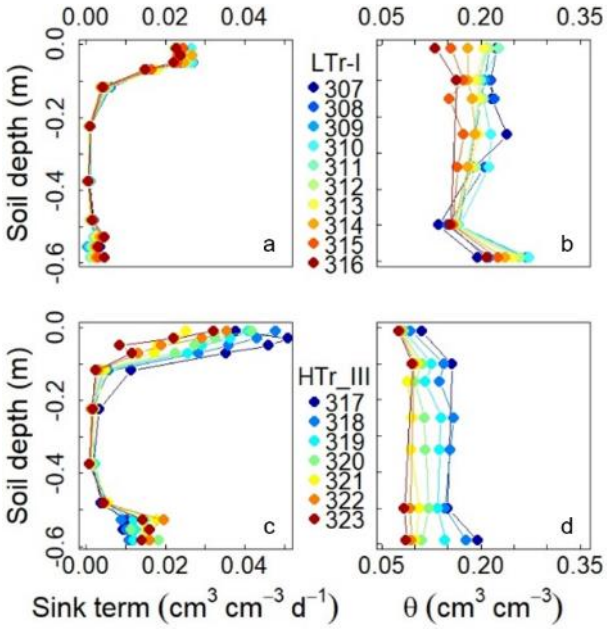

Figure 3-7 : a) Temporal changes in the sink term (cm^3 water cm^{-3} soil day^{-1}) and b) in volumetric soil water content profiles (θ, cm^3 cm^{-3}) during period of low transpiration rate I (LTr-I) and during period of high transpiration rate III (HTr-III) in the isotopic column (c-d).

4.1. Plant response to drought

The statistically significant correlations between measured and calculated variables are displayed in Fig. 3-8. In general, we interpret changes in the correlations between canopy conductance, G_s; transpiration rate, Tr; vapor pressure deficit, vpd; and soil water content, θ; as a stricter control over transpiration rate by *Centaurea jacea* L. through stomatal closure when both above- and below-ground conditions were dry. Before DaS 319, the relationships between θ and Tr, and between θ and G_s were not unique (i.e., there were several Tr or G_s values for one single θ value) and seemed to depend on vpd (empty circles in Fig. 3-8c and e, respectively). After DaS 319, both G_s and Tr decreased markedly with small changes in θ (filled circles in Fig. 3-8c and e, respectively). Interestingly, both CO_2 assimilation rate, A; and Tr were positively correlated to G_s (Fig. 3-8d and f, respectively). However, only the correlation between G_s and Tr changed with vpd: the higher the vpd, the higher the slope (0.002 for vpd < 1 kPa, 0.01 for 1 < vpd < 1.5 kPa and 0.02 for vpd > 1.5 kPa in Fig. 3-8f). We also observed a different and significant correlation between vpd and Tr when comparing the data before DaS 319 (slope = 4.14, r^2 = 0.68, p-value = $2.2x10^{-16}$) and after DaS 319 (slope = 5.87, r^2 = 0.86, p-value = $6.2x10^{-4}$).

Through stomatal closure in dry conditions, *C. jacea* L. displayed a slightly more efficient water use in laboratory conditions. We observed a slight increase in intrinsic water use efficiency, iWUE; and a constant instantaneous water use efficiency, WUE (Fig. 3-2e). Similarly, Kübert et al. (2021) observed an increase in iWUE and no

change or a small decline in WUE of *C. jacea* L. in dry conditions in the field. In our experiment, WUE and vpd were significantly and negatively correlated (slope = -3.70, $r^2 = 0.63$, p-value = $1.2x10^{-9}$) during the drought period. Yet, several studies reported higher WUE values in grassland species during drought (e.g., Judson et al., 2006; Gang et al., 2016; Yue et al., 2020). These contradictory outcomes could be attributed to differences in temporal and spatial scales: the studies of Gang et al. (2016) and Yue et al. (2020) encompassed data at a global scale and from several years. Alternatively, they could be attributed to the fact that, in the experiments conducted by Kübert et al. (2021) and in this study, lower θ (< 0.1 cm^3 cm^{-3}) and higher vpd (> 1 kPa) values were observed than those reported by Judson et al. (2006).

According to Sperry & Love (2015), water flux from the soil to the leaves can be described mathematically by a "supply function", in which Tr is expressed as a function of canopy xylem pressure (P_{canopy}) at constant θ. The slope of the relationship (also referred to as soil-canopy conductance by the authors) is positive and relatively linear at high xylem pressure (i.e., close to zero) and low to medium Tr, and decreases with decreasing xylem pressure (i.e., more negative) and increasing Tr. The slope approaches zero at high Tr and low P_{canopy}, while Tr approaches a constant maximum value referred to as a critical Tr value (associated with a critical P_{canopy} value) after which hydraulic failure takes place. In drier soils, the Tr(P_{canopy}) relationship is "flatter" than in wet soils and therefore, the critical Tr value is lower than in wetter soils. The authors argue that through stomatal closure the plants avoid reaching the critical Tr and P_{canopy} values, especially when vpd is high and the soil is dry. We hypothesize that the drop in G_s in our experiment observed at DaS 319 might have occurred to counteract the effect of high vpd and low θ. In other words, to avoid approaching a theoretical non-linear region of the relationship between Tr and leaf water potential, ψ_l (i.e., slope ≈ 0 at higher Tr and lower ψ_l values beyond the shown linear trend in Fig. 3-9). Additionally, the supply functions for DaS 322-327 (filled circles in Fig. 3-9) might have been flatter than those for the previous days, since vpd remained high and the soil had dried out significantly (Fig. 3-2b and f) after the stomatal closure on DaS 319.

The fact that the simultaneous drop of G_s and Tr occurred a few days before the relationship between Tr and ψ_l deviated from a relatively linear trend observed until DaS 321 (empty circles in Fig. 3-9) further supports our assumption of stomatal closure as a strategy to avoid hydraulic failure. Hayat et al. (2020) also observed a concomitant reduction in soil-canopy conductance, stomatal conductance, and Tr in maize plants when the soil was drying. They also argued that reducing Tr through stomatal closure following a reduction in soil-canopy conductance is an attempt to avoid what they call "non-linearities" in the Tr(P_{canopy}) relationship (i.e., approaching the critical Tr value). Investigating the temporal and spatial dynamics of the soil-canopy conductance and of hydraulic characteristics at the root-soil interface during our experiment (as done by Rodriguez-Dominguez & Brodribb (2020); Sperry et al. (2002) and as suggested by Carminati & Javaux (2020)) would have helped further substantiate our assumptions.

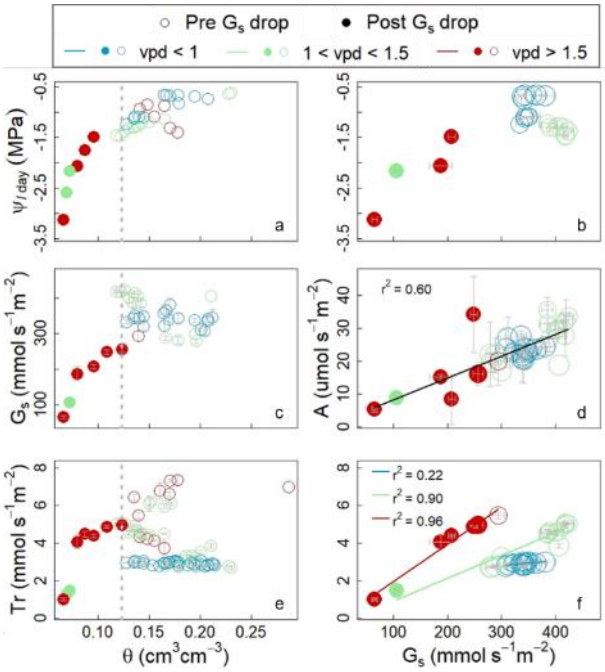

Figure 3-8 : Minimum leaf water potential during day (light panel on) ($\psi_{l\text{-}day}$, MPa), canopy conductance (G_s, mmol s^{-1} m^{-2}), and transpiration rate (Tr, mmol s^{-1} m^{-2}) as a function of soil water content (θ, cm^3 cm^{-3}) (a, c, and e, respectively). $\psi_{l\text{-}day}$, CO_2 assimilation rate (A, µmol s^{-1} m^{-2}), and Tr as a function of G_s (b, d, and f, respectively). The correlations in panels d and f were significant (i.e., p-value < 0.05). The dashed gray line in panels a, c, and e marks the soil water content value (θ, cm^3 cm^{-3}) on day after seeding (DaS) 319, when canopy conductance started dropping steadily to zero. Empty circles represent days before this drop (pre G_s drop) and filled circles represent days after this drop (post G_s drop). The color of the symbols represents vapor pressure deficit (vpd, kPa): blue for days with vpd below 1 kPa, green for days with vpd between 1 and 1.5 kPa, and red for days with vpd higher than 1.5 kPa. In panels b, d, and f, the symbol size represents the mean θ along the isotopic column (i.e., the bigger the circle, the higher the θ value on that day).

Moreover, reductions in soil-canopy conductance (followed by reductions in stomatal conductance and Tr) reported by Hayat et al. (2020) started at relatively high θ values (0.12 cm^3 cm^{-3}). In our study, θ was relatively high (around 0.12 cm^3 cm^{-3}) when G_s, Tr, and A, started decreasing on DaS 319 (Fig. 3-2b, d, and f). ψ_l was around -1.5 MPa at this point, a value observed on other DaS with higher θ and G_s values (empty circles in Fig. 3-8a and b). The results of Hayat et al. (2020) and our own potentially agree with the hypothesis of Gollan et al. (1985) that leaf gas exchange might be limited when a critical value of θ (alternatively, a critical value of soil water potential) is reached rather than when a critical leaf water potential is exceeded. Leaf gas exchange in the last days of the experiment was limited by both a drying soil and increasingly negative ψ_l values: G_s values decreased steadily with decreasing ψ_l values after DaS 319, while no trend was observed before this day (Fig. 3-8b).

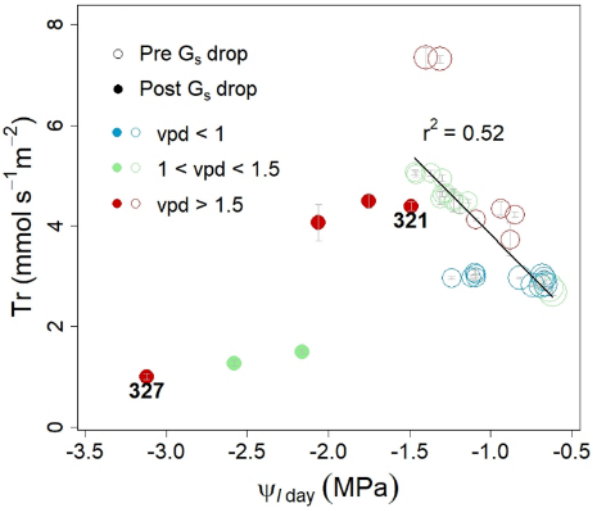

Figure 3-9 : Plant transpiration rate (Tr, mmol s^{-1} m^{-2}) as a function of minimum leaf water potential during day (light panel on) ($\psi_{l\text{-}day}$, MPa). The correlation is significant (i.e., p-value < 0.05). Empty circles represent days before day after seeding (DaS) 319, when canopy conductance started dropping steadily to zero (pre G_s drop). The filled circles represent days after DaS 319 (post G_s drop). The numbers next to two of the filled red circles are the DaS of the observation point. The color of the symbols represents vapor pressure deficit (vpd, kPa): blue for days with vpd below 1 kPa, green for days with vpd between 1 and 1.5 kPa, and red for days with vpd higher than 1.5 kPa. The symbol size represents the mean soil water content (θ, cm^3 cm^{-3}) along the isotopic column (i.e., the bigger the circle, the higher the θ value on that day).

4.2. Iso- or anysohydricity

Similar to Kübert et al. (2021), we observed that *C. jacea* L. could maintain relatively high Tr in dry soils and at high vpd by withstanding very low ψ_l values. This pointed towards an anisohydric behavior. However, a deeper analysis of the ψ_l values during the experiment revealed that this conclusion might be incomplete.

The correlation between $\psi_{l\text{-}day}$ (i.e., minimum ψ_l while the LED panel was on) and $\psi_{l\text{-}night}$ (i.e., maximum ψ_l while the LED panel was off) was below 1 (slope = 0.89, r^2 = 0.86, p-value = $2.2x10^{-16}$) during the experiment, indicating an isohydric behavior (Martínez-Vilalta et al., 2014; Y. Zhao et al., 2021). However, when considering the data before DaS 321 when θ dropped below ~0.10 cm^3 cm^{-3} only, the computed slope is above 1 (slope = 1.78, r^2 = 0.58, p-value = $2.8x10^{-9}$), pointing to an anisohydric behavior. Furthermore, the variation in $\Delta\psi_l = \psi_{l\text{-}day} - \psi_{l\text{-}night}$ was comparable to the variation observed in the anisohydric plant in the study of Zhao et al. (2021) (~0.40 MPa). Though, the median $\Delta\psi_l$ in our experiment (-0.47 MPa) was closer to the value calculated for the isohydric plant (~-0.77 MPa) of the same study (the value for the anisohydric plant was ~-1.70 MPa). Also, there was no significant correlation between G_s and $\psi_{l\text{-}day}$ (Fig. 3-8b), another characteristic of anisohydric behavior according to

Zhao et al. (2021), and ψ_l steadily dropped when θ decreased (see period HTr-II in Fig. 3-2c), also pointing towards anisohydricity.

The analysis presented in the last paragraph supports the idea that isohydric and anisohydric behavior should be viewed as a more or less continuous spectrum rather than a dichotomy (Martínez-Vilalta et al., 2014) and that it is possible for a species to display both behaviors. Alternatively, there have been recent calls to abandon the iso- and anisohydricity terms and instead assess plant performance during drought through parameters such as maximum transpiration rate, hydraulic conductance, and critical leaf water potential (Hochberg et al., 2018). According to Hochberg et al. (2018), by using these parameters, the effect of environmental factors could be eliminated when comparing the response of plant species or genotypes to drought.

4.3. RWU dynamics and drivers

In the following paragraphs we i) describe the role of root distribution (i.e., RLD) in RWU, ii) the impact of above- and below-ground dry conditions on RWU, and iii) water movement processes through the soil and the root system observed in our experiment.

4.3.1. RLD monitoring and its role in RWU

Using MRI to monitor root distribution and growth requires careful selection and preparation of the soil (e.g., removal of ferromagnetic particles), and characteristics of the pot (a bigger diameter decreases the signal-to-noise ratio of the images, and thus thin roots are not visible). By comparing root mass and length obtained from MRI and from destructive sampling (e.g., root extraction and scanning) using a particular soil, plant, and pot size, we can determine a root-diameter threshold (van Dusschoten et al., 2016), differences in root diameter in the soil profile, and correct θ measurements (van Dusschoten et al., 2020). The ten-fold difference between the MRI- and scan-derived RLD profiles could primarily stem from the fact that the average root diameter along the isotopic column was 0.36 ± 0.04 mm, right above the lower detection limit of MRI with the used coil and measurement settings (~0.3 mm). Beyond these differences and limitations, the RLD profiles from the MRI analysis agreed well with those obtained with WinRhizo™. This fact highlights the potential of MRI to monitor at a much higher temporal resolution (e.g., daily) and with a higher repeatability root development in the same plant individual.

In some studies, root distribution and RWU profiles are rather similar (e.g., for grass species in Mazzacavallo & Kulmatiski, 2015), whereas in other studies there is no clear and consistent association (e.g., Kühnhammer et al., 2020). In our study, RWU at the bottom of the isotopic column (45-60 cm) was consistently lower than RWU at the top (0-15 cm), even if the percentage of total root length and root volume in the same soil layers was comparable. On DaS 307, 33.9% and 31.5% of the total root length and volume, respectively, were located in the soil layer 0-15 cm, whereas 37.9% and 39.2% of the total root length and volume, respectively, were located in the soil layer 45-60 cm. On DaS 327, the soil layer 0-15 cm contained 34.8% and 39.4% of the total root length and volume, respectively, whereas the soil layer 45-60 cm contained 35.8% and 32.9% of the total root length and volume, respectively. Our

observations, like the results of Kulmatiski et al. (2010) regarding the overestimation of root activity from root mass, potentially confirm the conclusion drawn by Schenk (2008): most plants will develop the "shallowest possible" root and water extraction profile. This fits our observation that RWU from *C. jacea* L. was highest in layer 0-15 cm under varying hydroclimatic conditions. However, since we could not quantify root-mediated soil water redistribution (i.e., hydraulic lift) with our isotope-based methodology, we do not entirely rule out a potential underestimation of water extraction by deep roots (see section 4.3.3).

4.3.2. RWU dynamics under varying above- and below-ground environmental conditions

The comparison made between the δ^2H-$\delta^{18}O$-, δ^2H-, and $\delta^{18}O$-derived RWU profiles assisted in assessing potential isotope-specific (^2H or ^{18}O) fractionation during RWU or artifacts during the non-destructive sampling of soil water vapor and plant chamber water vapor. We did not observe neither isotope-specific fractionation during RWU nor methodological artifacts, since no statistically significant differences between RWU profiles were generally found, to the single exception of DaS 245 between δ^2H- and δ^2H-$\delta^{18}O$-derived RWU profiles. This is why we will only discuss the dynamics of δ^2H-$\delta^{18}O$-derived RWU profiles in this section.

The calculated RWU profiles in periods with high and low Tr were very similar in well-watered and dry conditions: up to 79% of RWU happened in the soil layer 0-15 cm and up to 44% of RWU happened in the soil layer 45-60 cm (see section 3.4 in this chapter). Hayat et al. (2019) also obtained similar relative RWU profiles from maize under uniform θ conditions when Tr was high and low. However, the RWU in their study shifted (i.e., was higher) to deeper wetter soil layers in non-uniform θ conditions. The investigation conducted by Warren (2011) also shows evidence of a RWU shift in *Centaurea diffusa* towards deeper soil layers when the shallow ones had dried out. There are numerous studies reporting higher water extraction from deeper wetter soil layers by trees (e.g., Ehleringer & Dawson, 1992; Volkmann et al., 2016). Nonetheless, there are some studies that reported no such shift in some tree species during drought (e.g., Gessler et al., 2022). In the case of grassland species, it has been observed that some still extract water from the top soil, even if θ is approaching permanent wilting point (Bachmann et al., 2015; Kulmatiski et al., 2010; Prechsl et al., 2015). Kühnhammer et al. (2020) proposed that significant RWU by *C. jacea* L. from shallow soil layers, even if water is available deeper in the soil profile, might be a strategy for maximizing the use of rainwater, especially when drought conditions prevail. Even if we did not observe a marked shift in RWU to wetter deeper layers (i.e., highest RWU values in layers with the highest θ values), we did observe an increase of RWU in wetter deeper layers when the soil layer 0-15 cm was drying out and when transpiration rate was high.

Not only water availability, root distribution (see section 4.3.1 in this chapter) and environmental factors (i.e., vpd or light intensity) were driving RWU, but also nutrient availability might have played a significant role in our experiment (Kulmatiski et al., 2017). Nutrients in irrigation water were added at the top and the bottom of the column

before the isotopic labelling started and most probably the amount of irrigation water was not sufficient to reach the middle section of the column and a gradient in nutrient content along the column was established. Alternatively, the addition of water for about 57 days on a daily basis from the top and the bottom in relatively small amounts could have been a driver of RWU of *C. jacea* L., since θ was locally and temporally very high at the top and at the bottom (Fig. 3-6d). A better strategy would probably be to add smaller amounts of water with a much higher δ-value for a shorter period at different depths, so that the changes in θ are homogeneous along the soil column and, to some extent, negligible (see chapter 5 section 2).

4.3.3. Redistribution of water in the soil

Mismatches between θ and RWU profiles, like the ones described in other studies and in section 3.4 in this chapter, are to be expected, since changes in θ are not only due to RWU, but also to soil water redistribution (Zarebanadkouki et al., 2013). This redistribution can happen through capillary forces or even through hydraulic lift (Couvreur et al., 2020; Meunier, Rothfuss, et al., 2017). Kühnhammer et al. (2020) described such mismatches in an experimental setup comparable to ours. For example, for some periods they observed daily changes in θ greater than daily changes in estimated RWU in depth 30-60 cm and almost no changes in θ in depth 1 cm, even though RWU there was high.

Soil water redistribution could also be the reason why the isotopic profile in layer 0-10 cm became progressively non-monotonic from DaS 318 onwards (Fig. 3-3d). Contrary to our observations, water diffusion promoted solely by the isotopic and θ gradients would have resulted in a gradual and homogeneous shift of the entire isotopic profile towards the middle. That is, the changes in the isotopic profile in the soil layer 0-30 cm would have been similar to those in the isotopic profile in the soil layer 30-60 cm. In a scenario where hydraulic lift took place, water extracted by the roots from the deepest soil layers (i.e., 55-60 cm characterized by a higher soil water potential, Fig. 3-7d) could have been released locally in soil layer 0-10 cm. This would have resulted in a greater increase of $\delta^{2}H$ and a greater decrease of $\delta^{18}O$ from day to day in soil layer 0-10 cm than in layer 10-55 cm. Such changes in the isotopic profile are observed in Fig. 3-3d, which could be evidence of hydraulic lift. In this case, calculation of the sink term using transpiration rate and soil water isotopic composition may lead to an underestimation of water uptake from the roots at the bottom of the column, since water extracted by these roots might have been released at the top and later taken up by the shallow roots. However, physically-based modeling (i.e., where hydraulic redistribution by roots can be simulated) is necessary to test the validity of this hypothesis (Rothfuss & Javaux, 2017), that is, distinguish between soil- and root-mediated water redistribution.

5. Conclusions

In the present study, we were able to obtain RWU profiles of *Centaurea jacea* L. with daily and centimeter resolution and to assess the ability of this plant to acclimate to challenging environmental conditions. The coupling between a semi-automated experimental system and the latest soil and plant water isotopic monitoring and root imaging techniques allowed for a fully non-destructive approach. The control of gas exchange at the leaf level in response to drought was proven mostly anisohydric, although at other moments during our experiment stomatal control could be described as isohydric. Under dry conditions, leaf water potential in this plant species reached low values, which allowed *C. jacea* L. to maintain high transpiration rates and relatively constant intrinsic water use efficiency values without causing hydraulic disruption in the soil-plant-atmosphere continuum. However, we also observed a decline in canopy conductance that potentially limited transpiration and carbon assimilation rates before leaf water potential and soil water content markedly decreased. Under well-watered conditions, transpiration rate was mainly driven by vapor pressure deficit and light intensity.

Under laboratory conditions, up to 79% of RWU by *C. jacea* L. occurred in shallow depths and up to 44% of RWU, in deeper soil layers. We were able to explain the adaptation of RWU patterns with both root distribution and water availability profiles. Even though *C. jacea* L. displayed effective adaptation strategies to a dry environment, its apparent and consistent reliance on water in shallow soil depths could negatively affect the performance and competitiveness of this species in a future climate, projected to be associated with more frequent and prolonged drought periods. Nevertheless, the significance of the activity of deep roots in the adaptation of *C. jacea* L. to dry conditions might have been underestimated, since we only quantified root water extraction for plant transpiration but not soil water redistribution through the roots.

6. Supplementary material

Table S3-1: p-values from the normality test (Shapiro-Wilk) used to determine if a parametric (t-test) or a non-parametric (Wilcoxon) statistical test was used to compare the δ^2H-$\delta^{18}O$-derived with the δ^2H- and $\delta^{18}O$-derived root water uptake profiles. The p-values from the t-test are marked with a (*). The rest was calculated with the Wilcoxon test. The p-values lower than 0.05 are marked with two (*).

	p-value from the normality test (Shapiro-Wilk)			**p-value from the paired test (Wilcoxon or t-test)**	
Days after seeding (DaS)	**$\delta^{18}O$-δ^2H-derived**	**$\delta^{18}O$-derived**	**δ^2H-derived**	**$\delta^{18}O$-δ^2H-derived vs. $\delta^{18}O$-derived**	**$\delta^{18}O$-δ^2H-derived vs. δ^2H-derived**
270	0.0517	0.0269	0.0152	0.7646	0.042**
271	0.0383	0.0528	0.025	1	0.3203
272	0.2053	0.005	0.3628	0.4131	0.1675*
273	0.0319	0.0113	0.0069	0.8311	0.0674
274	0.0079	0.0099	0.0108	0.5771	0.3203
275	0.0157	0.0067	0.0102	0.9658	0.5771
276	0.0425	0.0157	0.0152	0.8984	0.3652
277	0.0345	0.0017	0.0148	0.8311	0.4648
278	0.0327	0.0024	0.029	0.9658	0.2783
279	0.2688	0.0189	0.0487	0.6377	0.2783
280	0.0414	0.008	0.0598	0.8311	0.2061
281	0.0179	0.0049	0.0422	0.5195	0.6377
282	0.2434	0.0165	0.5698	0.8984	0.0718*
283	0.0132	0.0068	0.0585	0.5771	0.4648
284	0.0053	0.01	0.0598	0.3652	0.3203
285	0.0223	0.0054	0.0424	0.5195	0.3203
286	0.0171	0.0051	0.0431	0.8311	0.3652
287	0.0121	0.0074	0.0064	0.8311	0.2783
288	0.0169	0.0046	0.0159	0.8311	0.2783
289	0.0403	0.0109	0.037	0.7646	0.6377
290	0.0311	0.0125	0.0233	0.6377	0.5771
291	0.01	0.0054	0.0098	0.1475	0.8984
292	0.0269	0.0044	0.024	0.8984	0.4131
293	0.005	0.008	0.0025	0.8984	0.5195
294	0.002	0.0149	0.001	0.7002	0.4131

295	0.0024	0.0122	0.0082	0.8311	0.4648
296	0.0022	0.0069	0.0056	0.8311	0.4648
297	0.0075	0.0083	0.0041	0.7002	0.3652
298	0.0042	0.0125	0.0028	0.5771	0.7002
299	0.0081	0.0078	0.0042	0.3652	0.5195
300	0.0025	0.0034	0.005	0.5195	0.8984
301	0.0031	0.0269	0.0037	1	0.7646
302	0.0025	0.0243	0.0026	0.9658	0.5195
303	0.0039	0.0189	0.0029	0.8311	0.7002
304	0.0055	0.0068	0.0047	0.4648	0.6377
305	0.0107	0.0058	0.0059	0.4648	0.6377
306	0.0014	0.0249	0.0023	0.9658	0.8984
307	0.0029	0.0112	0.0059	0.5195	0.8311
308	0.0028	0.0062	0.0073	0.6377	0.8311
309	0.0028	0.0071	0.0133	0.9658	0.9658
310	0.0011	0.0091	0.0197	0.7646	1
311	0.0018	0.0134	0.0026	0.7646	0.3652
312	0.0031	0.0139	0.0035	0.6377	0.4131
313	0.0031	0.0085	0.0027	0.8311	0.5195
314	0.0028	0.0054	0.0017	0.9658	0.7646
315	0.0038	0.0028	0.0018	0.4131	0.3203
316	0.0063	0.006	0.0083	0.9658	0.1748
317	0.0218	0.0131	0.0022	0.6377	0.8984
318	0.0361	0.0093	0.0525	0.5195	0.4648
319	0.1194	0.0273	0.161	0.8311	0.3029*
320	0.4532	0.0104	0.1943	0.4131	0.1709*
321	0.1896	0.1979	0.1185	0.2862*	0.686*
322	0.3584	0.2951	0.0814	0.2105*	0.2394*
323	0.3318	0.5375	0.0108	0.492*	0.8984
324	0.0351	0.0349	0.0863	0.1748	0.4648
325	0.4973	0.0098	0.1724	1	0.3833*
326	0.4199	0.0088	0.5156	0.8984	0.3327*
327	0.1896	0.0021	0.2401	0.8984	0.3482*

Chapter 4

Root water uptake quantification: a comparison between probabilistic and physically-based modelling approaches

As mentioned at the beginning of chapter 3, a more in-depth assessment of the ecohydrological response to drought of *Centaurea jacea* L. was pursued in this third study. More specifically, we aimed at describing the interplay between soil-root and plant-atmosphere processes from a hydraulic perspective and comparing probabilistic- (chapter 3) and physically-based modelled RWU patterns (O.3). The link between a decrease in hydraulic conductance in the soil-root interface and in the leaves theorized in the discussion of the second study (chapter 3 section 3.4), potentially resulting in changes in the RWU profiles that might not have been captured with the isotopic approach (H.3) was tested.

Section 1 contains a short theoretical framework about physically-based RWU models, in which water flow and distribution depends on the dynamics of root (segments in 3D or system in 1D approaches) and soil hydraulic properties. Here, the emergence of an exponentially decreasing soil hydraulic gradient near the roots and its limiting effect on water uptake is highlighted.

Section 2 contains a description of the mechanistic hydraulic model of Vanderborght et al. (2021, 2023) – in its 1D version – employed to estimate RWU and two relevant hydraulic parameters: root system conductance (K_{rs}) and soil-root water tension ($H_{s,r}$) during selected days of the experiments described in chapter 3. Additionally, the parametrization of the model and estimations of K_{rs} in wet and homogeneous conditions are detailed.

The results and discussion of this third study in preparation are found in section 3. We modelled an exponential decrease of the root system conductance and of soil water tension near the roots in the last four days of the experiment from the second study in moderately dry soil and right after the decrease in canopy conductance. The probabilistic and physically-based RWU patterns had similar shapes for days with no water limitation: water uptake was significantly higher in shallow-depths. However, the location of maximum water extraction shifted from the surface to a depth of 10 cm only in the physically-based RWU profiles, associated with a significant decrease in soil water tension in the soil-root interface above 10 cm.

The main conclusions of this third study are summarized in section 4. We found evidence to support H.3: the root system conductance and soil water tension near the roots exponentially decreased resulting in adaptations in water uptake "missed" in the isotopic approach. The simple comparison between isotopic and hydraulic approaches to RWU quantification presented here broadened the ecohydrological assessment of the response to drought of *Centaurea jacea* L. at the single plant scale in controlled laboratory conditions. Nonetheless, employing integrative isotopic and hydraulic approaches for RWU quantification, as proposed by Dubbert et al. (2023), might be the best way forward to describe in a more realistic way water use strategies across scales. This could be achieved by including the influence of phenomena commonly overlooked on water uptake dynamics (e.g., root traits and contrasting resource uptake or allocation strategies) or isotope-based estimations (e.g., water travel and residence time or water pool mixing inside the plant) in a true isotope-enabled hydrodynamic approach (Dubbert et al., 2023).

1. Introduction

Water flow in the soil-plant-continuum may be investigated by coupling models describing soil water movement in the soil by solving Richardson-Richards equation (Richards, 1931; Richardson, 2007) and models quantifying root water uptake from the root hydraulic architecture (i.e. root system architecture accounting for root hydraulic properties (Draye et al., 2010)). One of the catalysts for this approach was the work of Van Den Honert (1948), describing plant water uptake as a catenary process, in which a gradient of decreasing water potential in a network of resistances along the soil-root axis produces (unidirectional) flow of water. Landsberg & Fowkes (1978) modelled a few decades later the dependency of water uptake along a root to its radial and axial hydraulic resistances, as well as the dependency of water uptake patterns on the spatio-temporal dynamics of root and soil hydraulic resistances. These studies and others have laid the ground for current models accounting for root hydraulic architecture in RWU quantification.

Thanks to three-dimensional (3D) microscopic explicit models accounting for the spatial distribution of radial and axial hydraulic conductances at the root segment level, important insights into the complex interactions between root segments and soil at a high temporal resolutions (e.g., hourly) have been documented (e.g., Doussan et al., 2006; Javaux et al., 2008; Schröder et al., 2009). However, these approaches are computationally costly and require estimations of root radial and axial hydraulic resistances at the root segment level, since these change with the developmental stage and position of the root segments in the system (Frensch et al., 1996; Meunier et al., 2018; Rieger & Litvin, 1999). This is why, 3D models (e.g., Vanderborght et al., 2021) and their parameters (e.g., Couvreur et al., 2014) have been upscaled to macroscopic (1D) models that carry a lower computational cost and require only average estimates of root axial and radial hydraulic conductivities along a soil profile, very convenient for field studies on the plot and global scales.

Going a step further, Vanderborght et al. (2023) in a 1D model and Schröder et al. (2008) in a 3D model demonstrated that the hydraulic properties of the soil (and not the properties of the roots) become limiting for the water uptake process below a certain soil water potential. They concluded that below this threshold (the magnitude of which depends on the soil type; Cai et al., 2022s) an additional hydraulic resistance in the soil-root interface should be considered. Most importantly, the effect of this resistance is enhanced by its non-linear relationship to the soil hydraulic conductivity curve resulting in a steep decrease of water potential near the root surface ($H_{s,r}$, L) in a drying soil. The results of these approaches when considering the soil limitation to water uptake under dry conditions match better experimental observations and shed light into the strategies of plants to avoid or delay water stress. However, Couvreur et al. (2014) did cautioned, that the assumption of horizontally homogeneous RLD and bulk soil water content in 1D approaches might lead to an overestimation of the collar potential for wide-row crops like maize and to potentially misidentifying the moment water stress sets in.

Due to the pivotal role root radial and axial hydraulic conductivities seem to play in the spatial and temporal distribution of RWU, accurate estimations of these parameters are considered necessary to also accurately quantify (macro- or microscopically) RWU. Nevertheless, this is not a trivial or easy task, especially when scaling root conductivity (intensive property) into conductance (extensive property), since the latter depends inversely on root wall thickness and root length but directly on root surface and xylem diameter (Bouda et al., 2018). Since it is likely that root radial and axial conductivities react in a coordinated fashion to and are also influenced by environmental changes (Bouda et al., 2018; Vetterlein & Doussan, 2016), estimating a root system conductance (K_{rs}, $L^3\ P^{-1}\ T^{-1}$), dependent on root radial, root axial, and soil hydraulic conductivities, might be a better strategy. This is further supported by the fact that both root radial and axial conductivities strongly depend on root order, age, and structure, and plant species (resulting in a variability that can only be accounted for in 3D models) and influence the "tradeoffs between root length utilization and water uptake capacity" (Zwieniecki et al., 2003).

Cai et al. (2022) found that the maximum K_{rs} (slope of the relationship between transpiration rate and leaf water potential in wet soil) was mainly dependent on root length and independent on soil type or plant species. However, K_{rs} decreased with decreasing θ and this decrease was related to both soil texture and plant species. Moreover, the effect of soil texture on the decrease of K_{rs} was related to the drop in soil water potential around the roots, similar to the findings of Vanderborght et al. (2023) and Schröder et al. (2008) regarding the effect of steep $H_{s,r}$ gradients on RWU.

Chapter 3 included the description of a drought experiment using a single plant of the species *Centaurea jacea* L. (brown knapweed) grown in a 60 cm soil column filled with a loamy sand in which we measured physiological and environmental parameters in a semi-automated manner. At the end of this drought experiment, canopy conductance declined at a relatively high bulk soil water content of ~0.12 $cm^3\ cm^{-3}$ and we hypothesized that this was related to a decrease in K_{rs} and $H_{s,r}$. In this study, we tested this assumption by modelling these two parameters with a 1D mechanistic model (Vanderborght et al., 2021, 2023) during eight (non-consecutive) days of the drought experiment. Additionally, a comparison of RWU profiles obtained with the upscaled model and the ones obtained with SIAR (see chapter 3 section 3.4) is done.

2. Materials and Methods

A brief description of the macroscopic mechanistic model of Vanderborght et al. (2021, 2023) is included in section 2.1 and the details of the parametrization, in section 2.2.

2.1. 1D mechanistic modelling of water flow from the soil to the roots

The 1D mechanistic model of Vanderborght et al. (2021, 2023) couples a 1D root system architecture model assuming horizontally heterogeneous soil water potential (Eq. 4-1; Couvreur et al., 2014; Vanderborght et al., 2021) and a 1D soil water flow

model. In this study, only water flow into the roots and not from one soil compartment to others was modelled.

$$Q = K_{\mathrm{rs}} SUF\left(H_{\mathrm{s,r}} - H_{\mathrm{collar}}\right)$$

Equation 4-1

with Q ($L^3\ T^{-1}$) the flux rate of water taken up by the roots in a soil layer, K_{rs} ($L^3\ P^{-1}\ T^{-1}$) the root system (equivalent) conductance, $H_{s,r}$ (L) the water potential at the soil-root interface, SUF (-) the standard uptake fraction (equal to the fraction of water taken up by the roots in that layer relative to the total root system water uptake under homogeneous soil-root interface water potentials), and H_{collar} (L) the water potential at the plant collar.

K_{rs} and SUF are the only root system hydraulic properties necessary to calculate RWU in this model and they are derived from the hydraulic conductances of the root segments (see section 2.2.1) and their connectivity (Vanderborght et al., 2021, 2023).

2.2. Model setup and parametrization

The detailed steps to estimated K_{rs} and $H_{s,r}$ in wet conditions from a network of hydraulic conductances and from the experimental data collected in the second study are detailed in the first two subsections. The last subsection contains the parametrization of the model.

2.2.1. Estimation of K_{rs} and SUF from a conductance network

The network of hydraulic conductances, designed to reflect the drought experiment is presented in Fig. 4-1a. We estimated K_{rs} using two strategies (Fig. 4-1b): taking into account i) root radial (k_r, $L\ P^{-1}\ T^{-1}$) and axial (k_x, $L^4\ P^{-1}\ T^{-1}$) conductivities, and ii) the soil hydraulic conductivity (k_s, $L^2\ P^{-1}\ T^{-1}$) in addition to k_x and k_r (i.e., taking into account the resistance in the perirhizal zone (Couvreur et al., 2020)). The pressure units in the hydraulic conductances and conductivities are normally expressed as water heads and hence cancelling out with the length units in the numerator. However, we will consistently include in this text all elements in the units.

Case i): K_r and K_x ($L^3\ P^{-1}\ T^{-1}$) in each soil layer were calculated using Eq. 4-2 and Eq. 4-3, respectively:

$$K_{\mathrm{r}_z} = k_{\mathrm{r}} * S_{\mathrm{root}_z}$$

Equation 4-2

$$K_{\mathrm{x}_z} = \frac{k_{\mathrm{x}}}{dz} * N_{\mathrm{segments}_z}$$

Equation 4-3

where S_{root_z} (L^2) is the root surface area in soil layer z, dz is the thickness of soil layer z (1 cm) and N_{segments_z} (-) is the number of dz-long (i.e., 1 cm) root segments in soil layer z.

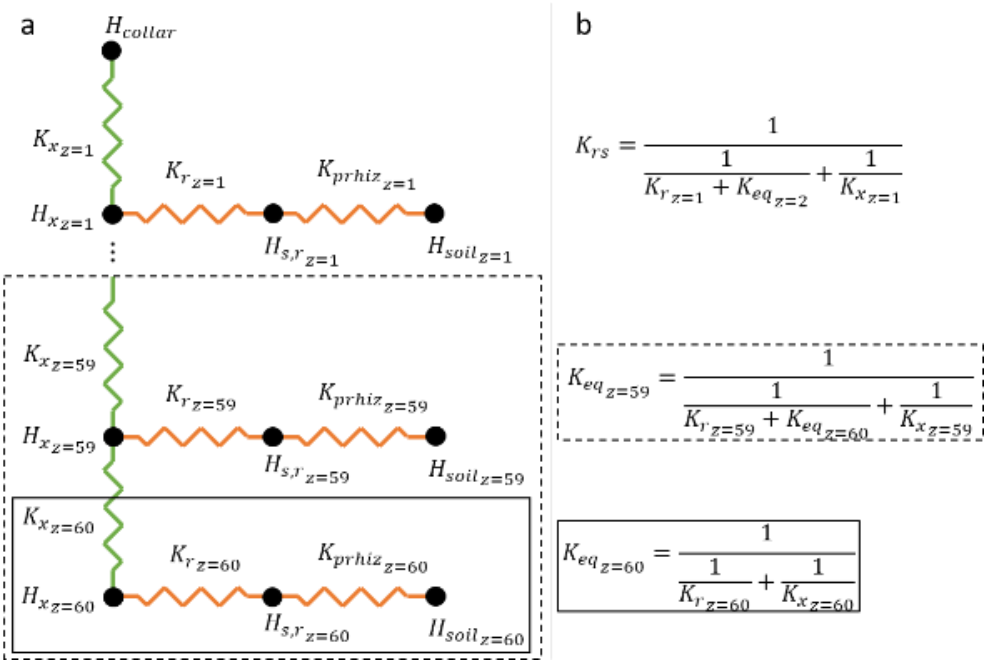

Figure 4-1 : a) 1D schematic representation of the soil-root hydraulic network of the experimental setup described in chapter 3. In each of the 60 (1 cm-thick) soil layers, water flow from the bulk soil (subscript *soil*) to the root xylem (subscript *x*) via the soil-root interface (subscript *s,r*) is governed by the differences in matric potentials (H) and the series of hydraulic conductances (K) in the perirhizal zone (subscript *prhiz*) and radially inside the root (subscript *r*). Water flow across soil layers is conditioned by the differences in H_x, the plant collar (with water potential H_{collar}), and the series of axial hydraulic conductances (K_x). b) Calculation of the root system conductance (K_{rs}) based only on K_r and K_x.

S_{root_z} was calculated using Eq. 4-4:

$$S_{\mathrm{root}_z} = \sum_{n=1}^{50} RL_{z_n} * \pi * D_{z_n}$$

Equation 4-4

where n (-) is the number of root diameter ranges (50 in total, from 0 to 5 mm in 0.1 mm steps), RL_{z_n} (L) is the total root length in soil layer z within the n diameter range and D_{z_n} (L) is the average root diameter in range n.

N_{segments_z} was further calculated using Eq. 4-5:

$$N_{\mathrm{segments}_z} = \frac{RL_z}{dz}$$

Equation 4-5

Case ii): K_x was calculated with Eq. 4-3, but K_r was calculated as follows (Eq. 4-6):

$$K_{\mathrm{r}_z} = \frac{2\pi r_{\mathrm{root}_z} \cdot RL_z \cdot B_z \cdot k_{\mathrm{r}} \cdot k_{\mathrm{s}_z}}{B_z \cdot k_{\mathrm{s}_z} + r_{\mathrm{root}_z} \cdot k_{\mathrm{r}}}$$

Equation 4-6

where r_{root} (L) is the weighted mean of the root radius (root length being the weight used), k_s ($L^2\ P^{-1}\ T^{-1}$) is the hydraulic conductivity of the soil, and B_z is a geometrical factor "simplifying the horizontal dimensions into radial domains between the bulk soil and root surfaces" (Couvreur et al., 2020; Schröder et al., 2009) all in soil layer z.

In a first approximation, k_{s_z} was considered to be a function of soil water content (Eq. 4-7; Mualem, 1976; van Genuchten, 1980):

$$k_{\mathrm{s}_z} = k_{\mathrm{sat}} \cdot \left(\frac{\theta_z - \theta_{\mathrm{res}}}{\theta_{\mathrm{sat}} - \theta_{\mathrm{res}}}\right)^{\lambda} \left(1 - \left(1 - \left(\frac{\theta_z - \theta_{\mathrm{res}}}{\theta_{\mathrm{sat}} - \theta_{\mathrm{res}}}\right)^{1/\mathrm{m}}\right)^{\mathrm{m}}\right)^2$$

Equation 4-7

where k_{sat} ($L^2\ P^{-1}\ T^{-1}$), λ (-) and m (-, equal to 1-1/n) are hydraulic parameters; θ_z, θ_{res}, and θ_{sat} are the soil water content ($L^3\ L^{-3}$) in soil layer z, residual, and saturated soil water content, respectively.

The geometrical factor B_z was calculated as follows (Eq. 4-8; Schröder et al., 2009):

$$B_z = \frac{2(1 - \rho_z^2)}{-2\rho_z^2 \cdot \ln \rho_z + \rho_z^2 - 1}$$

Equation 4-8

where ρ_z (-) is "the ratio of the distance between root segments and the root segments' averaged diameter" (Couvreur et al., 2020) and can be calculated as follows (Eq. 4-9):

$$\rho_z = \frac{\sqrt{\frac{1}{\pi RLD_z}}}{r_{\mathrm{root}_z}}$$

Equation 4-9

For the simulations conducted with the upscaled mechanistic model, Eq. 4-6 was solved numerically in an iterative process. This is because instead of k_s, an "effective conductivity" in the perirhizal zone is used (i.e., $\overline{k}_{prhiz}$), which depends on the water potential in the bulk soil and on $H_{s,r}$, as K_{rs} does (Vanderborght et al., 2023).

For the estimation of K_{rs} in wet and homogeneous conditions using the hydraulic conductance network, equivalent conductances (K_{eq_z}) were sequentially calculated starting with the deepest layer (i.e., z = 60 cm, Fig. 4-1b). Note that, as highlighted in Fig. 4-1b, the equivalent conductance in the shallowest layer (i.e., z = 1 cm) was that of the whole system, i.e., $K_{\mathrm{eq}_1} = K_{\mathrm{rs}}$.

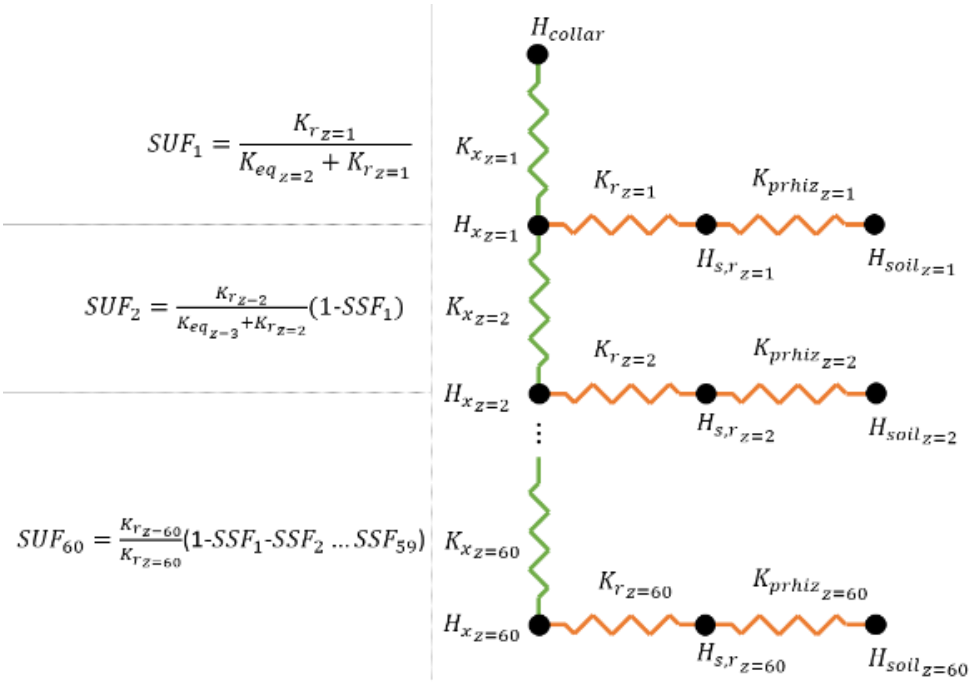

Figure 4-2 : Steps for the estimation of the standard uptake fraction (SUF, -) from the layer z-specific radial (K_{r_z}) and axial (K_{x_z}) hydraulic conductances.

Similarly, SUF from the hydraulic conductance network (SUF_{Knet}) was calculated in each 1 cm-thick soil layer. However, the sequential calculations started with the shallowest soil layer (i.e. z = 1 cm) yielding $SUF_{Knet} = \sum_{z=1}^{60} SUF_z$ (Fig. 4-2).

2.2.2. Estimation of K_{rs} with experimental data

Seven periods of the drought experiment in which vapor pressure deficit (vpd, kPa) around the plant in the first and last day of the period changed considerably were identified. These were days after seeding (DaS) 250-251 (period 1), 251-244 (period 2), 244-256 (period 3), 256-257 (period 4), 277-281 (period 5), 281-290 (period 6), and 290-291 (period 7). In each period *i* (1 through 7), K_{rs} was calculated using Eq. 4-10 as the slope of the relationship between transpiration rate (T_{act}, $L^3\ T^{-1}$) and leaf water potential (ψ_l, P) assuming constant soil water potential values around the roots (Fig. 4-3a):

$$K_{\mathrm{rs}_i} = \frac{T_{\mathrm{act}_{i_1}} - T_{\mathrm{act}_{i_n}}}{\psi_{\mathrm{l}_{i_n}} - \psi_{\mathrm{l}_{i_1}}}$$

Equation 4-10

where $T_{\mathrm{act}_{i_1}}$ and $T_{\mathrm{act}_{i_n}}$ are the plant transpiration rate on the first and last day of period *i*, respectively, and $\psi_{\mathrm{l}_{i_1}}$ and $\psi_{\mathrm{l}_{i_n}}$ is leaf water potential on the first and last day of period *i*, respectively.

Afterwards, a mean K_{rs} across sampling periods was used to estimate the daily soil water potential sensed by the plant or equivalent soil water potential ($\psi_{soil\ eq}$; Fig. 4-3a) for each day *j* for which experimental measurements were available (DaS 250-257, 277-296, 301-307, and 321-327). For any experimental day *j*, Eq. 4-10 can be re-written into Eq. 4-11:

$$mean\ K_{\mathrm{rs}} = \frac{T_{\mathrm{act\ day}_j} - T_{\mathrm{act\ night}_j}}{\psi_{\mathrm{l\ night}_j} - \psi_{\mathrm{l\ day}_j}}$$

Equation 4-11

where $T_{act\ day}$ and $T_{act\ night}$ ($\psi_{l\ day}$ and $\psi_{l\ night}$) are the transpiration rate (leaf water potential) during day and night, respectively.

If we assume $T_{act\ night} = 0$, then $\psi_{l\ night} = \psi_{soil\ eq}$ (Fig. 4-3a). Under this assumption and after rearranging Eq. 4-11, we obtain:

$$\psi_{\mathrm{soil\ eq}_j} = \frac{T_{\mathrm{act\ day}_j}}{mean\ K_{\mathrm{rs}}} + \psi_{\mathrm{l\ day}_j}$$

Equation 4-12

From this point onwards, transpiration rate and leaf water potential measurements during the day are represented by T_{act} and ψ_l, respectively. A variation in $\psi_{soil\ eq}$ was observed, which meant that our assumption of a constant $\psi_{soil\ eq}$ from one day to the next was not verified. Eq. 4-11 was modified and both $\psi_{soil\ eq}$ and K_{rs} were estimated again in an iterative process described here below and depicted in Fig. 4-3c:

1) K_{rs_j} was calculated using Eq. 4-13 as a mean value from day *j* to *j +1* (Fig. 4-3b):

$$K_{\mathrm{rs}_j} = \frac{T_{\mathrm{act}_j} + T_{\mathrm{act}_{j+1}}}{\psi_{\mathrm{soil\ eq}_j} + \psi_{\mathrm{soil\ eq}_{j+1}} - \psi_{\mathrm{l}_j} - \psi_{\mathrm{l}_{j+1}}}$$

Equation 4-13

2) Since a statistically significant correlation between the calculated K_{rs_j} values and the mean θ across the soil profile was found, $\psi_{\mathrm{soil\ eq}_j}$ was recalculated using Eq. 4-14 with K_{rs_j} calculated from the correlation with θ (i.e., $K_{\mathrm{rs}_j}(\theta_j)$). That is, K_{rs} was not constant between consecutive observation days, unless soil water content was also constant:

$$\psi_{\mathrm{soil\ eq}_j} = \frac{T_{\mathrm{act}_j}}{K_{\mathrm{rs}_j}(\theta_j)} + \psi_{\mathrm{l}_j}$$

Equation 4-14

The recalculated $\psi_{\mathrm{soil\ eq}_j}$ were fed into Eq. 4-13 (step 1) to estimate K_{rs_j} anew. Steps 1 and 2 were repeated ten times (arbitrary low number to test the convergence of the proposed recalculation loop).

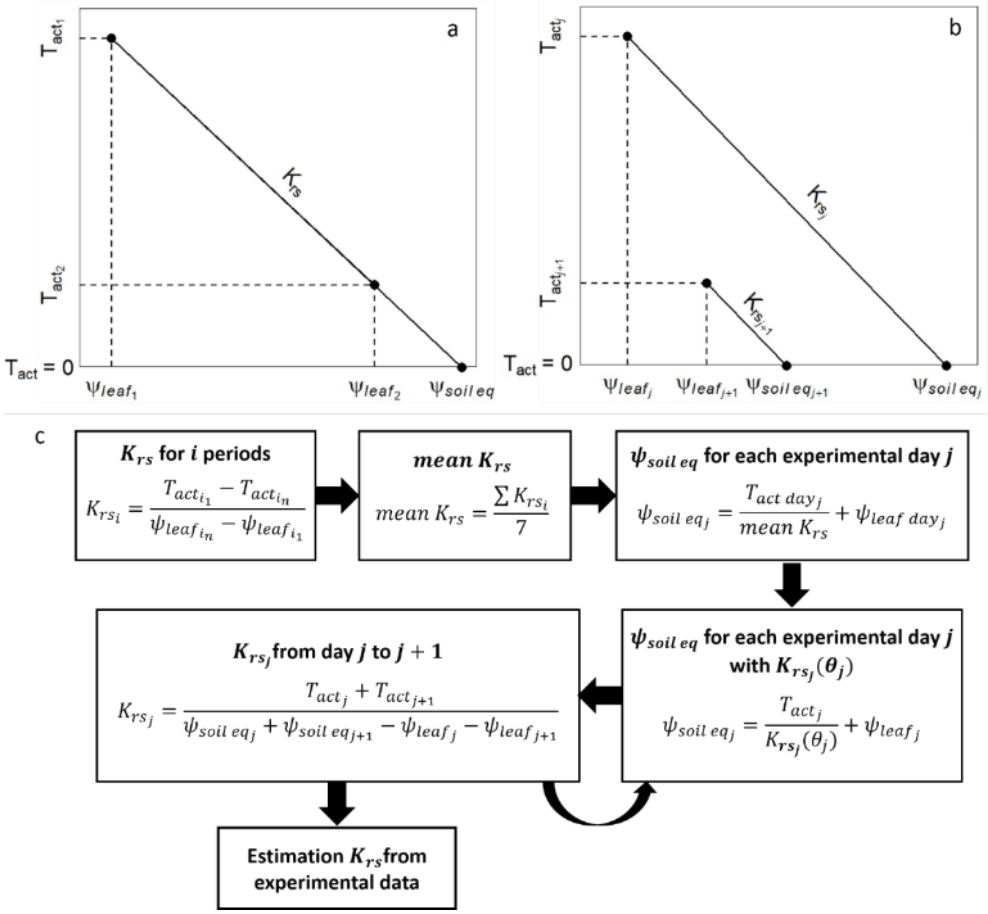

Figure 4-3 : a) Actual plant transpiration rate (T_{act}, $L^3\ T^{-1}$) expressed as a function of leaf water potential (ψ_l, P) either assuming a constant root system hydraulic conductance (K_{rs}, $L^3\ P^{-1}\ T^{-1}$) at the beginning and at the end of the selected periods or b) assuming K_{rs} was varying. c) Steps of the calculation of K_{rs} with the data from the drought experiment including an iterative recalculation of K_{rs_j} from day j to $j+1$ and of $\psi_{soil\ eq}$ for each experimental day j with $K_{rs_j}(\theta_j)$.

Two more strategies, both described in Cai et al. (2022), were employed to validate the estimation of K_{rs} with our experimental data and with the network of hydraulic conductances. First, we calculated the slope in the linear correlation between T_{act} and ψ_l in wet soil conditions (i.e., $K_{root\ max}$). Second, the magnitude of $K_{root\ max}$ was estimated from its correlation with total RL.

2.2.3. Modelling $H_{s,r}$, K_{rs}, SUF, and RWU

Vertical profiles (eleven soil depths of varying thickness) in eight (non-consecutive) days (DaS 275, 284, 304, 316, 323, 325, 326 and 327) of varying above- and below-ground environmental conditions of the drought experiment (Table 4-1) were used to model $H_{s,r}$, K_{rs}, SUF, and the sink term profiles with the upscaled mechanistic model.

The input variables (Table S4-1) were:

i. calculated mean values of root diameter weighted by root length (r_{root}, cm),
ii. measured RLD (cm cm^{-3}) determined via MRI,
iii. water flux into the roots derived from the sink term from the water stable isotope mixing model SIAR per root surface area (cm d^{-1}),
iv. bulk soil water potential (H_s, cm), calculated from θ measurements with the bimodal Mualem-van Genuchten water retention model (Fig. 4-4), and
v. SUF considered equal to the relative root length (rRL) profile ($SUF_{root} = \sum_{z=1}^{11} rRL = 1$) or the relative source contribution (i.e., relative root water uptake, rRWU) profiles ($SUF_{iso} = \sum_{z=1}^{11} rRWU = 1$) obtained with SIAR.

Table 4-1 : Daily mean values and standard deviation of the air temperature (T, °C), relative humidity (rh, %), vapor pressure deficit (vpd, kPa), soil water content (θ, cm^3 cm^{-3}), and transpiration rate (Tr, cm d^{-1}) during eight (non-consecutive) selected days of the drought experiment in days after seeding (DaS).

DaS	T (°C)	rh (%)	vpd (-)	θ (cm^3 cm^{-3})	Tr (cm d^{-1})
275	23.2 ± 0.3	53.1 ± 1.6	1.3 ± 0.0	0.15 ± 0.02	0.95 ± 0.06
284	24.4 ± 0.3	67.1 ± 1.4	1.0 ± 0.0	0.13 ± 0.01	0.72 ± 0.01
304	22.5 ± 0.1	70.3 ± 1.6	0.8 ± 0.0	0.16 ± 0.03	0.46 ± 0.01
316	22.7 ± 0.1	67.5 ± 1.0	0.9 ± 0.0	0.16 ± 0.02	0.43 ± 0.00
323	24.3 ± 0.2	39.0 ± 2.4	1.8 ± 0.1	0.08 ± 0.01	0.63 ± 0.06
325	22.7 ± 0.2	52.8 ± 1.1	1.3 ± 0.0	0.07 ± 0.01	0.23 ± 0.01
326	22.7 ± 0.1	50.3 ± 1.0	1.4 ± 0.0	0.07 ± 0.01	0.20 ± 0.01
327	22.7 ± 0.1	47.8 ± 1.1	1.4 ± 0.0	0.07 ± 0.01	0.16 ± 0.01

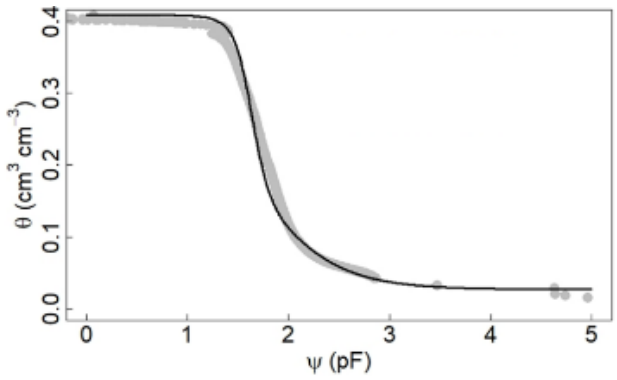

Figure 4-4 : Mualem-van Genuchten water retention curve (black continuous line) fitted to measurements (gray circles) in the standard soil (classified as a loamy sand) used in the drought experiment.

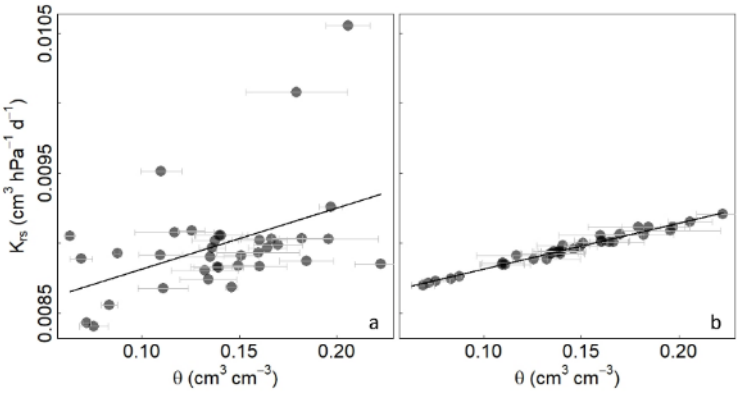

Figure 4-5 : a) The root system equivalent conductance (K_{rs}, cm^3 d^{-1} hPa^{-1}) as a function of soil water content (θ, cm^3 cm^{-3}) with the unmodified data from the drought experiment and b) after recalculating the equivalent soil water potential ($\psi_{soil\ eq}$) and K_{rs}.

Alongside these parameters, daily transpiration rate (T_{act}, cm d^{-1}; Table 4-1) and the estimated K_{rs} from experimental data (see section 2.2.2) were used in the model.

The following scenarios with SUF_{iso} and with SUF_{root} were considered:

a) unmodified input data and no decrease of soil hydraulic conductivity near the root surface (i.e., scenario "base"),
b) unmodified input data and nonlinear decrease of soil hydraulic conductivity near the root surface (i.e., scenario "nonlin"),
c) 3% overestimation of θ, 10% of root activity, and nonlinear decrease of soil hydraulic conductivity near the root surface (i.e., scenario "nonlin low").

3. Results and Discussion

The results of the different strategies to estimate K_{rs} and SUF (i.e., from the hydraulic conductance network, from the experimental data, and from root length) are presented and discussed in section 3.1. The results of the upscaled mechanistic model, especially the decrease in K_{rs} and $H_{s,r}$ in the last days of the drought experiment, are discussed in length in section 3.2. Finally, the similarities and differences between the probabilistic (second study) and physically-based RWU profiles (present study) are compared in section 3.3.

3.1. Analysis of the estimation strategies of K_{rs} and SUF

For the estimation of K_{rs} from the hydraulic conductance network (see section 2.2.1), k_r and k_x were set equal to 5.0x10^{-5} cm hPa^{-1} d^{-1} and 5.6x10^{-4} cm^4 hPa^{-1} d^{-1}, respectively. These values were taken from the ranges presented in Meunier et al. (2017). We were confident in the selected value for k_r when applying the model of Rieger & Litvin (1999), in which k_r is expressed as a function of root diameter, and obtained a value of 6.87x10^{-5} cm hPa^{-1} d^{-1}. The estimation of K_{rs} with K_{r_z} from Eq. 4-3 (i.e., considering only k_r) was 1x10^{-2} cm^3 d^{-1} hPa^{-1}. When both k_s and k_r were

considered in the calculation of K_{r_z} in Eq. 4-6, K_{rs} was 1.49x10^{-2} cm^3 d^{-1} hPa-^{1}. These two values are close to the mean K_{rs} across sampling periods (calculation described in section 2.2.2) which was 8.72x10^{-3} cm^3 hPa^{-1} d^{-1} and to $K_{root\ max}$ (Cai et al., 2022), when this was obtained from the slope in the linear correlation between T_{act} and ψ_l in wet soil (8.38x10^{-3} cm^3 d^{-1} hPa^{-1} with $\theta > 0.15$ cm^3 cm^{-3}). From the correlation between total RL and $K_{root\ max}$ also presented in Cai et al. (2022), we estimated three values for $K_{root\ max}$ for three different RL: 9.69x10^{-3} cm^3 hPa^{-1} d^{-1} (RL = ~3,000 cm, measured via MRI on DaS 75), 1.08x10^{-2} cm^3 hPa^{-1} d^{-1} (RL = ~10,000 cm, measured via MRI on DaS 307), and 0.17 cm^3 hPa^{-1} d^{-1} (RL = ~100,000 cm, measured destructively through harvesting and scanning of the roots on DaS 327). Note that only the values of $K_{root\ max}$ when considering RL from MRI measurements, which were only 3 and 10% of the RL from root scans, were very close to mean K_{rs}, the slope of $\psi_l(T_{act})$ in wet conditions and K_{rs} from the hydraulic conductance network.

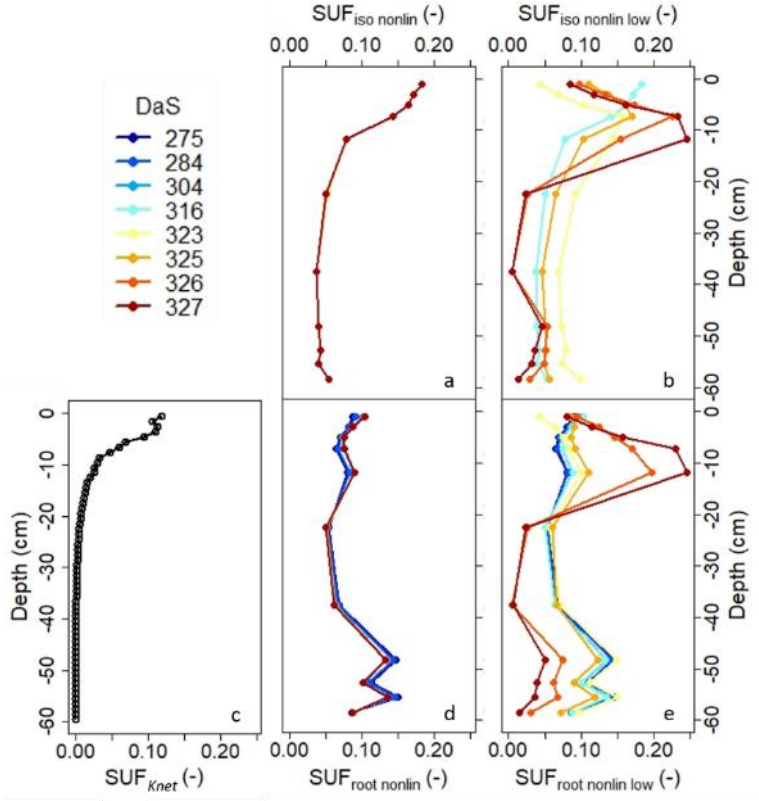

Figure 4-6 : Standard uptake fraction (SUF, -) modelled in eight (non-consecutive) days of the drought experiment with the upscaled mechanistic model considering an input SUF equal to relative RWU from the mixing model SIAR (SUF_{iso}; Parnell et al., 2010) in a) scenario "nonlin" and b) "nonlin low". Modelled SUF considering an input SUF equal to the relative root length (SUF_{root}) in d) scenario "nonlin" and e) "nonlin low". c) SUF calculated from the hydraulic conductance network (SUF_{Knet}).

During the recalculation of K_{rs} and $\psi_{soil\ eq}$ (see section 2.2.2), we tested the significance of the correlation of K_{rs} with plant age (DaS), T_{act}, and θ. Only K_{rs} and θ seemed to be significantly correlated (r^2 = 0.18, p-value = 0.006; Fig. 4-5a). The correlation between K_{rs} and θ after the first iteration for the recalculation of both K_{rs} and $\psi_{soil\ eq}$ is shown in Fig. 4-5b.

The modelled SUF_{iso} and SUF_{root} profiles in the "base" scenario (data not shown) were almost identical to the SUF_{iso} and SUF_{root} profiles in the "nonlin" scenario (Fig. 4-6a and d, respectively), as well as to the input profiles. In the "nonlin low" scenario, considerable shifts of the SUF_{iso} and SUF_{root} profiles in the last two to fours days of the experiment were observed (Fig. 4-6b and e, respectively). SUF increased in layer 7-20 cm and decreased in layer 0-7 and 20-60 cm in comparison to the preceding days. Overall, the simulated shifts in the SUF_{iso} and SUF_{root} profiles in scenario "nonlin low" were similar in direction and magnitude, even though the input profiles differed (rRWU and rRL, very similar to the $SUF_{iso\ nonlin}$ and $SUF_{root\ nonlin}$ profiles in the first four days; Fig. 4-6b and e). The SUF profile obtained from the hydraulic conductance network (SUF_{Knet}, section 2.2.1) differed considerably from both SUF_{iso} and SUF_{root} (Fig. 4-6c).

3.2. Exponential decrease of K_{rs} and $H_{s,r}$ in dry soil

We observed an exponential decrease of the modelled K_{rs} (magenta lines in Fig. 4-7) and of the average $H_{s,r}$ (magenta discontinuous lines in Fig. 4-8) in the last four days of the drought experiment under scenario "nonlin low" regardless of the input SUF. No noticeable decrease in the same period in either K_{rs}, nor $H_{s,r}$ was observed under scenarios "base" (data not shown) or "nonlin" (blue lines in Fig. 4-7 and solid magenta lines in Fig. 4-8). The modelled bulk soil water potential (H_{soil}) also decreased (although much less than $H_{s,r}$) under the "nonlin low" scenario (black discontinuous lines in Fig. 4-8).

Since the investigated plant is an herbaceous species (i.e., with a relatively short xylem path from the collar to the leaves), we were expecting measured leaf water potentials (H_{leaf}) and modelled collar potentials (H_{collar}) to be similar. However, except on DaS 327, they differed greatly (Fig. 4-8, maximum difference of 20,000 cm on DaS 326). We do not believe these discrepancies can be attributed to horizontal heterogeneities in root density or soil water content leading to an overestimation of simulated collar water potential (Couvreur et al., 2014), since the used column was relatively thin (diameter = 11 cm) and densely rooted. Cavitation, on the other hand, could explain the observed differences in leaf and collar water potential. However, we do not have experimental data to support this assumption.

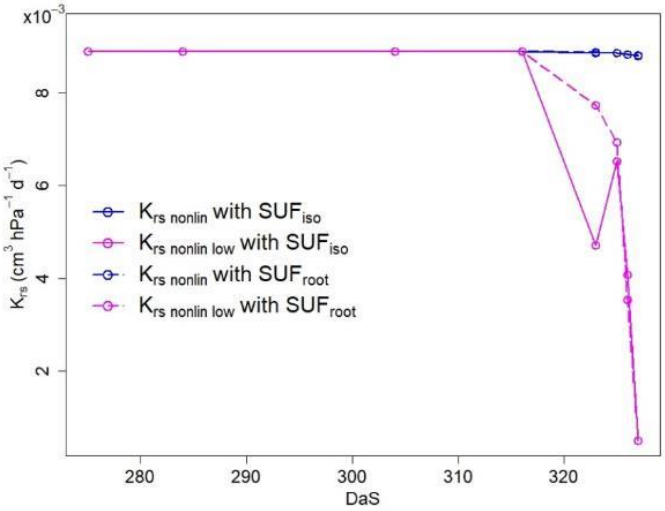

Figure 4-7 : Modelled root system conductance (K_{rs}, $cm^3\ hPa^{-1}\ d^{-1}$) in eight (non-consecutive) days of the drought experiment under scenario "nonlin" (blue lines) and "nonlin low" (magenta lines) with SUF_{iso} (solid lines) and SUF_{root} (dashed lines) using the upscaled mechanistic model.

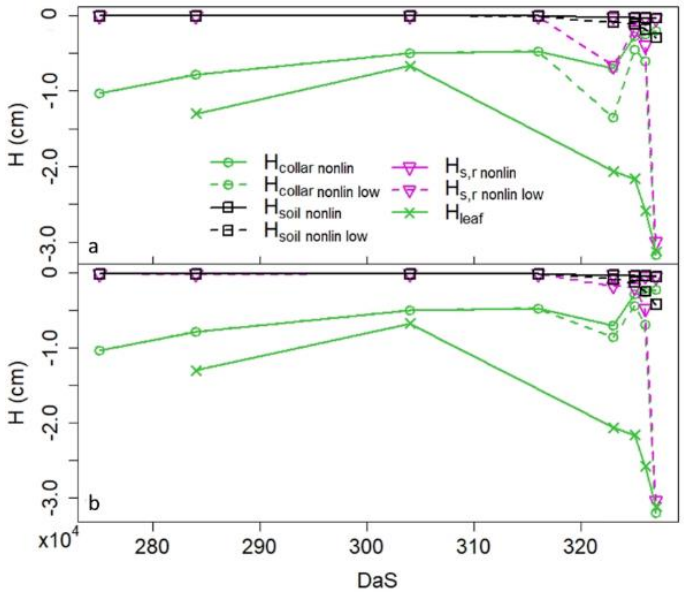

Figure 4-8 : Modelled water potential (H, cm) in the plant collar (subscript *collar*, green lines with circles), modelled average water potential in the bulk soil (subscript *soil*, black lines) and the soil-root interface (subscript *s,r*, magenta lines) under scenarios "nonlin" (solid lines) and "nonlin low" (dashed lines) a) with SUF_{iso} and b) SUF_{root} using the upscaled mechanistic model. Measured leaf water potential (subscript *leaf*, green lines with crosses) is included for comparison proposes.

3.3. Root water uptake quantification and dynamics from a hydraulic and a probabilistic perspective

In general, RWU simulated with the 1D mechanistic model under scenario "nonlin low" with SUF_{iso} and SUF_{root} and obtained from SIAR (Fig. 4-9) is consistently higher in soil layers 0-10 cm and 50-60 cm in comparison to the uptake in layer 10-50 cm in the first four days. While RWU simulated with SUF_{root} was equal or slightly higher at the bottom of the column than at the top, RWU obtained with SIAR and simulated with SUF_{iso} was much higher (< DaS 323) at the top than at the bottom.

Before DaS 323, a gradual decrease in RWU most markedly at the top and bottom of the column is observed in both the results of the 1D model and SIAR. However, on this day water uptake in soil layer 0-8 cm decreased (with a minimum value at the surface) and increased below 8 cm (most markedly in soil layer 50-60 cm) in the simulations of the 1D model (Fig. 4-9a and b). RWU in the SIAR profile in soil layers 0-10 cm (50-60 cm) also decreased (increased), but the maximum remained at the surface (Fig. 4-9c). The top 5 cm on DaS 323 were drier than the rest of the soil layers (yellow line in Fig. 4-9d) and Tr was high (Table 4-1). Water uptake probably decreased in this region and remained low because $H_{s,r}$ was much closer to H_{collar} than in previous days (compare lines in the yellow-red spectrum in Fig. 4-10b and d with the solid green line with crosses in Fig. 4-8) (Li et al., 2002).

Thomas et al. (2020) observed a shift in water uptake to the second highest root density region after θ in the most densely rooted region dropped below 15%. In our study, θ in all soil layers on DaS 323 was already below 10% and due to pot-bound roots the bottom soil layers contained as much or slightly more roots than the top. Therefore, and similar to the observations of these authors, an increase in RWU at the bottom of the column in our study made the most hydrological sense, since there the maximum water potential difference was reached and more root surface area than in the intermediate layers was available for water uptake. We believe the conclusion of Thomas et al. (2020) that RLD is a good root water uptake indicator only in wet conditions applies here. However, the picture is only complete when the hydraulic properties of the system are taken into account.

In the last three days of the experiment, Tr (Table 4-1) and H_{collar} (continuous green line with crosses in Fig. 4-8) in the drought experiment decreased considerably due to a drop in canopy conductance. RWU (Fig. 4-7a and b) and SUF (Fig. 4-6b and e) in the simulations of the 1D model progressively increased from the surface to a maximum value at depth 8 or 10 cm and decreased progressively towards the bottom of the column. Again, the decrease in soil layer 50-60 cm was more pronounced than that in soil layer 10-50 cm. The decrease in RWU in the same period in comparison to previous periods is also observed in the SIAR profiles, but it remained slightly higher in soil layer 0-5 cm than in soil layer 5-10 cm until the end (Fig. 4-9c). From the 1D simulations, we concluded that RWU in these last days in soil layer 5-10 cm increased because this layer presented the path of less hydraulic resistance until the end of the drought experiment (i.e., higher $H_{s,r}$ than above 5 cm and below 10 cm, Fig. 4-10b and d), whereas it decreased with increasing depth because hydraulic resistance increased

with depth (increasingly lower $H_{s,r}$). We see here the preponderance of the dependency of RWU patterns to whole system hydraulics in dry conditions and the lessening of the influence of RLD (Draye et al., 2010). The monitoring of the plant in the drought experiment stopped at DaS 327 since the plant died. On this day, $H_{s,r}$ across the soil profile was equal to H_{leaf} and Tr then stopped.

Only by assuming an overestimation of 3% of the θ measurements and 10% of root length involved in water uptake do we observe significant changes in the hydraulic properties of the root system and, consequently, differences between the probabilistic and physically-based RWU profiles. The latter assumption could be supported by the findings of several studies. In wet conditions, uptake is mostly happening in the proximal part of the roots (furthest part from the tip), once these regions dry out, root water uptake shifts to the distal part of the roots (closest to the root tip) and water transport in the rest of the root is happening on the axial and not radial direction (Hsiao & Xu, 2000). Doussan et al. (2006) modelled the development of an extraction front some hours after water uptake started and observed that not all roots take up water at any given time. Furthermore, evidence suggests that young roots are more "RWU-active" than older mature roots, which mostly transport water to the leaves (Bechmann et al., 2014). The main reason is that mature roots have a lower radial hydraulic conductivity due to their higher "endodermal development (suberin lamellae, cell wall thickening)" (Frensch et al., 1996). The investigated plant, a dicot, in the drought experiment was almost one year old at the end, so it is safe to assume that a high percentage of the root segments were suberized (with a lower radial conductivity) or behind a potential uptake front (where the water potential difference had dissipated) and likely not actively taking up water. Furthermore, the closet values of $K_{root\ max}$ from the correlation with root length (see section 3.1) was when we used the MRI-derived root length values, which were 3% and 10% lower than the scan-derived ones.

The assumed overestimation of θ in scenario "nonlin low" is partly supported by the decreased accuracy of the used frequency domain sensors (EC-5; Decagon Devices, USA) of around 1-2 % volume, when temperature, electric conductivity, and supply voltage effects on the readings are taken into account (Bogena et al., 2007). The low spatial resolution or proximity to roots (in spite of the corrections done for root volume) could account for further errors in the measurements resulting in overestimation of θ. Relatively small measurement uncertainties in θ measurements (like the 3% in our assumption) in the "dry end" of the retention curve (Fig. 4-4) result in considerably large inaccuracies in the estimation of soil water tension.

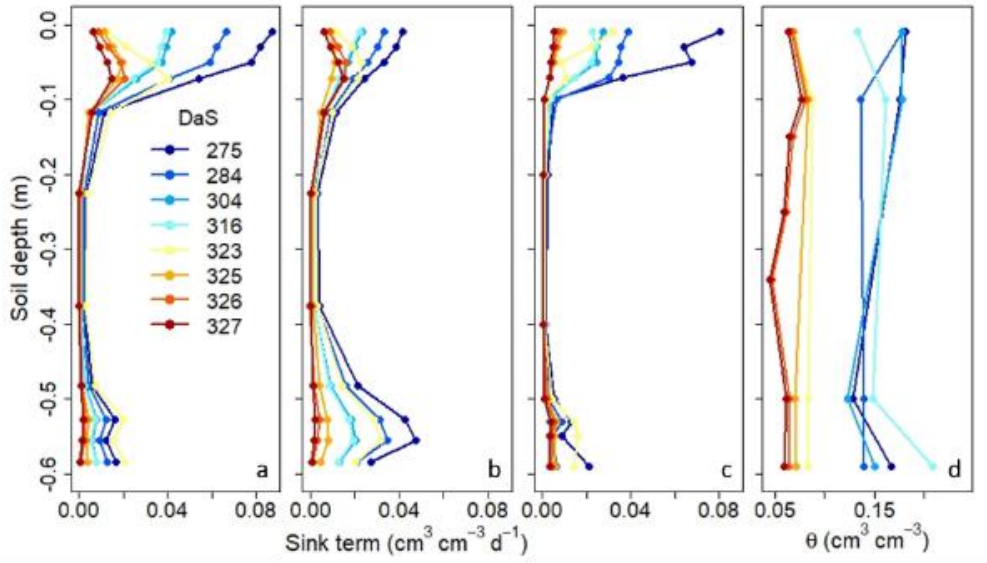

Figure 4-9 : Root water uptake profiles (sink term, $cm^3\ cm^{-3}\ d^{-1}$) modelled with the upscaled mechanistic model under scenario "nonlin low" a) with SUF_{iso}, b) with SUF_{root}, c) obtained with SIAR, and d) soil water content (θ, $cm^3\ cm^{-3}$) profiles in eight (non-consecutive) days of the drought experiment.

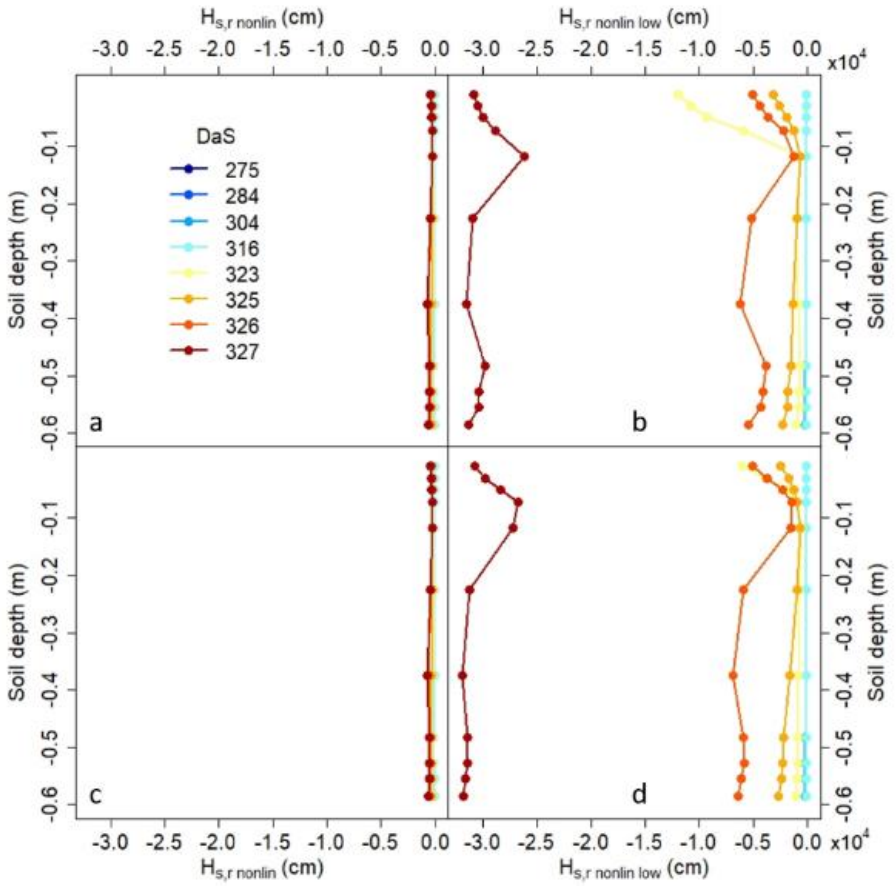

Figure 4-10 : Water potential at the soil-root interface ($H_{s,r}$, cm) modelled with the upscaled mechanistic model under a) scenario "nonlin" and b) scenario "nonlin low" with SUF_{iso}, and under c) scenario "nonlin" and d) scenario "nonlin low" with SUF_{root} in eight (non-consecutive) days of the drought experiment.

4. Conclusions

Only under the "nonlin low" scenario an exponential drop of K_{rs} and $H_{s,r}$ in the last four days of the drought experiment was observed. In previous (non-consecutive) four days, bulk soil water potential was uniform and above or around 0.15 cm^3 cm^{-3}, consequently $H_{s,r}$ profiles were close to zero and the modelled RWU was highest in soil layers 0-10 cm (decreasing values with depth) and 50-60 cm (increasing values with depth), where most of the roots were. In the last four days, a shift in the maximum RWU from right below the surface to a depth of 10 cm was modelled, explained by increasingly negative $H_{s,r}$ values, first at the surface and then along the soil profile. On DaS 323, RWU increased markedly in soil layer 50-60 cm, since this was one of the most advantageous hydraulic pathway under high Tr and drying out of soil layer 0-15 cm. SUF decreased (increased) in soil layers 0-5 cm (20-60 cm) compared to the four preceding days. Later, RWU at the bottom decreased and SUF remained low in layer 0-5 cm, increased even more in layer 5-20 cm, and decreased below 20 cm. The increase (decrease) in RWU at the bottom (top) of the column was also observed in the profiles obtained with SIAR. However, no decrease in RWU in soil layer 0-5 cm was observed.

Coupling of probabilistic and hydraulic approaches for the quantification of RWU could allow a broader insight into the dynamic interactions in the soil-plant-atmosphere continuum and the description of breaking or tipping points (see chapter 5 section 3). For example, certain soil layers could be eliminated as water sources in SIAR based on the presence of steep water potential gradients in the soil-root interface. Finally, we highlight the necessity of accounting for the nonlinear decrease in soil hydraulic conductivity near the roots in macro- and microscopic hydraulic models especially in dry conditions to accurately model experimental results.

5. Supplementary material

Table S4-1 : Input parameters for the modelling of the root system equivalent conductance (K_{rs}, $L^3\ P^{-1}\ T^{-1}$), the soil-root interface water potential ($H_{s,r}$, L), the standard uptake fraction (SUF, -), and root water uptake (sink term, $L^3\ L^{-3}\ T^{-1}$) with the 1D mechanistic model described in Vanderborght et al. (2023) in eight (non-consecutive) days (days after seeding – DaS – 275, 284, 304, 316, 323, 325, 326 and 327) of the drought experiment.

DaS	Depth (cm)	Root diameter (cm)	RLD (cm cm^{-3})	Water flux into the roots (cm d^{-1})	Matric potential (cm)	SUFroot (-)	SUFiso (-)
275	2	0.0257	3.20	0.049324	58.49	0.087326	0.205258
275	4	0.0285	2.88	0.042774	58.67	0.080989	0.169065
275	6	0.0267	2.54	0.041589	58.85	0.069260	0.173592
275	8.5	0.0258	1.81	0.030976	59.05	0.064334	0.12128
275	15	0.0267	0.84	0.004292	60.23	0.080046	0.042239
275	30	0.0276	0.24	0.002289	65.95	0.053841	0.048588
275	45	0.0275	0.30	0.001451	73.93	0.068176	0.032075
275	51.5	0.0275	1.55	0.005029	79.65	0.147256	0.04818
275	54	0.0275	3.15	0.015529	74.95	0.112415	0.043807
275	57	0.027	3.63	0.005884	69.32	0.150144	0.034152
275	60	0.0285	2.09	0.006964	63.17	0.086214	0.081763
284	2	0.0257	3.40	0.030766	59.24	0.091826	0.168717
284	4	0.0285	2.97	0.030437	62.43	0.082717	0.158532
284	6	0.0267	2.62	0.027239	65.62	0.070783	0.149825
284	8.5	0.0258	1.91	0.032875	69.21	0.067528	0.169616
284	15	0.0267	0.88	0.007476	73.59	0.082674	0.096951
284	30	0.0276	0.24	0.001530	73.58	0.052922	0.04281
284	45	0.0275	0.30	0.001577	73.57	0.066713	0.04595
284	51.5	0.0275	1.52	0.003510	73.56	0.143220	0.044319
284	54	0.0275	3.09	0.013404	73.41	0.109154	0.049827
284	57	0.027	3.56	0.004059	73.27	0.145803	0.031044
284	60	0.0285	2.12	0.002741	73.12	0.086660	0.042408
304	2	0.0257	3.83	0.022364	59.24	0.101528	0.193927
304	4	0.0285	3.17	0.021713	59.17	0.086445	0.178825
304	6	0.0267	2.80	0.019744	59.10	0.074068	0.171723
304	8.5	0.0258	2.15	0.016704	59.02	0.074415	0.136282
304	15	0.0267	0.96	0.003369	60.02	0.088341	0.069092

304	30	0.0276	0.23	0.001176	66.76	0.050939	0.052005
304	45	0.0275	0.29	0.000868	76.16	0.063557	0.039979
304	51.5	0.0275	1.46	0.001296	82.91	0.134519	0.025884
304	54	0.0275	2.95	0.005543	79.16	0.102125	0.03258
304	57	0.027	3.40	0.004795	74.32	0.136443	0.057984
304	60	0.0285	2.18	0.001705	69.04	0.087620	0.041719
316	2	0.0257	3.90	0.017874	78.88	0.102949	0.163709
316	4	0.0285	3.20	0.020471	75.75	0.086991	0.178084
316	6	0.0267	2.82	0.017352	72.62	0.074549	0.15941
316	8.5	0.0258	2.19	0.016326	69.10	0.075424	0.140689
316	15	0.0267	0.97	0.004730	65.06	0.089171	0.102453
316	30	0.0276	0.23	0.001271	66.63	0.050649	0.059398
316	45	0.0275	0.29	0.000627	68.83	0.063095	0.030492
316	51.5	0.0275	1.45	0.001861	70.41	0.133245	0.039235
316	54	0.0275	2.93	0.007054	65.47	0.101095	0.043793
316	57	0.027	3.38	0.002596	60.28	0.135072	0.033157
316	60	0.0285	2.20	0.001919	54.62	0.087760	0.04958
323	2	0.0257	3.90	0.027425	375.86	0.102949	0.171659
323	4	0.0285	3.20	0.020459	330.52	0.086991	0.121631
323	6	0.0267	2.82	0.007176	285.19	0.074549	0.045051
323	8.5	0.0258	2.19	0.013643	234.18	0.075424	0.080344
323	15	0.0267	0.97	0.002994	173.09	0.089171	0.04432
323	30	0.0276	0.23	0.002205	180.72	0.050649	0.070398
323	45	0.0275	0.29	0.001124	191.38	0.063095	0.037363
323	51.5	0.0275	1.45	0.005814	199.02	0.133245	0.083785
323	54	0.0275	2.93	0.023640	206.22	0.101095	0.100306
323	57	0.027	3.38	0.014970	212.18	0.135072	0.130686
323	60	0.0285	2.20	0.006482	218.68	0.087760	0.114457
325	2	0.0257	3.90	0.007409	358.54	0.102949	0.125743
325	4	0.0285	3.20	0.006141	323.34	0.086991	0.098988
325	6	0.0267	2.82	0.004141	288.15	0.074549	0.07049
325	8.5	0.0258	2.19	0.003979	248.55	0.075424	0.063532
325	15	0.0267	0.97	0.001195	205.99	0.089171	0.047958
325	30	0.0276	0.23	0.000794	241.83	0.050649	0.068726
325	45	0.0275	0.29	0.000651	291.84	0.063095	0.058715
325	51.5	0.0275	1.45	0.003120	327.67	0.133245	0.121905

325	54	0.0275	2.93	0.009532	342.15	0.101095	0.109666
325	57	0.027	3.38	0.004804	350.79	0.135072	0.113715
325	60	0.0285	2.20	0.002518	360.22	0.087760	0.120562
326	2	0.0257	3.90	0.005937	396.26	0.102949	0.118669
326	4	0.0285	3.20	0.005209	355.53	0.086991	0.098882
326	6	0.0267	2.82	0.003761	314.80	0.074549	0.075399
326	8.5	0.0258	2.19	0.004030	268.97	0.075424	0.075794
326	15	0.0267	0.97	0.001206	263.19	0.089171	0.057022
326	30	0.0276	0.23	0.000703	423.99	0.050649	0.071642
326	45	0.0275	0.29	0.000536	741.84	0.063095	0.056951
326	51.5	0.0275	1.45	0.002350	457.83	0.133245	0.108153
326	54	0.0275	2.93	0.008410	446.29	0.101095	0.113943
326	57	0.027	3.38	0.003817	480.97	0.135072	0.106405
326	60	0.0285	2.20	0.002077	518.81	0.087760	0.117141
327	2	0.0257	3.90	0.004467	461.07	0.102949	0.11314
327	4	0.0285	3.20	0.004364	414.92	0.086991	0.104989
327	6	0.0267	2.82	0.003185	368.76	0.074549	0.080907
327	8.5	0.0258	2.19	0.004180	316.83	0.075424	0.099604
327	15	0.0267	0.97	0.001268	308.25	0.089171	0.075949
327	30	0.0276	0.23	0.000589	485.19	0.050649	0.076143
327	45	0.0275	0.29	0.000392	882.40	0.063095	0.052751
327	51.5	0.0275	1.45	0.001442	555.51	0.133245	0.084067
327	54	0.0275	2.93	0.006040	557.52	0.101095	0.103695
327	57	0.027	3.38	0.002919	612.74	0.135072	0.10313
327	60	0.0285	2.20	0.001478	672.97	0.087760	0.105624

Chapter 5

Conclusions and future prospects

Across scales, weather-related extremes such as drought and heat waves are affecting the carbon and water cycles and are projected to intensify due to naturally occurring positive feedback especially between vegetation and atmospheric conditions (Bastos et al., 2013; Frank et al., 2015; IPCC, 2021; Seneviratne et al., 2006). Under this scenario, understanding the processes occurring at the vegetation-atmosphere and soil-vegetation interfaces and influencing water movements in space and time is central towards a meaningful assessment of the effects of climate change. Ecosystems with higher sensitivity to changes in water availability (mainly from precipitation) such as grasslands are especially vulnerable to more frequent droughts and heatwaves, since here there is a higher dependency of biotic processes to abiotic ones (Jentsch et al., 2011;Yang et al., 2016). This also makes them an interesting subject for ecohydrological studies, in which a mechanistic understanding of the interplay between ecophysiological and hydrological phenomena is pursued (Dubbert, Piayda, et al., 2014; Newman et al., 2006). With such an approach, the detrimental effect of fertilization on ecosystem-level resistance to drought of grasslands through biodiversity loss (mainly of forb species) was described (Kübert et al., 2019; Stampfli et al., 2018; Zeiter et al., 2016). Drought resistance and recovery, and ultimately maintenance of ecosystem productivity and services, in grasslands depend on species and functional group richness (Tilman & Downing, 1994; Tilman & El Haddi, 1992).

Water stable isotopes have been used for several decades as tracers of water in the soil-plant-atmosphere continuum rendering crucial insights into the aforementioned interactions. More specifically, through water isotopic determinations (δ^2H and $\delta^{18}O$) in the soil and vegetation links between RWU, plant transpiration, and climatic conditions as well as dominance of biotic or abiotic control mechanisms can be explored with a range of established methodologies (e.g., Beyer et al., 2016; Meinzer et al., 1999; Meunier et al., 2017; Sun et al., 2014). Nevertheless, limitations of some of these methodologies, especially during soil or plant sampling and water extraction, result in uncertainties of the isotopic determinations and lack of spatio-temporal representation, ultimately reducing the confidence in the enabled insights (e.g., Beyer & Penna, 2021; Duvert et al., 2022; Gilg et al. 2004; He et al., 2023; Orlowski, Pratt, et al. 2016; Santos Pires et al., 2022; Zuecco et al., 2022). Many of these limitations are addressed with in situ non-destructive online isotopic techniques coupling laser-based spectroscopy and continuous sampling of soil or plant water vapor (e.g., Beyer et al., 2020; Dubbert, Cuntz, et al., 2014; Kühnhammer et al., 2022; Oerter et al., 2017; Rothfuss et al., 2013, 2015; Volkmann, Kühnhammer, et al., 2016; Volkmann & Weiler, 2014; Wang et al., 2012). This approach, in combination with "destructive" techniques, could provide the still needed description of soil-texture- and soil-water-tension-related potential isotopic fractioning effects that should be accounted for in RWU quantification. Furthermore, spatio-temporal dynamics of RWU are potentially better captured when in situ non-destructive isotopic monitoring is employed (Beyer & Penna, 2021).

Since spatio-temporal variability renders RWU quantification challenging, water availability or root density profiles are used as proxies for RWU in some soil-vegetation-atmosphere transfer models, which normally leads to acceptably accurate

estimations of water flux in well-watered conditions (Kühnhammer et al., 2022). However, water and nutrient availability or root density might not be the predominant drivers of RWU in dry soils and direct profile comparisons might be misleading. The latest results obtained with 3D and 1D mechanistic hydraulic models, accounting for soil and root hydraulic properties, have provided evidence of the increasing influence of an exponential decrease of water potential near the roots in drying soils on RWU patters (e.g., Schröder et al., 2008; Vanderborght et al., 2023). Moreover, it could be hypothesized that the development of such a steep water potential gradient near the roots could be linked to the onset of – or even trigger – water stress and of corresponding protective measures by the plant. The necessary mechanistic understanding of the interactions in the plant-atmosphere and soil-plant interfaces could be achieved through comparisons between probabilistic isotope-based and the aforementioned physically-based approaches to RWU quantification and concurrent monitoring of plant-physiology and above- and below-ground environmental conditions (Dubbert et al., 2023; Rothfuss & Javaux, 2017).

With such an ecohydrological approach – monitoring of both ecophysiology and environmental variables – the main objective of this doctoral project was to assess the response of the grassland species *Centaurea jacea* L. to drought in controlled conditions in the laboratory at the single plant level in a semi-automated and non-destructive manner. This forb species was investigated because it was the dominant forb species in the semi-natural temperate grassland in the southwest of Germany, where the ecohydrological assessment of the response to drought at the community scale was investigated (Kübert et al., 2019, 2020, 2021) in the same research program this doctoral project was imbedded in.

1. Soil-mediated and antecedent water effects on soil water isotopic composition

Because relative contributions of soil water to xylem water would be estimated with isotopic determinations of soil and plant transpiration, the objective of the first published study in this doctoral project was to describe potential soil-texture- and soil-water-tension-related isotopic fractionating effects when using established destructive isotopic techniques and the in situ non-destructive online technique described in Rothfuss et al. (2013, 2015) (O.1 in chapter 1 section 5). The results of this first study would help determine if further correction steps had to be undertaken when estimating soil water δ-values in a loamy sand with the in situ online method to ensure reliable RWU estimations in the second study. The hypothesis was that there would not be a dependency of soil water δ-values on neither soil texture nor soil water tension (H.1 in chapter 1 section 5).

A spike experiment with two "chemically inert" soils, quartz sand and the loamy sand, was conducted and soil water isotopic determinations via three methodologies based on destructive sampling – cryogenic vacuum distillation, centrifugation, and direct water vapor equilibration–, from pressure-extracted water, and from the in situ online method were compared. Since no "pure" soil-texture or soil-water-tension-related

fractionating effects were observed using the loamy sand, no further measures, beyond using isotopic standards, in the in situ online method in the semi-automated experimental setup in the second study were undertaken.

The significant differences among the isotopic determinations with the studied methods were explained partly by well-documented methodological limitations, especially with the destructive isotopic techniques and in dry soil: fractionation due to incomplete water extraction or evaporation during sampling. But also partly by the specificities of our experimental setup: evaporation inside the pressure extractors. If evaporation during the pressure-mediated water extraction steps could be avoided or its fractionating effect quantified, potential soil-texture-related fractionation in other soil types, especially clay-rich ones, could be investigated with the presented setup and methodological framework. More than two cycles of soil saturation-desaturation could be performed to investigate the mixing of isotopically distinct mobile and immobile water with a wider range of isotopic techniques. Even the effect of oven-drying and subsequent saturation in the isotopic composition of extracted soil water could be investigated with such an approach. The presented experimental framework could be used to describe isotopic fractionating processes related to soil texture and moisture status and history at higher scales than the soil-pore scale in natural soils. The results of such studies could be compared to those of water flow and solute transport models (e.g., HYDRUS incorporating water stable isotope transport; Zhou et al., 2021) to better describe spatial and temporal isotope distribution and exchange dynamics in the soil, which could help systematically test controversial hypothesis such as ecohydrological separation.

Testing soil-related fractionating processes should be a prerequisite for probabilistic isotope-based RWU quantification and the use of in situ non-destructive methodologies, also in combination with destructive techniques, could possess a higher potential to render more precise isotopic determinations (due to a higher repeatability). Furthermore, in situ techniques could render the investigation of less understood fractionating processes in the soil-plant continuum resulting in mismatches between xylem and soil water – not only in trees – less challenging (e.g., water transport through the roots, mycorrhizal activity, root decomposition, transport delays; see chapter 1 section 2; Barbeta et al., 2020; Vargas et al., 2017). Confidence in the insights into these fractionating processes could increase and biases in RWU estimations could diminish with standardized methodological frameworks overarching all steps in isotopic monitoring: from experimental design, through sampling, and isotopic determinations as detailed by Ceperley et al., (2024).

2. Ecohydrological assessement of the response to drought of *Centaurea jacea* L.

Concurrent non-destructive monitoring of plant physiology, as well as above- and below-ground environmental conditions was recorded for 87 days to assess the ecohydrological response of a single individual of the grassland species *Centaurea jacea* L. to varying hydroclimatic conditions from an isotopic perspective (O.2 in

chapter 1 section 5). The hypothesis that *Centaurea jacea* L. displayed efficient water use and short-term dynamic RWU patterns in dry conditions was tested (H.2 in chapter 1 section 5).

C. jacea L. extracted consistently and in varying hydroclimatic conditions most water from the upper soil layers 0-15 cm – up to 79% – and in some periods up to 44% from the bottom soil layer 45-60 cm, especially in periods of high transpiration rate. In wet soil (mean $\theta > 0.12$ cm^3 cm^{-3} at DaS < 319), plant transpiration seemed to be controlled by light intensity and vpd. After DaS 319, leaf gas exchange was likely constrained by the recorded reduction in canopy conductance pre-dating a leaf and soil water content exponential decrease at the end of the experiment (until DaS 327) and resulting in a maintenance of water use efficiency.

Improvements in the presented semi-automated setup could enable better insights into the interactions in the soil-plant-atmosphere continuum at the plant or small plot scale under both edaphic and atmospheric drought. For instance, soil water tension should be directly measured (e.g., via psychrometers) instead of estimated from soil water content measurements and a water retention curve, as done in the second study of this doctoral project. Small errors in soil water content measurements in the "dry end" of the retention curve may result in significant uncertainties in estimations of soil water tension.

The frequency with which labelled water is added to the soil should be considerably decreased, for example to one or two events, which means that an extremer δ-value of the labeling water is necessary. Additionally, and with a few modifications to the used custom-made isotopic column, water could be added at different depths of the soil profile, not just at the top and the bottom. Thus, other strategies aimed at decoupling the information provided by each water isotopologue could be tested. In the second study, we attempted this with orthogonal profiles but did not achieve this decoupling, probably evidenced by the fact that RWU profiles from one or both isotopes were statistically indistinguishable (see chapter 3 section 3.4). For example, a combination of monotonic and non-monotonic vertically mirrored isotopic profile resulting in a different $\delta^{18}O$- $\delta^{2}H$ pair combination at each depth could be tested (Le Gall, personal communication). Nonetheless, this must be weighed against the time and computational cost of comparing the results of multi-source mixing models using the profiles of one or both isotopologues (Le Gall, personal communication), especially, if full integration of isotopic and hydrodynamic models is envisioned (Dubbert et al., 2023; see also section 3 in this chapter and chapter 1 section 4).

In similar semi-automated experimental setups, single and compounded effects of the availability of further resources – e.g., light and (micro)nutrients – or microbial activity in the soil and the mycorrhiza on water and carbon cycling could be investigated, also in combination with destructive sampling. For example, Le Gall et al. (2024) incorporated measurements of enzymatic activity and identification of soil microorganisms, nitrogen, and carbon labeling and sampling of biomass. Moreover, the "naturalness" of this approach could be increased if humidity inside the climate chamber enclosing the aerial parts of the plant is increased during the simulated night (i.e., lights off) to avoid atmospheric forcing of plant transpiration, not occurring in

"natural" conditions. Additionally, increases in light intensity and air temperature should follow smoother trends in the simulated night-day cycle, as exemplified by Le Gall et al. (2024) with the programming of sigmoidal functions for these two environmental parameters. This showcases the capabilities of the water-cooled LED panel employed in this doctoral project and in Le Gall et al. (2024), which provided constant, homogeneous, and automatic control of the light-intensity while helping avoid an undesired heating effect inside the plant chamber, which would influence plant transpiration. Through a better experimental design to simulate, for example, spring or summer and intermittent or extended drought, broader insights into the nature and long-term effectiveness of the drought resistance strategies of *C. jacea* L. or, better yet, crop variants, could be enabled (e.g., wheat; Le Gall et al., 2024).

Incorporating MRI-enabled root phenotyping in the presented semi-automated experimental setup contributed to the aforementioned "naturalness" (Lobet, 2017). Le Gall et al. (2024) described significant improvements to the MRI-platform allowing scanning of wider columns than the ones used in the second study, which could contain two plant individuals or even small trees, without increasing the detection limit, i.e., limiting the observation of fine roots. Additionally, they increased the throughput of this technique, a weakness of MRI (Lobet, 2017), by increasing the replicates. These improvements mean that plant-plant interactions and species-specific water use strategies in a competition-facilitation context could be investigated in laboratory controlled conditions (Le Gall et al., 2024) and data sets to test and improve transfer models with high spatio-temporal resolution can be produced (Giraud et al., 2023). Here we would recommend to conduct the experiments in younger plants or increase the length of the columns (Le Gall et al., 2024) to avoid pot-bound roots at the bottom, decreasing the naturalness of the setup and introducing influencing factors, difficult to describe, in the analysis of RWU dynamics. Furthermore, shoot phenotyping (e.g., leaf area index estimations) would be an important addition enabling insights into changes in carbon allocation during drought (e.g., shift to below-ground carbon allocation, see chapter 1 section 1; Kahmen et al., 2005). Especially because root surface area can be over an order of magnitude greater than leaf area in grasslands and fine roots (see next paragraph) is estimated to represent 33% of global annual net primary productivity (Jackson et al., 1997).

The readily available (non-destructive) root phenotyping techniques (among them MRI) in ecohydrological studies could contribute to the description of the fundamental role of fine root biomass in water and nutrient uptake. The ability of fine roots (< 2 mm) to absorb water is considered higher than that of thicker root segments, since they are more permeable. This is especially true in herbaceous species (McCully, 1999). However, the link between (fine) root biomass or root vertical distribution to root water uptake is neither straightforward nor direct, because root activity (i.e., the rate of water uptake per root length) and root plasticity (i.e., the rate of change in active root distributions) are highly dynamic (Kulmatiski, 2024). This in turn is closely related to mechanisms plants display to isolate or facilitate access to soil resources of root segments or complete sections (see chapter 1 section 4; Carminati et al., 2016; Carminati & Vetterlein, 2013). Thus, the influence of "root activity, root

plasticity, and soil water flow" (Kulmatiski, 2024) should no longer be overlooked when investigating drivers and dynamics of RWU (see section 3 in this chapter).

3. Probabilistic and physically-based RWU quantification

In the second study, the hypothesis that through stomatal closure reaching a critical plant transpiration threshold after which hydraulic failure might occur due to dry above-ground (high vpd) and below-ground (low θ) environmental conditions was being avoided was formulated. In this scenario, a drop in soil water tension in the soil-root interface and of root system conductance could have been related to the observed canopy conductance drop (H.3). Thus, the aim in the third study was to broaden the insights of the response to drought of *Centaurea jacea* L. by linking soil-plant and plant-atmosphere processes, as well as by comparing probabilistic and physically-based RWU estimates (O.3).

The modelling of the temporal and spatial dynamics of hydraulic parameters, namely the root system conductance (K_{rs}) and water tension at the soil-root interface ($H_{s,r}$) of *C. jacea* L. during selected days of the semi-automated drought experiment with the 1D mechanistic model of Vanderborght et al. (2021, 2023) shed more light into the plasticity of this grassland species in dry conditions. By assuming that only 10% of the total root length was actively taking up water, that soil water content measurements were overestimated by 3%, and accounting for the non-linear decrease of soil conductivity near the roots, an exponential decrease of K_{rs} and $H_{s,r}$ at relatively high bulk soil water content was modelled. These results support our hypothesis that the decline in canopy conductance in the drought experiment in the last days was linked to a change in the hydraulic properties around and of the root system.

The relatively straightforward comparison between probabilistic and physically-based RWU and estimation of relevant hydraulic parameters in the soil-plant continuum in the third study rendered interesting insights into the dynamic water uptake dynamics of *Centaurea jacea* L. Improvements in similar approaches would include (re)calculation of probabilistic RWU profiles with exclusion of sources if a certain local soil water tension or maximum extractable water threshold is exceeded (Dubbert et al., 2023; Kühnhammer et al., 2020). Nonetheless, it would have been much more challenging to incorporate additional parameters and their short-term dynamics (e.g., root activity or plasticity, residence and arrival times of water, as well as mixing inside the plant) without recurring to oversimplifying assumptions, such as a uniform 10% of total root length actively taking up water. These assumptions are of course necessary if the computational and time costs outweigh the potential improvements in the estimations without these simplifications.

The trade-off between computational cost and simplicity is even more relevant when "the inverse problem of reproducing target plant water isotope ratios with the hydrodynamic approach is posed in a probabilistic framework" (Dubbert et al., 2023) as done by De Deurwaerder et al. (2021) in their "inverse plant hydraulic model". Using a Bayesian statistical framework, uncertainties and biases in the estimations of

vertical distributions of absorbing root surfaces – direct measurements being challenging and labor intensive – are calculated in this model with water isotopic data and accounting for uncertainties in these determinations and for dynamics of biophysical parameters. They provided evidence of the underestimation of uncertainties in plant xylem isotopic composition by not including biophysical information (e.g., sap flow velocity) in the analysis and recommended characterizing heterogeneities in isotopic composition and water tension in the soil. They present an interesting positive feedback while using this model between both optimized data collection and experimental design and reduction of uncertainties and biases in vertical distributions of absorbing root surfaces. On the one hand, more variables can be accounted for in such isotope-enabled physically-based models such as microscopic soil and root hydraulic dynamics, or the role of mycorrhizal colonization (De Deurwaerder et al., 2021). On the other hand, open questions on isotope discrimination at different interfaces of the soil-plant continuum (e.g., during transport into and through the plant xylem or in the mycorrhiza) must be answered to keep improving transfer models.

References

Adams, R. E., Hyodo, A., SantaMaria, T., Wright, C. L., Boutton, T. W., & West, J. B. (2020). Bound and mobile soil water isotope ratios are affected by soil texture and mineralogy, whereas extraction method influences their measurement. *Hydrological Processes*, *34*, 991–1003. https://doi.org/10.1002/hyp.13633

Allen, M. F. (2007). Mycorrhizal Fungi: Highways for Water and Nutrients in Arid Soils. *Vadose Zone Journal*, *6*(2), 291–297. https://doi.org/10.2136/vzj2006.0068

Allen, V. G., Batello, C., Berretta, E. J., Hodgson, J., Kothmann, M., Li, X., McIvor, J., Milne, J., Morris, C., Peeters, A., & Sanderson, M. (2011). An international terminology for grazing lands and grazing animals. *Grass and Forage Science*, *66*, 2–29. https://doi.org/10.1111/j.1365-2494.2010.00780.x

Allison, G. B., Barnes, C. J., Hughes, M. W., & Leaney, F. W. J. (1984). Effect of climate and vegetation on oxygen-18 and deuterium profiles in soils. *International Atomic Energy Agency (IAEA) International Symposium on Isotope Hydrology in Water Resources Development*, 105–123.

Allison, G. B., & Hughes, M. W. (1983). The use of natural tracers as indicators of soil-water movement in a temperate semi-arid region. *Journal of Hydrology*, *60*, 157–173. https://doi.org/10.1016/0022-1694(83)90019-7

Altman, D. G., & Bland, J. M. (1983). Measurement in Medicine : The Analysis of Method Comparison Studies. *Journal of the Royal Statistical Society*, *32*(3), 307–317.

Araguás-Araguás, L., Rozanski, K., Gonfiantini, R., & Louvat, D. (1995). Isotope effects accompanying vacuum extraction of soil water for stable isotope analyses. *Journal of Hydrology*, *168*, 159–171. https://doi.org/10.1016/0022-1694(94)02636-P

Asbjornsen, H., Mora, G., & Helmers, M. J. (2007). Variation in water uptake dynamics among contrasting agricultural and native plant communities in the Midwestern U.S. *Agriculture, Ecosystems and Environment*, *121*(4), 343–356. https://doi.org/10.1016/j.agee.2006.11.009

Bachmann, D., Gockele, A., Ravenek, J. M., Roscher, C., Strecker, T., Weigelt, A., & Buchmann, N. (2015). No evidence of complementary water use along a plant species richness gradient in temperate experimental grasslands. *PLoS ONE*, *10*(1), 1–14. https://doi.org/10.1371/journal.pone.0116367

Barbeta, A., Gimeno, T. E., Clavé, L., Fréjaville, B., Jones, S. P., Delvigne, C., Wingate, L., & Ogée, J. (2020). An explanation for the isotopic offset between soil and stem water in a temperate tree species. *New Phytologist*, *227*(3), 766–779. https://doi.org/10.1111/nph.16564

Bariac, T., Rambal, S., Jusserand, C., & Berger, A. (1989). Evaluating water fluxes of field-grown alfalfa from diurnal observations of natural isotope concentrations, energy budget and ecophysiological parameters. *Agricultural and Forest Meteorology*, *48*, 263–283.

Barnes, C. J., & Allison, G. B. (1983). The distribution of deuterium and 18O in dry soils 1. Theory. *Journal of Hydrology*, *60*, 141–156.

Barnes, C. J., & Allison, G. B. (1984). The distribution of deuterium and 18O in dry soils 3. Theory for Non-isothermal Water Movement. *Journal of Hydrology*, *74*, 119–135.

Bastos, A., Gouveia, C. M., Trigo, R. M., & Running, S. W. (2013). Comparing the impacts of 2003 and 2010 heatwaves in NPP over Europe. *Biogeosciences Discussions*, *10*, 15879–15911. https://doi.org/10.5194/bgd-10-15879-2013

Bechmann, M., Schneider, C., Carminati, A., Vetterlein, D., Attinger, S., & Hildebrandt, A. (2014). Effect of parameter choice in root water uptake models - the arrangement of root hydraulic properties within the root architecture affects dynamics and efficiency of root water uptake. *Hydrology and Earth System Sciences*, *18*(10), 4189–4206. https://doi.org/10.5194/hess-18-4189-2014

Beyer, M., Hamutoko, J. T., Wanke, H., Gaj, M., & Koeniger, P. (2018). Examination of deep root water uptake using anomalies of soil water stable isotopes, depth-controlled isotopic labeling and mixing models. *Journal of Hydrology*, *566*(August), 122–136. https://doi.org/10.1016/j.jhydrol.2018.08.060

Beyer, M., Koeniger, P., Gaj, M., Hamutoko, J. T., Wanke, H., & Himmelsbach, T. (2016). A deuterium-based labeling technique for the investigation of rooting depths, water uptake dynamics and unsaturated zone water transport in semiarid environments. *Journal of Hydrology*, *533*, 627–643. https://doi.org/10.1016/j.jhydrol.2015.12.037

Beyer, M., Kühnhammer, K., & Dubbert, M. (2020). In situ measurements of soil and plant water isotopes: A review of approaches, practical considerations and a vision for the future. *Hydrology and Earth System Sciences*, *24*, 4413–4440. https://doi.org/10.5194/hess-24-4413-2020

Beyer, M., & Penna, D. (2021). On the Spatio-Temporal Under-Representation of Isotopic Data in Ecohydrological Studies. *Frontiers in Water*, *3*(March), 1–9. https://doi.org/10.3389/frwa.2021.643013

Biodiversity Information Sytem for Europe. (2024). *Grasslands*. https://biodiversity.europa.eu/natura2000/en/grasslands

Bland, J. M., & Altman, D. G. (1996). Statistics Notes: Measurement error and correlation coefficients. *BMJ*, *312*(1654). https://doi.org/10.1136/bmj.313.7048.41

Bland, J. M., & Altman, D. G. (1999). Measuring agreement in method comparison studies. *Statistical Methods in Medical Research*, *8*, 135–160. https://doi.org/10.1002/sim.5955

Blum, A. (2011). *Plant Breeding for Water-Limited Environments*. Springer Science+Business Media. https://doi.org/10.1007/978-1-4419-7491-4

Bogena, H. R., Huisman, J. A., Oberdörster, C., & Vereecken, H. (2007). Evaluation of a low-cost soil water content sensor for wireless network applications. *Journal of Hydrology*, *344*(1–2), 32–42. https://doi.org/10.1016/j.jhydrol.2007.06.032

Bouda, M., Brodersen, C., & Saiers, J. (2018). Whole root system water conductance responds to both axial and radial traits and network topology over natural range of trait variation. *Journal of Theoretical Biology*, *456*, 49–61. https://doi.org/10.1016/j.jtbi.2018.07.033

Bowers, W. H., Mercer, J. J., Pleasants, M. S., & Williams, D. G. (2020). A combination of soil water extraction methods quantifies the isotopic mixing of waters held at separate tensions in soil. *Hydrology and Earth System Sciences*, *24*(8), 4045–4060. https://doi.org/10.5194/hess-24-4045-2020

Bowling, D. R., Schulze, E. S., & Hall, S. J. (2017). Revisiting streamside trees that do not use stream water: can the two water worlds hypothesis and snowpack isotopic effects explain a missing water source? *Ecohydrology*, *10*(1), 1–12. https://doi.org/10.1002/eco.1771

Braud, I., Bariac, T., Gaudet, J. P., & Vauclin, M. (2005). SiSPAT-Isotope, a coupled heat, water and stable isotope (HDO and H 218O) transport model for bare soil. Part I. Model description and first verifications. *Journal of Hydrology*, *309*, 277–300. https://doi.org/10.1016/j.jhydrol.2004.12.013

Brooks, R. J., Barnard, H. R., Coulombe, R., & McDonnell, J. J. (2010). Ecohydrologic separation of water between trees and streams in a Mediterranean climate. *Nature Geoscience*, 1–5. https://doi.org/10.1038/ngeo722

Burgess, J. (1978). *Metal ions in solution*. John Wiley and Sons Limited.

Cai, G., Ahmed, M. A., Abdalla, M., & Carminati, A. (2022). Root hydraulic phenotypes impacting water uptake in drying soils. *Plant Cell and Environment*, *45*(3), 650–663. https://doi.org/10.1111/pce.14259

Caldeira, C. F., Jeanguenin, L., Chaumont, F., & Tardieu, F. (2014). Circadian rhythms of hydraulic conductance and growth are enhanced by drought and improve plant performance. *Nature Communications*, *5*, 1–9. https://doi.org/10.1038/ncomms6365

Carminati, A., & Javaux, M. (2020). Soil Rather Than Xylem Vulnerability Controls Stomatal Response to Drought. *Trends in Plant Science*, *25*(9), 868–880. https://doi.org/10.1016/j.tplants.2020.04.003

Carminati, A., & Vetterlein, D. (2013). Plasticity of rhizosphere hydraulic properties as a key for efficient utilization of scarce resources. *Annals of Botany*, *112*, 277–290. https://doi.org/10.1093/aob/mcs262

Carminati, A., Zarebanadkouki, M., Kroener, E., Ahmed, M. A., & Holz, M. (2016). Biophysical rhizosphere processes affecting root water uptake. *Annals of Botany*, *118*, 561–571. https://doi.org/10.1093/aob/mcw113

Ceperley, N., Gimeno, T. E., Jacobs, S. R., Beyer, M., Dubbert, M., Fischer, B., Geris, J., Holko, L., Kübert, A., Le Gall, S., Lehmann, M. M., Llorens, P., Millar, C., Penna, D., Prieto, I., Radolinski, J., Scandellari, F., Stockinger, M., Stumpp, C., … Rothfuss, Y. (2024). Toward a common methodological framework for the sampling, extraction, and isotopic analysis of water in the Critical Zone to study vegetation water use. *Wiley Interdisciplinary Reviews: Water*, *January*, 1–33. https://doi.org/10.1002/wat2.1727

Chen, G., Auerswald, K., & Schnyder, H. (2016). 2H and 18O depletion of water close to organic surfaces. *Biogeosciences*, *13*, 3175–3186. https://doi.org/10.5194/bg-13-3175-2016

Chitra-Tarak, R., Xu, C., Aguilar, S., Anderson-Teixeira, K. J., Chambers, J., Detto, M., Faybishenko, B., Fisher, R. A., Knox, R. G., Koven, C. D., Kueppers, L. M., Kunert, N., Kupers, S. J., McDowell, N. G., Newman, B. D., Paton, S. R., Pérez, R., Ruiz, L., Sack, L., … McMahon, S. M. (2021). Hydraulically-vulnerable trees survive on deep-water access during droughts in a tropical forest. *New Phytologist*, *231*(5), 1798–1813. https://doi.org/10.1111/nph.17464

Christmann, A., Weiler, E. W., Steudle, E., & Grill, E. (2007). A hydraulic signal in root-to-shoot signalling of water shortage. *The Plant Journal*, *52*, 167–174. https://doi.org/10.1111/j.1365-313X.2007.03234.x

Couvreur, V., Rothfuss, Y., Meunier, F., Bariac, T., Biron, P., Durand, J. L., Richard, P., Javaux, M., & Javaux, M. (2020). Disentangling temporal and population variability in plant root water uptake from stable isotopic analysis: when rooting depth matters in labeling studies. *Hydrology and Earth System Sciences*, *24*(6), 3057–3075. https://doi.org/10.5194/hess-24-3057-2020

Couvreur, V., Vanderborght, J., Beff, L., & Javaux, M. (2014). Horizontal soil water potential heterogeneity : simplifying approaches for crop water dynamics models. *Hydrology and Earth System Sciences*, *18*, 1723–1743. https://doi.org/10.5194/hess-18-1723-2014

Couvreur, V., Vanderborght, J., & Javaux, M. (2012). A simple three-dimensional macroscopic root water uptake model based on the hydraulic architecture approach. *Hydrology and Earth System Sciences*, *16*, 2957–2971. https://doi.org/10.5194/hess-16-2957-2012

Cowan, I. R., & Farquhar, G. D. (1977). Stomatal function in relation to leaf metabolism and environment: Stomatal function in the regulation of gas exchange. *Cambridge: At the University Press*, 471–505.

Craig, H. (1961). Isotopic Variations in Meteoric Waters. *Science*, *133*(3465), 1702–1703. https://doi.org/http://dx.doi.org/10.1126/science.133.3465.1702

Craig, H., & Gordon, L. I. (1965). Deuterium and oxygen 18 variations m the ocean and the marine atmosphere. In *Stable Isotopes in Oceanographic Studies and Paleotemperatures*. http://scholar.google.com/scholar?hl=en&btnG=Search&q=intitle:Deuterium+and+oxygen+18+variations+m+the+ocean+and+the+marine+atmosphere#0

Craine, J. M., Wedin, D. A., Chapin III, F. S., & Reich, P. B. (2002). Relationship between the structure of root systems and resource use for 11 North American grassland plants. *Plant Ecology*, *165*, 85–100. https://doi.org/10.1023/A

Crausbay, S. D., Ramirez, A. R., Carter, S. L., Cross, M. S., Hall, K. R., Bathke, D. J., Betancourt, J. L., Colt, S., Cravens, A. E., Dalton, M. S., Dunham, J. B., Hay, L. E., Hayes, M. J., McEvoy, J., McNutt, C. A., Moritz, M. A., Nislow, K. H., Raheem, N., & Sanford, T. (2017). Defining ecological drought for the twenty-first century. *Bulletin of the American Meteorological Society*, *98*(12), 2543–

2550. https://doi.org/10.1175/BAMS-D-16-0292.1

De Deurwaerder, H. P. T., Visser, M. D., Meunier, F., Detto, M., Hervé-Fernández, P., Boeckx, P., & Verbeeck, H. (2021). Robust Estimation of Absorbing Root Surface Distributions From Xylem Water Isotope Compositions With an Inverse Plant Hydraulic Model. *Frontiers in Forests and Global Change*, *4*(July), 1–14. https://doi.org/10.3389/ffgc.2021.689335

De Smedt, F., & Wierenga, P. J. (1979). A Generalized Solution for Solute Flow in Soils With Mobile and Immobile Water. *Water Resources Research*, *15*(5), 1137–1141.

Deseano Diaz, P., Nong, T., Brüggemann, N., Dubbert, M., Javaux, M., Orlowski, N., Vereecken, H., & Rothfuss, Y. (2023). Insights into tension-mediated and antecedent water effects on soil water isotopic composition. *Vadose Zone Journal*, *22*(6), 1–19. https://doi.org/10.1002/vzj2.20288

Deseano Diaz, P., van Dusschoten, D., Kübert, A., Brüggemann, N., Javaux, M., Merz, S., Vanderborght, J., Vereecken, H., Dubbert, M., & Rothfuss, Y. (2023). Response of a grassland species to dry environmental conditions from water stable isotopic monitoring: no evident shift in root water uptake to wetter soil layers. *Plant and Soil*, *482*(1–2), 491–512. https://doi.org/10.1007/s11104-022-05703-y

Dongmann, G., Nürnberg, H. W., Förstel, H., & Wagener, K. (1974). On the Enrichment of H2180 in the Leaves of Transpiring Plants. *Radiation and Environmental Biophysics*, *52*, 41–52. https://doi.org/10.1007/BF01323099

Doussan, C., Pierret, A., Garrigues, E., & Pagès, L. (2006). Water uptake by plant roots: II - Modelling of water transfer in the soil root-system with explicit account of flow within the root system - Comparison with experiments. *Plant and Soil*, *283*(1–2), 99–117. https://doi.org/10.1007/s11104-004-7904-z

Draye, X., Kim, Y., Lobet, G., & Javaux, M. (2010). Model-assisted integration of physiological and environmental constraints affecting the dynamic and spatial patterns of root water uptake from soils. In *Journal of Experimental Botany*. https://doi.org/10.1093/jxb/erq077

Dubbert, M., Couvreur, V., Kübert, A., & Werner, C. (2023). Plant water uptake modelling: added value of cross-disciplinary approaches. *Plant Biology*, *25*(1), 32–42. https://doi.org/10.1111/plb.13478

Dubbert, M., Cuntz, M., Piayda, A., & Werner, C. (2014). Oxygen isotope signatures of transpired water vapor: The role of isotopic non-steady-state transpiration under natural conditions. *New Phytologist*, *203*(4), 1242–1252. https://doi.org/10.1111/nph.12878

Dubbert, M., Piayda, A., Cuntz, M., Correia, A. C., Costa e Silva, F., Pereira, J. S., & Werner, C. (2014). Stable oxygen isotope and flux partitioning demonstrates understory of an oak savanna contributes up to half of ecosystem carbon and water exchange. *Frontiers in Plant Science*, *5*, 1–17. https://doi.org/10.3389/fpls.2014.00530

Dubbert, M., & Werner, C. (2019). Water fluxes mediated by vegetation: emerging

isotopic insights at the soil and atmosphere interfaces. *New Phytologist*, *221*(4), 1754–1763. https://doi.org/10.1111/nph.15547

Duvert, C., Canham, C. A., Barbeta, A., Alvarez Cortes, D., Chandler, L., Harford, A. J., Leggett, A., Setterfield, S. A., Humphrey, C. L., & Hutley, L. B. (2022). Deuterium depletion in xylem water and soil isotopic effects complicate the assessment of riparian tree water sources in the seasonal tropics. *Ecohydrology*, *15*(6), 1–17. https://doi.org/10.1002/eco.2383

Ehhalt, D. Von, & Knott, K. (1965). Kinetische Isotopentrennung bei der Verdampfung von Wasser. *Tellus*, *17*(3), 389–397. https://doi.org/10.3402/tellusa.v17i3.9060

Ehleringer, J. R., & Dawson, T. E. (1992). Water uptake by plants: perspectives from stable isotope composition. *Plant, Cell & Environment*, *15*(9), 1073–1082. https://doi.org/10.1111/j.1365-3040.1992.tb01657.x

Ellsworth, P. Z., & Williams, D. G. (2007). Hydrogen isotope fractionation during water uptake by woody xerophytes. *Plant and Soil*, *291*(1–2), 93–107. https://doi.org/10.1007/s11104-006-9177-1

Eurostat. (2022). *Utilised Agricultural Area by Categories*. https://ec.europa.eu/eurostat/web/products-datasets/-/tag00025

Evaristo, J., Jasechko, S., & McDonnell, J. J. (2015). Global separation of plant transpiration from groundwater and streamflow. *Nature*, *525*, 91–94. https://doi.org/10.1038/nature14983

Evaristo, J., McDonnell, J. J., & Clemens, J. (2017). Plant source water apportionment using stable isotopes: A comparison of simple linear, two-compartment mixing model approaches. *Hydrological Processes*, 1–9. https://doi.org/10.1002/hyp.11233

Farquhar, G. D., & Lloyd, J. (1993). Carbon and Oxygen Isotope Effects in the Exchange of Carbon Dioxide between Terrestrial Plants and the Atmosphere. *Stable Isotopes and Plant Carbon-Water Relations*, 47–70. https://doi.org/10.1016/b978-0-08-091801-3.50011-8

Figueroa-Johnson, M. A., Tindall, J. A., & Friedel, M. (2007). A Comparison of 18Oδ Composition of Water Extracted from Suction Lysimeters, Centrifugation, and Azeotropic Distillation. *Water, Air, and Soil Pollution*, *184*(1–4), 63–75. https://doi.org/10.1007/s11270-007-9399-8

Forzieri, G., Feyen, L., Russo, S., Vousdoukas, M., Alfieri, L., Outten, S., Migliavacca, M., Bianchi, A., Rojas, R., & Cid, A. (2016). Multi-hazard assessment in Europe under climate change. *Climatic Change*, *137*(1–2), 105–119. https://doi.org/10.1007/s10584-016-1661-x

Frank, D., Reichstein, M., Bahn, M., Thonicke, K., Frank, D., Mahecha, M. D., Smith, P., van der Velde, M., Vicca, S., Babst, F., Beer, C., Buchmann, N., Canadell, J. G., Ciais, P., Cramer, W., Ibrom, A., Miglietta, F., Poulter, B., Rammig, A., … Zscheischler, J. (2015). Effects of climate extremes on the terrestrial carbon cycle: Concepts, processes and potential future impacts. *Global Change Biology*, *21*(8), 2861–2880. https://doi.org/10.1111/gcb.12916

Frensch, J., Hsiao, T. C., & Steudle, E. (1996). Water and solute transport along developing maize roots. *Planta*, *198*(3), 348–355. https://doi.org/10.1007/BF00620050

Gaines, K. P., Meinzer, F. C., Duffy, C. J., Thomas, E. M., & Eissenstat, D. M. (2016). Rapid tree water transport and residence times in a Pennsylvania catchment. *Ecohydrology*, *9*, 1554–1565. https://doi.org/10.1002/eco.1747

Gaj, M., Beyer, M., Koeniger, P., Wanke, H., Hamutoko, J., & Himmelsbach, T. (2016). In situ unsaturated zone water stable isotope (2H and 18O) measurements in semi-arid environments: a soil water balance. *Hydrology and Earth System Sciences*, *20*(2), 715–731. https://doi.org/10.5194/hess-20-715-2016

Gaj, M., Lamparter, A., Woche, S. K., Bachmann, J., McDonnell, J. J., & Stange, C. F. (2019). The Role of Matric Potential, Solid Interfacial Chemistry, and Wettability on Isotopic Equilibrium Fractionation. *Vadose Zone Journal*, 1–11. https://doi.org/10.2136/vzj2018.04.0083

Gaj, M., & McDonnell, J. J. (2019). Possible soil tension controls on the isotopic equilibrium fractionation factor for evaporation from soil. *Hydrological Processes*, *33*(11), 1629–1634. https://doi.org/10.1002/hyp.13418

Gang, C., Wang, Z., Chen, Y., Yang, Y., Li, J., Cheng, J., Qi, J., & Odeh, I. (2016). Drought-induced dynamics of carbon and water use efficiency of global grassland from 200 to 2011. *Ecological Indicators*, *67*, 788–797.

Gat, J. R., & Gonfiantini, R. (1981). *Stable Isotope Hydrology. Deuterium and Oxygen-18 in the Water Cycle* (IAEA (ed.)).

Gaudet, J. P., Jégat, H., Vachaud, G., & Wierenga, P. J. (1977). Soil Science Society of America. *Soil Science Society of America Journal*, *41*(4), 665–671. https://doi.org/10.2136/sssaj1940.03615995000400c0132x

Geris, J., Tetzlaff, D., McDonnell, J., Anderson, J., Paton, G., & Soulsby, C. (2015). Ecohydrological separation in wet, low energy northern environments? A preliminary assessment using different soil water extraction techniques. *Hydrological Processes*, *29*, 5139–5152. https://doi.org/10.1002/hyp.10603

Geris, J., Tetzlaff, D., McDonnell, J. J., & Soulsby, C. (2017). Spatial and temporal patterns of soil water storage and vegetation water use in humid northern catchments. *Science of the Total Environment*, *595*, 486–493. https://doi.org/10.1016/j.scitotenv.2017.03.275

Gerke, H. H., & van Genuchten, M. T. (1993). A Dual-Porosity Model for Simulating the Preferential Movement of Water and Solutes in Structured Porous Media. *Water Resources Research*, *29*(2), 305–319. https://doi.org/10.1029/92WR02339

Gessler, A., Bächli, L., Rouholahnejad Freund, E., Treydte, K., Schaub, M., Haeni, M., Weiler, M., Seeger, S., Marshall, J., Hug, C., Zweifel, R., Hagedorn, F., Rigling, A., Saurer, M., & Meusburger, K. (2022). Drought reduces water uptake in beech from the drying topsoil, but no compensatory uptake occurs from deeper soil layers. *New Phytologist*, *233*(1), 194–206.

https://doi.org/10.1111/nph.17767

Gilg, H. A., Girard, J.-P., & Sheppard, S. M. F. (2004). Conventional and Less Conventional Techniques for Hydrogen and Oxygen Isotope Analysis of Clays, Associated Minerals and Pore Waters in Sediments and Soils. In P. A. de Groot (Ed.), *Handbook of Stable Isotope Analytical Techniques* (pp. 38–61). Elsevier.

Giraud, M., Le Gall, S., Harings, M., Javaux, M., Leitner, D., Meunier, F., Rothfuss, Y., van Dusschoten, D., Vanderborght, J., Vereecken, H., Lobet, G., & Schnepf, A. (2023). CPlantBox : a fully coupled modelling platform for the water and carbon fluxes in the soil-plant-atmosphere continuum. *In Silico Plants*, *5*, 1–36. https://doi.org/10.1093/insilicoplants/diad009

Goebel, T. S., & Lascano, R. J. (2012). System for High Throughput Water Extraction from Soil Material for Stable Isotope Analysis of Water. *Journal of Analytical Sciences, Methods and Instrumentation*, *02*(04), 203–207. https://doi.org/10.4236/jasmi.2012.24031

Gollan, T., Turner, N. C., & Schulze, E. D. (1985). The responses of stomata and leaf gas exchange to vapour pressure deficits and soil water content. *Oecologia*, *65*, 356–362.

Gray, S. B., & Brady, S. M. (2016). Plant developmental responses to climate change. *Developmental Biology*, *419*, 64–77. https://doi.org/10.1016/j.ydbio.2016.07.023

Harpole, W. S., Potts, D. L., & Suding, K. N. (2007). Ecosystem responses to water and nitrogen amendment in a California grassland. *Global Change Biology*, *13*(11), 2341–2348. https://doi.org/10.1111/j.1365-2486.2007.01447.x

Hayat, F., Ahmed, M. A., Zarebanadkouki, M., Cai, G., & Carminati, A. (2019). Measurements and simulation of leaf xylem water potential and root water uptake in heterogeneous soil water contents. *Advances in Water Resources*, *124*, 96–105.

Hayat, F., Ahmed, M. A., Zarebanadkouki, M., Javaux, M., Cai, G., & Carminati, A. (2020). Transpiration Reduction in Maize (Zea mays L) in Response to Soil Drying. *Frontiers in Plant Science*, *10*(January), 1–8. https://doi.org/10.3389/fpls.2019.01695

He, D., Wen, M., Wang, Y., Du, G., Zhang, C., He, H., Jin, J., Li, M., & Si, B. (2023). Xylem water cryogenic vacuum extraction: Testing correction methods with CaviTron-based apple twig sampling. *Journal of Hydrology*, *621*(March), 129572. https://doi.org/10.1016/j.jhydrol.2023.129572

Hegi, G. (1954). *Illustrierte Flora von Mitteleuropa. Mit besonderer Berücksichtigung von Oesterreich, Deutschland und der Schweiz. Zum Gebrauche in den Schulen und zum Selbstunterricht*.

Hejcman, M., Hejcmanová, P., Pavlů, V., & Beneš, J. (2013). Origin and history of grasslands in central europe - A review. *Grass and Forage Science*, *68*, 345–363. https://doi.org/10.1111/gfs.12066

Hillel, D. (2003). *Introduction to Environmental Soil Physics*. Academic Press.

Hochberg, U., Rockwell, F. E., Holbrook, N. M., & Cochard, H. (2018). Iso /

Anisohydry : A Plant – Environment Interaction Rather Than a Simple Hydraulic Trait. *Trends in Plant Science*, *23*(2), 112–120. https://doi.org/10.1016/j.tplants.2017.11.002

Horita, J., & Wesolowski, D. J. (1994). Liquid-vapor fractionation of oxygen and hydrogen isotopes of water from the freezing to the critical temperature. *Geochimica et Cosmochimica Acta*, *58*(16), 3425–3437. papers2://publication/uuid/F9BCD32F-8569-4ACF-81AF-08518BF40A32

Hsiao, T. C., & Xu, L. K. (2000). Sensitivity of with of roots versus leaves to water stress: Biophysical analysis and relation to water. *Journal of Experimental Botany*, *51*(350), 1595–1616. https://doi.org/10.1093/jexbot/51.350.1595

Hsieh, J. C. C., Savin, S. M., Kelly, E. F., & Chadwick, O. A. (1998). Measurement of soil-water δ18O values by direct equilibration with CO2. *Geoderma*, *82*, 255–268. https://doi.org/10.1016/S0016-7061(97)00104-3

IAEA. (2019). *2H and 18O in water samples*. https://nucleus.iaea.org/rpst/referenceproducts/referencematerials/Stable_Isotopes/2H18O-water-samples/index.htm

IPBES. (2018). *Summary for policymakers of the regional assessment report on biodiversity and ecosystem services for Europe and Central Asia of the Intergovernmental Science-Policy Platform on Biodiversity and Ecosystem Services*.

IPCC. (2021). Climate Change 2021: The Physical Science Basis. In *IPCC*.

Jackson, R. B., Mooney, H. A., & Schulze, E. D. (1997). A global budget for fine root biomass, surface area, and nutrient contents. *Proceedings of the National Academy of Sciences of the United States of America*, *94*, 7362–7366. https://doi.org/10.1073/pnas.94.14.7362

Javaux, M., Schröder, T., Vanderborght, J., & Vereecken, H. (2008). Use of a Three-Dimensional Detailed Modeling Approach for Predicting Root Water Uptake. *Vadose Zone Journal*, *7*, 1079–1088. https://doi.org/10.2136/vzj2007.0115

Javot, H., & Maurel, C. (2002). The role of aquaporins in root water uptake. *Annals of Botany*, *90*, 301–313. https://doi.org/10.1093/aob/mcf199

Jentsch, A., Kreyling, J., Elmer, M., Gellesch, E., Glaser, B., Grant, K., Hein, R., Lara, M., Mirzae, H., Nadler, S. E., Nagy, L., Otieno, D., Pritsch, K., Rascher, U., Schädler, M., Schloter, M., Singh, B. K., Stadler, J., Walter, J., … Beierkuhnlein, C. (2011). Climate extremes initiate ecosystem-regulating functions while maintaining productivity. *Journal of Ecology*, *99*, 689–702. https://doi.org/10.1111/j.1365-2745.2011.01817.x

Judson, P. H., Germino, M. J., Wraith, J. M., Olson, B. E., & Swan, M. B. (2006). Advantages in water relations contribute to greater photosynthesis in Centaurea maculosa compared with established grasses. *International Journal of Plant Sciences*, *167*(2), 269–277.

Kahmen, A., Perner, J., & Buchmann, N. (2005). Diversity-dependent productivity in semi-natural grasslands following climate perturbations. *Functional Ecology*, *19*, 594–601. https://doi.org/10.1111/j.1365

Knapp, A. K., & Smith, M. D. (2001). Variation Among Biomes in Temporal Dynamics of Aboveground Primary Production. *Science*, *291*, 481–484.

Knighton, J., Kuppel, S., Smith, A., Soulsby, C., Sprenger, M., & Tetzlaff, D. (2020). Using isotopes to incorporate tree water storage and mixing dynamics into a distributed ecohydrologic modelling framework. *Ecohydrology*, *13*(1–17). https://doi.org/10.1002/eco.2201

Koeniger, P., Marshall, J. D., Link, T., & Mulch, A. (2011). An inexpensive, fast, and reliable method for vacuum extraction of soil and plant water for stable isotope analyses by mass spectrometry. *Rapid Communications in Mass Spectrometry*, *25*, 3041–3048. https://doi.org/10.1002/rcm.5198

Kübert, A. (2019). *Extreme Drought and Nitrogen Loading in Grasslands : Assessing the Impact on Vegetation-Soil-Atmosphere Processes Across Scales*.

Kübert, A., Götz, M., Kuester, E., Piayda, A., Werner, C., Rothfuss, Y., & Dubbert, M. (2019). Nitrogen Loading Enhances Stress Impact of Drought on a Semi-natural Temperate Grassland. *Frontiers in Plant Science*, *10*(August), 1–16. https://doi.org/10.3389/fpls.2019.01051

Kübert, A., Kuester, E., Götz, M., Dubbert, D., Eiblmeier, M., Werner, C., Rothfuss, Y., & Dubbert, M. (2021). Combined experimental drought and nitrogen loading: the role of species-dependent leaf level control of carbon and water exchange in a temperate grassland. *Plant Biology*, *23*(3), 427–437. https://doi.org/10.1111/plb.13230

Kübert, A., Paulus, S., Dahlmann, A., Werner, C., Rothfuss, Y., Orlowski, N., & Dubbert, M. (2020). Water Stable Isotopes in Ecohydrological Field Research: Comparison Between In Situ and Destructive Monitoring Methods to Determine Soil Water Isotopic Signatures. *Frontiers in Plant Science*, *11*(April), 1–13. https://doi.org/10.3389/fpls.2020.00387

Kühnhammer, K., Dahlmann, A., Iraheta, A., Gerchow, M., Birkel, C., Marshall, J. D., & Beyer, M. (2022). Continuous in situ measurements of water stable isotopes in soils, tree trunk and root xylem: Field approval. *Rapid Communications in Mass Spectrometry*, *36*(5), 1–19. https://doi.org/10.1002/rcm.9232

Kühnhammer, K., Kübert, A., Brüggemann, N., Deseano Diaz, P., van Dusschoten, D., Javaux, M., Merz, S., Vereecken, H., Dubbert, M., & Rothfuss, Y. (2020). Investigating the root plasticity response of Centaurea jacea to soil water availability changes from isotopic analysis. *New Phytologist*, *226*(1), 98–110. https://doi.org/10.1111/nph.16352

Kulmatiski, A. (2024). Water matching : an explanation for plant growth and coexistence in water - limited systems. *Discover Soil*. https://doi.org/10.1007/s44378-024-00002-7

Kulmatiski, A., Adler, P. B., Stark, J. M., & Tredennick, A. T. (2017). Water and nitrogen uptake are better associated with resource availability than root biomass. *Ecosphere*, *8*(3). https://doi.org/10.1002/ecs2.1738

Kulmatiski, A., Beard, K. H., Verweij, R. J. T., & February, E. C. (2010). A depth-

controlled tracer technique measures vertical, horizontal and temporal patterns of water use by trees and grasses in a subtropical savanna. *New Phytologist*, *188*(1), 199–209. https://doi.org/10.1111/j.1469-8137.2010.03338.x

Kutschera, L., & Lichtenegger, E. (1992). *Wurzelatlas mitteleuropaeischer Gruenlandpflanzen*. Fischer.

Landon, M. K., Delin, G. N., Komor, S. C., & Regan, C. P. (1999). *Comparison of the stable-isotopic composition of soil water collected from suction lysimeters, wick samplers, and cores in a sandy unsaturated zone*. *224*, 45–54.

Landsberg, J. J., & Fowkes, N. D. (1978). Water movement through plant roots. *Annals of Botany*, *42*(3), 493–508. https://doi.org/10.1093/oxfordjournals.aob.a085488

Le Gall, S., van Duschoten, D., Lattacher, A., Giraud, M., Harings, M., Deseano Diaz, P., Sircan, A., Poll, C., Lobet, G., & Javaux, M. (2024). Investigating the impact on water fluxes and physiological development of the combination of contrasted root wheat cultivars from isotopic analysis. *EGU General Assembly 2024*.

Leaney, F. W., Osmond, C. B., Allison, G. B., & Ziegler, H. (1985). Hydrogen-isotope composition of leaf water in C3 and C4 plants: its relationship to the hydrogen-isotope composition of dry matter. *Planta*, *164*, 215–220. https://doi.org/10.1007/BF00396084

Leitinger, G., Ruggenthaler, R., Hammerle, A., Lavorel, S., Schirpke, U., Clement, J. C., Lamarque, P., Obojes, N., & Tappeiner, U. (2015). Impact of droughts on water provision in managed alpine grasslands in two climatically different regions of the Alps. *Ecohydrology*, *8*(8), 1600–1613. https://doi.org/10.1002/eco.1607

Li, Y., Fuchs, M., Cohen, S., Cohen, Y., & Wallach, R. (2002). Water uptake profile response of corn to soil moisture depletion. *Plant, Cell and Environment*, *25*(4), 491–500. https://doi.org/10.1046/j.1365-3040.2002.00825.x

Lin, G., & Sternberg, L. da S. L. (1993). Hydrogen Isotopic Fractionation by Plant Roots during Water Uptake in Coastal Wetland Plants. *Stable Isotopes and Plant Carbon-Water Relations*, 497–510. https://doi.org/10.1016/b978-0-08-091801-3.50041-6

Lin, Y., & Horita, J. (2016). An experimental study on isotope fractionation in a mesoporous silica-water system with implications for vadose-zone hydrology. *Geochimica et Cosmochimica Acta*, *184*, 257–271. https://doi.org/10.1016/j.gca.2016.04.029

Lobet, G. (2017). *Root phenotyping platforms*. Figshare. https://doi.org/https://doi.org/10.6084/m9.figshare.4706254.v1

Lobet, G., Couvreur, V., Meunier, F., Javaux, M., & Draye, X. (2014). Plant Water Uptake in Drying Soils. *Plant Physiology*, *164*, 1619–1627. https://doi.org/10.1104/pp.113.233486

Mackie, K. A., Stampfli, A., Zeiter, M., & Bloor, J. M. G. (2019). Plant functional groups mediate drought resistance and recovery in a multisite grassland experiment. *Journal of Ecology*, *107*, 937–949. https://doi.org/10.1111/1365-

2745.13102

Majoube, M. (1971). Fractionnement en oxygène 18 et en deutérium entre l'eau et sa vapeur. *Journal of Chemical Physics*, *68*, 1423–1436.

Marshall, J. D., Cuntz, M., Beyer, M., Dubbert, M., & Kuehnhammer, K. (2020). Borehole Equilibration: Testing a New Method to Monitor the Isotopic Composition of Tree Xylem Water in situ. *Frontiers in Plant Science*, *11*, 1–14. https://doi.org/10.3389/fpls.2020.00358

Martínez-Vilalta, J., Poyatos, R., Aguadé, D., Retana, J., & Mencuccini, M. (2014). A new look at water transport regulation in plants. *New Phytologist*, *204*(1), 105–115. https://doi.org/10.1111/nph.12912

Maseda, P. H., & Fernández, R. J. (2006). Stay wet or else: Three ways in which plants can adjust hydraulically to their environment. *Journal of Experimental Botany*, *57*(15), 3963–3977. https://doi.org/10.1093/jxb/erl127

Mathieu, R., & Bariac, T. (1996). A numerical model for the simulation of stable isotope profiles in drying soils. *Journal of Geophysical Research*, *101*, 12685–12696.

Mazzacavallo, M. G., & Kulmatiski, A. (2015). Modelling water uptake provides a new perspective on grass and tree coexistence. *PLoS ONE*, *10*(12), 1–16. https://doi.org/10.1371/journal.pone.0144300

McCully, M. E. (1999). ROOTS IN SOIL: Unearthing the Complexities of Roots and Their Rhizospheres. *Annual Review of Plant Physiology and Plant Molecular Biology*, *50*, 695–718.

McDonnell, J. J. (2014). The two water worlds hypothesis: ecohydrological separation of water between streams and trees? *Wiley Interdisciplinary Reviews: Water*, *1*, 323–329. https://doi.org/10.1002/wat2.1027

Meinzer, F. C., Andrade, J. L., Goldstein, G., Holbrook, N. M., Cavelier, J., & Wright, S. J. (1999). Partitioning of soil water among canopy trees in a seasonally dry tropical forest. *Oecologia*, *121*(3), 293–301. https://doi.org/10.1007/s004420050931

Meinzer, F. C., Brooks, J. R., Domec, J. C., Gartner, B. L., Warren, J. M., Woodruff, D. R., Bible, K., & Shaw, D. C. (2006). Dynamics of water transport and storage in conifers studied with deuterium and heat tracing techniques. *Plant, Cell and Environment*, *29*(1), 105–114. https://doi.org/10.1111/j.1365-3040.2005.01404.x

Meißner, M., Köhler, M., Schwendenmann, L., Hölscher, D., & Dyckmans, J. (2014). Soil water uptake by trees using water stable isotopes (δ2H and δ18O)—a method test regarding soil moisture, texture and carbonate. *Plant Soil*, *367*, 327–335. https://doi.org/10.1007/s11104-013-1970-z

Mennekes, D., Rinderer, M., Seeger, S., & Orlowski, N. (2021). Ecohydrological travel times derived from in situ stable water isotope measurements in trees during a semi-controlled pot experiment. *Hydrology and Earth System Sciences*, *25*, 4513–4530. https://doi.org/10.5194/hess-25-4513-2021

Merlivat, L. (1978). Molecular diffusivities of H2160, HD160, and H2180 in gases.

Journal of Chemical Physics, *69*(6), 2864–2871.

Merlivat, L., & Coantic, M. (1975). Study of mass transfer at the air-water interface by an isotopic method. *Journal of Geophysical Research*, *80*(24), 3455–3464. https://doi.org/10.1029/JC080i024p03455

Meunier, F., Couvreur, V., Draye, X., Vanderborght, J., & Javaux, M. (2017). Towards quantitative root hydraulic phenotyping: novel mathematical functions to calculate plant-scale hydraulic parameters from root system functional and structural traits. *Journal of Mathematical Biology*, *75*(5), 1133–1170. https://doi.org/10.1007/s00285-017-1111-z

Meunier, F., Rothfuss, Y., Bariac, T., Biron, P., Richard, P., Durand, J.-L., Couvreur, V., Vanderborght, J., & Javaux, M. (2017). Measuring and Modeling Hydraulic Lift of Lolium multiflorum Using Stable Water Isotopes. *Vadose Zone Journal*, *17*(1), 160134. https://doi.org/10.2136/vzj2016.12.0134

Meunier, F., Zarebanadkouki, M., Ahmed, M. A., Carminati, A., Couvreur, V., & Javaux, M. (2018). Hydraulic conductivity of soil-grown lupine and maize unbranched roots and maize root-shoot junctions. *Journal of Plant Physiology*, *227*, 31–44.

Michot, L. J., Villiéras, F., François, M., Bihannic, I., Pelletier, M., & Cases, J.-M. (2002). Water organisation at the solid-aqueous solution interface. *Geoscience*, *334*, 611–631.

Millar, C., Janzen, K., Nehemy, M. F., Koehler, G., Hervé-Fernández, P., Wang, H., Orlowski, N., Barbeta, A., & McDonnell, J. J. (2022). On the urgent need for standardization in isotope-based ecohydrological investigations. *Hydrological Processes*, *36*(10), 1–16. https://doi.org/10.1002/hyp.14698

Mualem, Y. (1976). A New Model for Predicting the Hydraulic Conductivity of Unsaturated Porous Media. *Water Resources Research*, *12*(3), 513–522.

Münnich, K. O., Clarke, W. B., Fischer, K. H., Flothmann, D., Kromer, B., Roether, W., Siegenthaler, U., Top, Z., & Weiss, W. (1978). Gas Exchange and Evaporation Studies in a Circular Wind Tunnel, Continuous Radon-222 Measurements at Sea, and Tritium/Helium-3 Measurements in a Lake. In A. Favre & K. Hasselmann (Eds.), *NATO Conference on Turbulent Fluxes through the Sea Surface, Wave Dynamics, and Prediction, France, 1977* (pp. 151–166). Plenum Press.

Murray, F. W. (1966). On the Computation of Saturation Vapor Pressure. *Journal of Applied Meteorology*, 203–204.

Newberry, S. L., Nelson, D. B., & Kahmen, A. (2017). Cryogenic vacuum artifacts do not affect plant water-uptake studies using stable isotope analysis. *Ecohydrology*, *10*(8), 1–10. https://doi.org/10.1002/eco.1892

Newberry, S. L., Prechsi, U. E., Pace, M., & Kahmen, A. (2017). Tightly bound soil water introduces isotopic memory effects on mobile and extractable soil water pools. *Isotopes in Environmental and Health Studies*, *53*(4), 368–381.

Newman, B. D., Wilcox, B. P., Archer, S. R., Breshears, D. D., Dahm, C. N., Duffy, C. J., McDowell, N. G., Phillips, F. M., Scanlon, B. R., & Vivoni, E. R. (2006).

Ecohydrology of water-limited environments: A scientific vision. *Water Resources Research, 42*, 1–15. https://doi.org/10.1029/2005WR004141

O'Neil, J. R., & Truesdell, A. H. (1991). Oxygen isotope fractionation studies of solute-water interactions. *Stable Isotopes Geochemistry*, *3*, 17–25.

Oerter, E. J., & Bowen, G. (2017). In situ monitoring of H and O stable isotopes in soil water reveals ecohydrologic dynamics in managed soil systems. *Ecohydrology*, *10*, 1–13. https://doi.org/10.1002/eco.1841

Oerter, E. J., & Bowen, G. J. (2019). Spatio-temporal heterogeneity in soil water stable isotopic composition and its ecohydrologic implications in semiarid ecosystems. *Hydrological Processes*, *33*, 1724–1738. https://doi.org/10.1002/hyp.13434

Oerter, E. J., Perelet, A., Pardyjak, E., & Bowen, G. (2017). Membrane inlet laser spectroscopy to measure H and O stable isotope compositions of soil and sediment pore water with high sample throughput. *Rapid Communications in Mass Spectrometry*, *31*(1), 75–84. https://doi.org/10.1002/rcm.7768

Ogle, K., Tucker, C., & Cable, J. M. (2014). Beyond simple linear mixing models: process-based isotope partitioning of ecological processes. *Ecological Applications*, *24*(1), 181–195. https://doi.org/10.1890/12-1970.1

Orlowski, N., & Breuer, L. (2020). Sampling soil water along the pF curve for δ2H and δ18O analysis. *Hydrological Processes*, *34*(25), 4959–4972. https://doi.org/10.1002/hyp.13916

Orlowski, N., Breuer, L., Angeli, N., Boeckx, P., Brumbt, C., Cook, C. S., Dubbert, M., Dyckmans, J., Gallagher, B., Gralher, B., Herbstritt, B., Hervé-Fernández, P., Hissler, C., Koeniger, P., Legout, A., Macdonald, C. J., Oyarzún, C., Redelstein, R., Seidler, C., … McDonnell, J. J. (2018). Inter-laboratory comparison of cryogenic water extraction systems for stable isotope analysis of soil water. *Hydrology and Earth System Sciences*, *22*, 3619–3637.

Orlowski, N., Breuer, L., & McDonnell, J. J. (2016). Critical issues with cryogenic extraction of soil water for stable isotope analysis. *Ecohydrology*, *9*(1), 3–10. https://doi.org/10.1002/eco.1722

Orlowski, N., Frede, H. G., Brüggemann, N., & Breuer, L. (2013). Validation and application of a cryogenic vacuum extraction system for soil and plant water extraction for isotope analysis. *Journal of Sensors and Sensor Systems*, *2*(2), 179–193. https://doi.org/10.5194/jsss-2-179-2013

Orlowski, N., Pratt, D. L., & McDonnell, J. J. (2016). Intercomparison of soil pore water extraction methods for stable isotope analysis. *Hydrological Processes*, *30*, 3434–3449.

Parnell, A. C., Inger, R., Bearhop, S., & Jackson, A. L. (2010). Source partitioning using stable isotopes: Coping with too much variation. *PLoS ONE*, *5*(3), 1–5. https://doi.org/10.1371/journal.pone.0009672

Penna, D., Geris, J., Hopp, L., & Scandellari, F. (2020). Water sources for root water uptake: using stable isotopes of hydrogen and oxygen as a research tool in agricultural and agroforestry systems. *Agriculture, Ecosystems & Environment*,

291, 1–30. https://doi.org/https://doi.org/10.1016/j.agee.2019.106790.

Pflugfelder, D., Metzner, R., Dusschoten, D., Reichel, R., Jahnke, S., & Koller, R. (2017). Non-invasive imaging of plant roots in different soils using magnetic resonance imaging (MRI). *Plant Methods*, *13*(1), 1–9. https://doi.org/10.1186/s13007-017-0252-9

Phillips, F. M., & Bentley, H. W. (1987). Isotopic fractionation during ion filtration: I. Theory. *Geochimica et Cosmochimica Acta*, *51*, 683–695. https://doi.org/10.1016/0016-7037(87)90079-2

Poca, M., Coomans, O., Urcelay, C., Zeballos, S. R., Bodé, S., & Boeckx, P. (2019). Isotope fractionation during root water uptake by Acacia caven is enhanced by arbuscular mycorrhizas. *Plant and Soil*, *441*, 485–497. https://doi.org/10.1007/s11104-019-04139-1

Ponce Campos, G. E., Moran, M. S., Huete, A., Zhang, Y., Bresloff, C., Huxman, T. E., Eamus, D., Bosch, D. D., Buda, A. R., Gunter, S. A., Scalley, T. H., Kitchen, S. G., McClaran, M. P., McNab, W. H., Montoya, D. S., Morgan, J. A., Peters, D. P. C., Sadler, E. J., Seyfried, M. S., & Starks, P. J. (2013). Ecosystem resilience despite large-scale altered hydroclimatic. *Nature*, 349–352. https://doi.org/10.1038/nature11836

Prechsl, U. E., Burri, S., Gilgen, A. K., Kahmen, A., & Buchmann, N. (2015). No shift to a deeper water uptake depth in response to summer drought of two lowland and sub-alpine C3-grasslands in Switzerland. *Oecologia*, *177*(1), 97–111. https://doi.org/10.1007/s00442-014-3092-6

Quade, M., Brüggemann, N., Graf, A., Vanderborght, J., Vereecken, H., & Rothfuss, Y. (2018). Investigation of Kinetic Isotopic Fractionation of Water During Bare Soil Evaporation. *Water Resources Research*, *54*, 6909–6928. https://doi.org/10.1029/2018WR023159

Quade, M., Klosterhalfen, A., Graf, A., Brüggemann, N., Hermes, N., Vereecken, H., & Rothfuss, Y. (2019). In-situ monitoring of soil water isotopic composition for partitioning of evapotranspiration during one growing season of sugar beet (Beta vulgaris). *Agricultural and Forest Meteorology*, *266–267*(December 2018), 53–64. https://doi.org/10.1016/j.agrformet.2018.12.002

R Core Team. (2020).

Richard, T., Mercury, L., Massault, M., & Michelot, J. L. (2007). Experimental study of D/H isotopic fractionation factor of water adsorbed on porous silica tubes. *Geochimica et Cosmochimica Acta*, *71*(5), 1159–1169. https://doi.org/10.1016/j.gca.2006.11.028

Richards, L. A. (1931). Capillary conduction of liquids through porous mediums. *Journal of Applied Physics*, *1*(5), 318–333. https://doi.org/10.1063/1.1745010

Richardson, L. F. (2007). *Weather Prediction by Numerical Process* (2nd ed.). Cambridge University Press. https://doi.org/10.1017/CBO9780511618291

Rieger, M., & Litvin, P. (1999). Root system hydraulic conductivity in species with contrasting root anatomy. *Journal of Experimental Botany*, *50*(331), 201–209. https://doi.org/10.1093/jxb/50.331.201

Rodriguez-Dominguez, C. M., & Brodribb, T. J. (2020). Declining root water transport drives stomatal closure in olive under moderate water stress. *New Phytologist*, *225*(1), 126–134. https://doi.org/10.1111/nph.16177

Rothfuss, Y., & Javaux, M. (2017). Reviews and syntheses: Isotopic approaches to quantify root water uptake: A review and comparison of methods. *Biogeosciences*, *14*, 2199–2224. https://doi.org/10.5194/bg-14-2199-2017

Rothfuss, Y., Merz, S., Vanderborght, J., Hermes, N., Weuthen, A., Pohlmeier, A., Vereecken, H., & Brüggemann, N. (2015). Long-term and high-frequency non-destructive monitoring of water stable isotope profiles in an evaporating soil column. *Hydrology and Earth System Sciences*, *12*, 3893–3918. https://doi.org/10.5194/hess-19-4067-2015

Rothfuss, Y., Quade, M., Brüggemann, N., Graf, A., Vereecken, H., & Dubbert, M. (2021). Reviews and syntheses: Gaining insights into evapotranspiration partitioning with novel isotopic monitoring methods. *Biogeosciences*, *18*(12), 3701–3732. https://doi.org/10.5194/bg-18-3701-2021

Rothfuss, Y., Vereecken, H., & Brüggemann, N. (2013). Monitoring water stable isotopic composition in soils using gas-permeable tubing and infrared laser absorption spectroscopy. *Water Resources Research*, *49*, 3747–3755. https://doi.org/10.1002/wrcr.20311

Santos Pires, S., Herbstritt, B., Stumpp, C., Weiler, M., & Stockinger, M. P. (2022). Influence of sample preparation procedures on water stable isotopes in plant organs using the water-vapour equilibrium method. *Ecohydrology*, *15*(4), 1–14. https://doi.org/10.1002/eco.2444

Schneider, J., Kiemle, S., Heck, K., Rothfuss, Y., Braud, I., Helmig, R., & Vanderborght, J. (2024). Analysis of experimental and simulation data of evaporation-driven isotopic fractionation in unsaturated porous media. *Vadose Zone Journal* , *May*, 1–21. https://doi.org/10.1002/vzj2.20363

Schröder, T., Javaux, M., Vanderborght, J., Körfgen, B., & Vereecken, H. (2008). Effect of Local Soil Hydraulic Conductivity Drop Using a Three-Dimensional Root Water Uptake Model. *Vadose Zone Journal*, *7*(3), 1089–1098. https://doi.org/10.2136/vzj2007.0114

Schröder, T., Javaux, M., Vanderborght, J., Körfgen, B., & Vereecken, H. (2009). Implementation of a Microscopic Soil–Root Hydraulic Conductivity Drop Function in a Three-Dimensional Soil–Root Architecture Water Transfer Model. *Vadose Zone Journal*, *8*(3), 783–792. https://doi.org/10.2136/vzj2008.0116

Schymanski, S. J., Sivapalan, M., Roderick, M. L., Beringer, J., & Hutley, L. B. (2008). Hydrology and Earth System Sciences An optimality-based model of the coupled soil moisture and root dynamics. *Hydrol. Earth Syst. Sci*, *12*, 913–932. www.hydrol-earth-syst-sci.net/12/913/2008/

Seleiman, M. F., Al-Suhaibani, N., Ali, N., Akmal, M., Alotaibi, M., Refay, Y., Dindaroglu, T., Abdul-Wajid, H. H., & Battaglia, M. L. (2021). Drought stress impacts on plants and different approaches to alleviate its adverse effects. *Plants*, *10*, 1–25. https://doi.org/10.3390/plants10020259

Seneviratne, S. I., Lüthi, D., Litschi, M., & Schär, C. (2006). Land-atmosphere coupling and climate change in Europe. *Nature*, *443*, 205–209. https://doi.org/10.1038/nature05095

Sheil, D. (2014). How plants water our planet: advances and imperatives. *Trends in Plant Science*, *19*(4), 209–211. https://doi.org/10.1016/j.tplants.2014.01.002

Sofer, Z., & Gat, J. R. (1972). Activities and concentrations of oxygen-18 in concentrated aqueous salt solutions: analytical and geophysical implications. *Earth and Planetary Science Letters*, *15*, 232–238.

Sperry, J. S., Hacke, U. G., Oren, R., & Comstock, J. P. (2002). Water deficits and hydraulic limits to leaf water supply. *Plant, Cell and Environment*, *25*(2), 251–263. https://doi.org/10.1046/j.0016-8025.2001.00799.x

Sperry, J. S., & Love, D. M. (2015). What plant hydraulics can tell us about responses to climate-change droughts. *New Phytologist*, *207*(1), 14–27. https://doi.org/10.1111/nph.13354

Sprenger, M., Herbstritt, B., & Weiler, M. (2015). Established methods and new opportunities for pore water stable isotope analysis. *Hydrological Processes*, *29*, 5174–5192. https://doi.org/10.1002/hyp.10643

Sprenger, M., Tetzlaff, D., Buttle, J., Laudon, H., Leistert, H., Mitchell, C. P. J., Snelgrove, J., Weiler, M., & Soulsby, C. (2018). Measuring and Modeling Stable Isotopes of Mobile and Bulk Soil Water. *Vadose Zone Journal*, *17*(1), 1–18. https://doi.org/10.2136/vzj2017.08.0149

Stampfli, A., Bloor, J. M. G., Fischer, M., & Zeiter, M. (2018). High land-use intensity exacerbates shifts in grassland vegetation composition after severe experimental drought. *Global Change Biology*, *24*, 2021–2034. https://doi.org/10.1111/gcb.14046

Sun, S. J., Meng, P., Zhang, J. S., & Wan, X. (2014). Hydraulic lift by Juglans regia relates to nutrient status in the intercropped shallow-root crop plant. *Plant and Soil*, *374*(1–2), 629–641. https://doi.org/10.1007/s11104-013-1888-5

Tardieu, F., Granier, C., & Muller, B. (2011). Water deficit and growth. Co-ordinating processes without an orchestrator? *Current Opinion in Plant Biology*, *14*, 283–289. https://doi.org/10.1016/j.pbi.2011.02.002

Tardieu, F., & Simonneau, T. (1998). Variability among species of stomatal control under fluctuating soil water status and evaporative demand: modelling isohydric and anisohydric behaviours. *Journal of Experimental Botany*, *49*, 419–432.

Thielemann, L., Gerjets, R., & Dyckmans, J. (2019). Effects of soil-bound water exchange on the recovery of spike water by cryogenic water extraction. *Rapid Communications in Mass Spectrometry*, *33*(5), 405–410. https://doi.org/10.1002/rcm.8348

Thomas, A., Yadav, B. K., & Šimůnek, J. (2020). Root water uptake under heterogeneous soil moisture conditions: an experimental study for unraveling compensatory root water uptake and hydraulic redistribution. *Plant and Soil*, *457*(1–2), 421–435. https://doi.org/10.1007/s11104-020-04738-3

Thompson, S. E., Harman, C. J., Heine, P., & Katul, G. G. (2010). Vegetation-

infiltration relationships across climatic and soil type gradients. *Journal of Geophysical Research*, *115*, 1–12. https://doi.org/10.1029/2009jg001134

Thorburn, P. J., Walker, G. R., & Brunel, J. -P. (1993). Extraction of water from Eucalyptus trees for analysis of deuterium and oxygen-18: laboratory and field techniques. *Plant, Cell & Environment*, *16*(3), 269–277. https://doi.org/10.1111/j.1365-3040.1993.tb00869.x

Tilman, D., & Downing, J. A. (1994). Biodiversity and stability in grasslands. *Nature*, *367*(6461), 363–365. https://doi.org/10.1038/367363a0

Tilman, D., & El Haddi, A. (1992). Drought and Biodiversity in Grasslands. *Oecologia*, *89*, 257–264.

Tsuruta, K., Yamamoto, H., Katsuyama, M., Kosugi, Y., Okumura, M., & Matsuo, N. (2019). Effects of cryogenic vacuum distillation on the stable isotope ratios of soil water. *Hydrological Research Letters*, *13*(1), 1–6. https://doi.org/10.3178/hrl.13.1

Van Den Honert, T. H. (1948). Water transport in plants as a catenary process. *Discussions of the Faraday Society*, *3*(146), 146–153. https://doi.org/10.1039/DF9480300146

van Dusschoten, D., Kochs, J., Kuppe, C. W., Sydoruk, V. A., Couvreur, V., Pflugfelder, D., & Postma, J. A. (2020). Spatially resolved root water uptake determination using a precise soil water sensor. *Plant Physiology*, *184*(3), 1221–1235. https://doi.org/10.1104/pp.20.00488

van Dusschoten, D., Metzner, R., Kochs, J., Postma, J. A., Pflugfelder, D., Bühler, J., Schurr, U., & Jahnke, S. (2016). Quantitative 3D analysis of plant roots growing in soil using magnetic resonance imaging. *Plant Physiology*, *170*(3), 1176–1188. https://doi.org/10.1104/pp.15.01388

van Genuchten, M. T. (1980). A Closed-form Equation for Predicting the Hydraulic Conductivity of Unsaturated. *Soil Science Society of America Journal*, *44*, 892–898. https://doi.org/10.1016/j.pan.2017.07.214

Vanderborght, J., Couvreur, V., Meunier, F., Schnepf, A., Vereecken, H., Bouda, M., & Javaux, M. (2021). From hydraulic root architecture models to macroscopic representations of root hydraulics in soil water flow and land surface models. *Hydrology and Earth System Sciences*, *25*(9), 4835–4860. https://doi.org/10.5194/hess-25-4835-2021

Vanderborght, J., Leitner, D., Schnepf, A., Couvreur, V., Vereecken, H., & Javaux, M. (2023). Combining root and soil hydraulics in macroscopic representations of root water uptake. *Vadose Zone Journal*, *December 2022*, 1–22. https://doi.org/10.1002/vzj2.20273

Varado, N., Braud, I., & Ross, P. J. (2006). Development and assessment of an efficient vadose zone module solving the 1D Richards' equation and including root extraction by plants. *Journal of Hydrology*, *323*(1–4), 258–275. https://doi.org/10.1016/j.jhydrol.2005.09.015

Vargas, A. I., Schaffer, B., Yuhong, L., & Sternberg, L. da S. L. (2017). Testing plant use of mobile vs immobile soil water sources using stable isotope experiments.

New Phytologist, *215*(2), 582–594. https://doi.org/10.1111/nph.14616

Vetterlein, D., & Doussan, C. (2016). Root age distribution: how does it matter in plant processes? A focus on water uptake. *Plant and Soil*, *407*(1–2), 145–160. https://doi.org/10.1007/s11104-016-2849-6

Vetterlein, D., Phalempin, M., Lippold, E., Schlüter, S., Schreiter, S., Ahmed, M. A., Carminati, A., Duddek, P., Jorda, H., Bienert, G. P., Bienert, M. D., Tarkka, M., Ganther, M., Oburger, E., Santangeli, M., Javaux, M., & Vanderborght, J. (2022). Root hairs matter at field scale for maize shoot growth and nutrient uptake, but root trait plasticity is primarily triggered by texture and drought. *Plant and Soil*, *478*, 119–141. https://doi.org/10.1007/s11104-022-05434-0

Volkmann, T. H. M., Haberer, K., Gessler, A., & Weiler, M. (2016). High-resolution isotope measurements resolve rapid ecohydrological dynamics at the soil-plant interface. *New Phytologist*, *210*(3), 839–849. https://doi.org/10.1111/nph.13868

Volkmann, T. H. M., Kühnhammer, K., Herbstritt, B., Gessler, A., & Weiler, M. (2016). A method for in situ monitoring of the isotope composition of tree xylem water using laser spectroscopy. *Plant Cell and Environment*, *39*(9), 2055–2063. https://doi.org/10.1111/pce.12725

Volkmann, T. H. M., & Weiler, M. (2014). Continual in situ monitoring of pore water stable isotopes in the subsurface. *Hydrology and Earth System Sciences*, *18*(5), 1819–1833. https://doi.org/10.5194/hess-18-1819-2014

von Caemmerer, S., & Farquhar, G. D. (1981). Some relationships between the biochemistry of photosynthesis and the gas exchange of leaves. *Planta*, *153*(4), 376–387. https://doi.org/10.1007/BF00384257

Walker, G. R., Woods, P. H., & Allison, G. B. (1994). Interlaboratory comparison of methods to determine the stable isotope composition of soil water. *Chemical Geology*, *111*(1–4), 297–306. https://doi.org/10.1016/0009-2541(94)90096-5

Wang, L., Good, S. P., Caylor, K. K., & Cernusak, L. A. (2012). Direct quantification of leaf transpiration isotopic composition. *Agricultural and Forest Meteorology*, *154–155*, 127. https://doi.org/10.1016/j.agrformet.2011.10.018

Warren, C. P. (2011). *Isotopic Tracer Reveals Depth-Specific Water Use Patterns Between Two Adjacent Native and Non- native Plant Communities*. Utah State University.

Wassenaar, L. ., Hendry, M. J., Chostner, V. L., & Lis, G. P. (2008). High Resolution Pore Water δ 2 H and δ 18 O Measurements by Laser Spectroscopy. *Environmental Science & Technology*, *42*(24), 9262–9267.

Wen, M., Si, B., Lu, Y., & Wang, H. (2021). Water recovery rate and isotopic signature of cryogenic vacuum extracted spiked soil water following oven-drying at different temperatures. *Hydrological Processes*, *35*(6). https://doi.org/10.1002/hyp.14248

Wever, L. A., Flanagan, L. B., & Carlson, P. J. (2002). Seasonal and interannual variation in evapotranspiration, energy balance and surface conductance in a northern temperate grassland. *Agricultural and Forest Meteorology*, *112*(1), 31–49. https://doi.org/10.1016/S0168-1923(02)00041-2

White, R., Murray, S., & Rohweder, M. (2000). Pilot Analysis of Global Ecosystems: Grassland Ecosystems. In *World Resources Institute*.

Yakir, D., DeNiro, M. J., & Rundel, P. W. (1989). Isotopic inhomogeneity of leaf water: Evidence and implications for the use of isotopic signals transduced by plants. *Geochimica et Cosmochimica Acta*, *53*, 2769–2773. https://doi.org/10.1016/0016-7037(89)90147-6

Yakir, D., & Sternberg, L. da S. L. (2000). International Association for Ecology The Use of Stable Isotopes to Study Ecosystem Gas Exchange. *Oecologia*, *123*, 297–311.

Yang, Y., Guan, H., Batelaan, O., McVicar, T. R., Long, D., Piao, S., Liang, W., Liu, B., Jin, Z., & Simmons, C. T. (2016). Contrasting responses of water use efficiency to drought across global terrestrial ecosystems. *Scientific Reports*, *6*, 1–8. https://doi.org/10.1038/srep23284

Yue, P., Zhang, Q., Zhang, L., Yang, Y., Wei, W., Yang, Z., Li, H., Wang, S., & Sun, X. (2020). Biometeorological effects on carbon dioxide and water-use efficiency within a semiarid grassland in the Chinese Loess Plateau. *Journal of Hydrology*, *590*(August), 125520. https://doi.org/10.1016/j.jhydrol.2020.125520

Zarebanadkouki, M., Kim, Y. X., & Carminati, A. (2013). Where do roots take up water? Neutron radiography of water flow into the roots of transpiring plants growing in soil. *New Phytologist*, *199*(4), 1034–1044. https://doi.org/10.1111/nph.12330

Zeiter, M., Schärrer, S., Zweifel, R., Newbery, D. M., & Stampfli, A. (2016). Timing of extreme drought modifies reproductive output in semi-natural grassland. *Journal of Vegetation Science*, *27*(2), 238–248. https://doi.org/10.1111/jvs.12362

Zhao, L., Wang, L., Cernusak, L. A., Liu, X., Xiao, H., Zhou, M., & Zhang, S. (2016). Significant Difference in Hydrogen Isotope Composition Between Xylem and Tissue Water in Populus Euphratica. *Plant Cell and Environment*, *39*(8), 1848–1857. https://doi.org/10.1111/pce.12753

Zhao, Y., Wang, L., Knighton, J., Evaristo, J., & Wassen, M. (2021). Contrasting adaptive strategies by Caragana korshinskii and Salix psammophila in a semiarid revegetated ecosystem. *Agricultural and Forest Meteorology*, *300*(May 2020), 108323. https://doi.org/10.1016/j.agrformet.2021.108323

Zhou, T., Šimůnek, J., & Braud, I. (2021). Adapting HYDRUS-1D to simulate the transport of soil water isotopes with evaporation fractionation. *Environmental Modelling and Software*, *143*. https://doi.org/10.1016/j.envsoft.2021.105118

Zimmermann, U., Ehhalt, D., & Münnich, K. O. (1967). Soil-water movement and evapotranspiration: changes in the isotopic composition of the water. *Proc. Symp. Isotop. Hydrology*, 567–585.

Zuecco, G., Amin, A., Frentress, J., Engel, M., Marchina, C., Anfodillo, T., Borga, M., Carraro, V., Scandellari, F., Tagliavini, M., Zanotelli, D., Comiti, F., & Penna, D. (2022). A comparative study of plant water extraction methods for isotopic analyses: Scholander-type pressure chamber vs. cryogenic vacuum

distillation. *Hydrology and Earth System Sciences*, *26*(13), 3673–3689. https://doi.org/10.5194/hess-26-3673-2022

Zwicke, M., Picon-Cochard, C., Morvan-Bertrand, A., Prud'homme, M. P., & Volaire, F. (2015). What functional strategies drive drought survival and recovery of perennial species from upland grassland? *Annals of Botany*, *116*(6), 1001–1015. https://doi.org/10.1093/aob/mcv037

Zwieniecki, M. A., Thompson, M. V., & Holbrook, N. M. (2003). Understanding the hydraulics of porous pipes: Tradeoffs between water uptake and root length utilization. *Journal of Plant Growth Regulation*, *21*(4), 315–323. https://doi.org/10.1007/s00344-003-0008-9